UNIVERSIDADE DA BEIRA INTERIOR
Engenharia

Adaptive Gurney Flap for Rotor Blades

Bruno Ricardo Barros Dias

Dissertação para obtenção do Grau de Mestre em
Engenharia Aeronáutica
(Ciclo de Estudos Integrado)

Orientador: Prof. Doutor Pedro Vieira Gamboa
Co-orientador: Prof. Doutor José Miguel Almeida da Silva

Covilhã, October 2013

Dedicatória

Este projecto é dedicado aos meus pais e a minha namorado pelo suporte dado este anos.

Acknowledges

I would like to thank all the teachers of the Department of Aerospace Ciências by knowledge transmitted throughout this 6 years, particularly to my counsellors, Prof. Pedro Gamboa and Prof. José Silva for all support provided for the realization of this project.
I thank the Active Space Technologies for giving me the opportunity to work on this project mainly to Eng. Nuno Sousa all support provided.
To my dear parents who have made enough sacrifices for that had an excellent training leave a profound gratitude and dedicate them this project. Finally I would also say a thank you to my dear girlfriend for having patience and being present in the hardest times.

Resumo

Desde muito tempo vários esforços tem sido feitos de maneira a optimizar o rotor dos helicópteros com o objectivo de reduzir a emissão de poluentes. Durante vários anos foram feitas várias optimizações estrutrais na pá do rotor.
Estudos recentes numéricos e experimentais mostram que para melhor a performance do rotor várias considerações aerodinâmicas têm que ser levadas em conta.
O principal objectivo deste trabalho é estudar e optimizar um mecanismo preliminar constituído por um flap dinâmico que consiga controlar a camada limite na pá. O flap escolhido foi o Gurney Flap, desenvolvido nos anos 70 por um piloto de automóveis com o intuito de provocar uma downforce de maneira a melhorar o desempenho do automovél. A razão desta escolha deve-se por o flap ter uma superfície relativamente pequena com baixas forças de inércia permitindo baixos consumos de energia e sem adicionar extra carga para na pá. A utilização deste flap demonstrou o aumento as propriedades aerodinâmicas de pá, portanto, reduzindo o consumo de combustÃvel.
Para este estudos várias análises estruturais foram realizadas usando softwares comerciais entre eles; análises cináticas, de maneira a estudar o deslocamento, velocidade e aceleraçao do mecanismo e também do sistema de actuação; análises dinâmica, possibilitando o calculo de tensões e deformações do sistema sujeito a várias cargas de inécia e por fim uma análise modal, bastante importante devido ao mecanismo estar sujeito a uma frequência de actuação.
Depois de conduzidas estas análises foi possivél optimizar o peso da desenho inicial em cerca de 50% respeitando todos os requerimentos impostos e as características do material. Foram estudados dois tipos de sistema de de actuação deixando em aberto a escolha do actuador.

Palavras-chave

Gurney Flap, Mecanismo Activo, Análise Modal, An'alise Estática, An'alise Diâmica

Abstract

Various efforts have been made in order to optimize the helicopter rotor with the objective to reduce the emission of pollutants. For several years many studies have conducted to a structural optimization of rotor blade.
Recent experimental and numerical studies show that for the best performance of the rotor several aerodynamic considerations must be taken into account.
The main objective of this work is to study and optimize a preliminary mechanism consisting in a dynamic flap that can control the boundary layer on the blade. The chosen flap was a Gurney flap which was developed in the 70's by a race driver in order to cause a downforce improving the performance of the race cars. The reason for this choice is due to the flap having a relatively small surface with low inertial forces allowing low energy consumption and without adding extra load to the blade. The use of this flap has demonstrated to increase the aerodynamics properties of blade therefore reducing the fuel consumption.
For this study a number of structural analyses were performed using commercial software between them: kinematics analysis in order to study the displacement, velocity and acceleration of the mechanism and also the actuation system; dynamic analysis , enabling the calculation of stress and strain of the system subjected to various inertial loads, and finally, a modal analysis, very important due to the mechanism being subject to a high frequency of actuation.
After these analyses was possible to optimize the design of the mass in about 50% respecting all the requirements imposed and the characteristics of the material. There are two types of actuation system, while leaving open the choice of the actuator.

Keywords

Gurney Flap, Active Mechanism, Modal Analysis, Static Analysis, Dynamic Analysis

Contents

List of Figures

List of Tables

List of Symbols

Acronyms

AST	Active Space Technologies
CFD	Computational Fluid Dynamics
FEM	Finite Elements Method
GF	Gurney Flap
MiTE	Miniature Trailing-Edge Efectors
UBI	Universidade da Beira Interior

Roman Symbols

a	$[m/s^2]$	Acceleration
c	[m]	chord
c_l		Lift coefficient
c_D		Drag coefficient
F	[N]	Force
f	[Hz]	Frequency
g	$[m/s^2]$	Gravity acceleration
M	[N/m]	Moment
m	[kg]	Mass
r	[m]	Distance actuator to rotating axle
T	[s]	Period
v	$[m/s^2]$	Velocity
y	[m]	Displacement Y direction
x	[m]	Displacement X direction

Greek symbols

α	$[rad/s^2]$	Angular Acceleration
θ	$[rad]$	Angle of rotation
ω	$[rad/s]$	Angular velocity

Subscripts

1	Point 1
2	Point 2
3	Point 3
actua	Actuator
ext	External/Environment acceleration
I	Inertia
support	Support
y	Y direction
x	X direction

Chapter 1

Introduction

For several years an effort is being made by several companies to improve the rotorcraft blade in order to turn the travels more pleasant and less expensive. In the past most of these efforts were focused to the structural dynamics of the blade, nowadays, some studies are conducted to improve the aerodynamic characteristics, controlling the flow, in order to increase the rotor performance.

In order to control the aerodynamics of the blade section to the maximum performance the rotorcraft airfoil must follow some features such as a high maximum lift coefficient allowing a rotor with lower solidity and lighter weight; a good lift-to-drag ratio which causes a low power consumption and low autorotative rate of descent; a low pitching moments that minimizes vibrations and blade torsion moments and other many considerations.

To control the flow in the rotor blade, the boundary-layer control methods such as suction or blowing, used in conventional aircraft wings, is not convenient mostly to the fact of addition of weight, need of power and complexity of the required pumps and tubes to actuate the system. An effective solution to control the flow is the use of trailing edge flaps which allows the control of aerodynamics of a blade increasing the performance of the vehicle and also has the ability to suppress the vibration of the rotor, thus, increasing the passenger comfort and reducing the fatigue life of the components. An additional possibility to control the aerodynamics of a rotor blade is the use of Gurney Flaps, shown by Fig.1.1 distributed along the blade.
Gurney Flaps were originally developed by race pilot Dan Gurney in the early 1970s. The objective of this flap was to increase the downforce generated by the wing of the car, improving traction during acceleration, braking and cornering. He noticed great improvements during the races. More recently several studies are being made to include these flaps in the helicopter's blades.

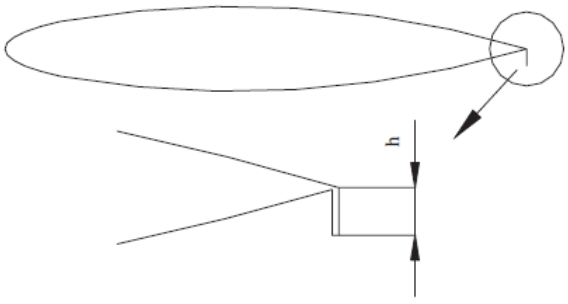

Fig. 2. Gurney flap configuration.

Figure 1.1: Gurney flap configuration.

Gurney Flaps are small plates placed perpendicular to the flow near the trailing edges of an arfoil, thus, having a much smaller wetted area and considerably less inertia than a traditional flap, consequently, smaller forces are required to actuate it when compared to a traditional flap. These types of flaps generate lift due to an effective increase in the camber of the airfoil, when used in a rotor blade, the flap would typically be deployed when the blade is retreating to prevent

stall due to lower speeds of a retreating blade.

1.1 Objectives

The main goal of this research is to design an active Gurney flap actuation system to be installed in a rotorcraft blade. An initial design was provided by the Portuguese company Active Space Technologies and an extensive study will be made to optimize the system in order to minimize the weight and the total deformation respecting several requirements, imposed by the AST, which will be mentioned in the following chapter. A kinematic and dynamic study of the mechanism will be conducted by commercial software, Ansys v13, and afterwards will be compared with a numerical code, using basic kinematics and dynamics equations, made in Matlab. With both methods it is possible to analyse the requirements which the actuator has to provide to the system. The main challenges encountered are the size constraints, the frequency required, to obtain better aerodynamics characteristics, and the inertial forces created by the accelerations provoked by the motion of the blade, mainly the centrifugal force which is typically on the order of hundreds of g's. The airfoil chosen for this project is a modified NACA 0012 with 90mm chord, and a Gurney flap located at 95% of the chord having a height of 1.5% of the chord. The reasons of these dimensions are to allow wind-tunnel tests with an actuation of the GF.
The ultimate goal of this project is to compete to the Clean Sky Project, a project concerned to minimize the emission of pollutants.

1.2 State of the Art

1.2.1 Aerodynamics of a Gurney Flap

An experimental study of the GF was first conducted by [1] on a Newman airfoil. He found that the GF with only a 1.25% chord length gave high-lift coefficient by increasing lift but reducing drag at the same time. [1] also found that the flap height should be kept between 1%C and 2%C in order to maximize the aerodynamic benefits from this simple high-lift device, Fig.1.2 shows the lift and drag coefficients of NACA0012 airfoil with the GF's obtained by [3].

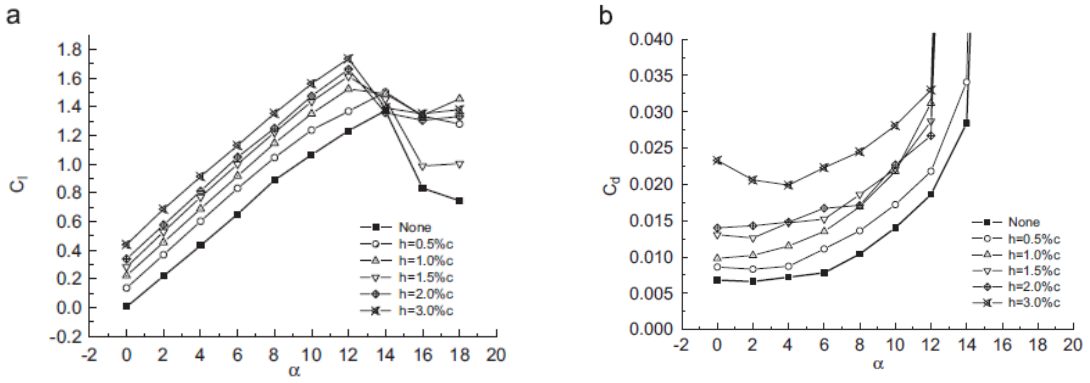

Figure 1.2: Lift and Drag coefficients vs. angle of attack: (a) lift coefficient and (b) drag coefficient. [1]

From Fig.1.2(a) it is possible to see an increase of the maximum lift coefficient increasing the Gurney Flap height. The figure also shows that the stall angle is reduced, while the zero-lift angle

of attack becomes increasingly more negative with an increase in the GF height. These results suggest that the effect of the GF is to increase the effective camber of the airfoil. Similar results were reported by several authors for different airfoils.

As shown in Fig.1.2(b), the drag polar, an increase of the flap height increases the drag in the same way, becoming more significantly for Gurney Flap with a height more than 2%C.

Fig.1.3 presents the result of lift-to-drag ratio vs. lift coefficient. There are large drag penalties associated with the GF at low-to-moderate lift coefficients, which can be increased with the flap height. At higher lift coefficients, however, both the lift and drag are increased. The effect of the Gurney Flap on the maximum lift-to-drag ratio is small, but the lift coefficient for a given lift-to-drag ratio is significantly increased.

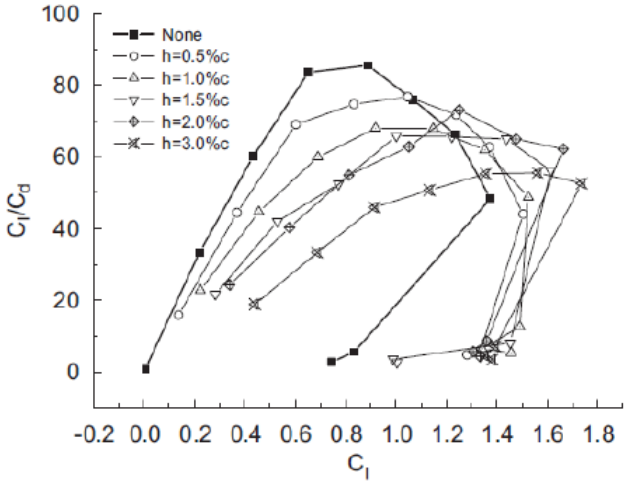

Figure 1.3: Lift-to-drag ratio vs. lift coefficient [1]

[4] suggested that the flap should be closed during cruise due the drag penalties at lower to moderate lift coefficients.
Fig.1.4 shows that the nose-down pitching moment is increased with the GF, confirming that the effective camber is increased with the GF.

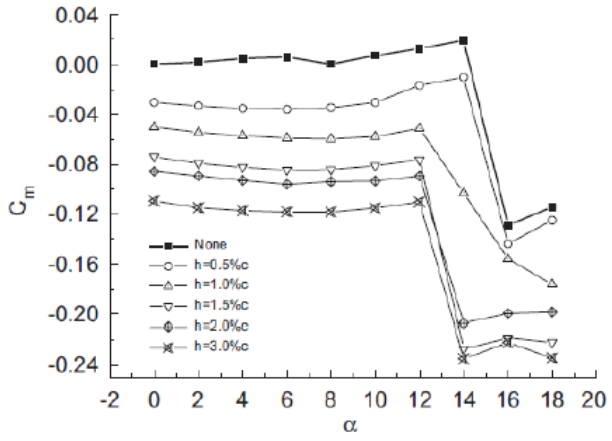

Figure 1.4: Quarter-chord pitching moment vs. angle of attack.[4]

[5] suggested that the size of the optimum GF for best lift-to-drag ratio is determined by the flow condition at the trailing edge on the pressure side of airfoil.

Fig.1.5 represents an airfoil with Gurney Flap configuration located at different positions with with a $\phi = 90°$ and $height = 1.5\%$C.

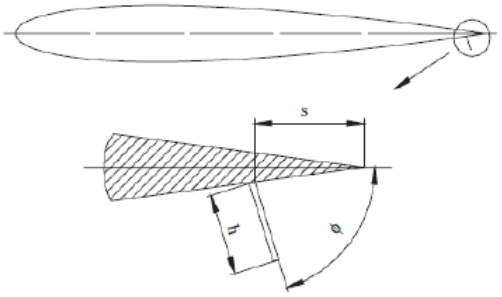

Figure 1.5: Gurney Flap Configuration. [4]

Fig.1.6 shows an increased lift coefficient with a reduced stall angle and the angle of zero lift. However, the increment of lift coefficient decreased when the GF was shifted forward away from the trailing edge, weakening the lift-enhancing effects of the flap, concluding the best position is at $s = 0$.

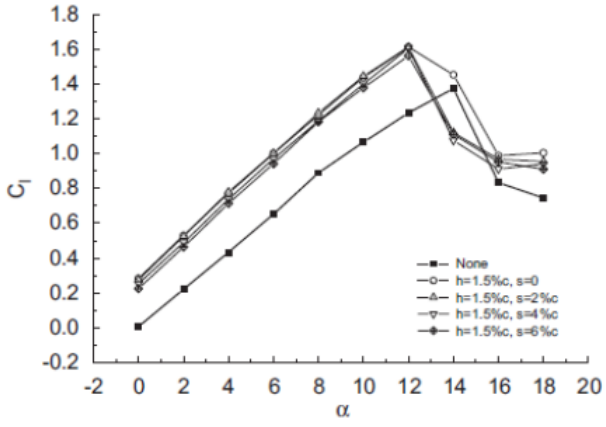

Figure 1.6: Lift coefficient vs. angle of attack for different flap locations.[4]

The drag polars (Fig.1.7) indicate that the GF always increases the drag whenever they are mounted.

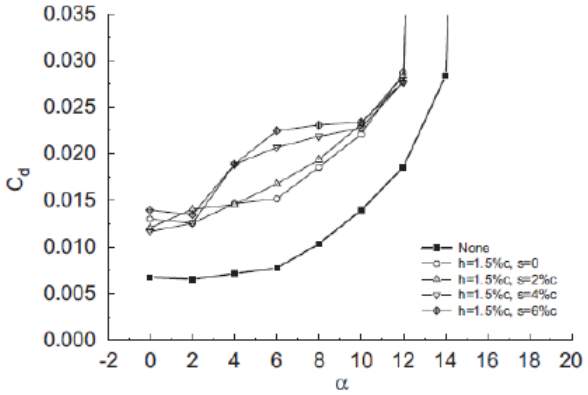

Figure 1.7: Drag coefficient vs. angle of attack for different flap locations.[4]

In Fig.1.8 it is possible to see the lift-to-drag ratio presenting that the GF can provide with an enhanced in this ratio when c_l>1.2, although no increase in lift-to-drag ratio can be observed when c_l<1.2. The best performance can be obtained when the GF is mounted at the trailing edge of the airfoil (s=0). The lift-enhancement effect is weakened when the flap is moved forwards.

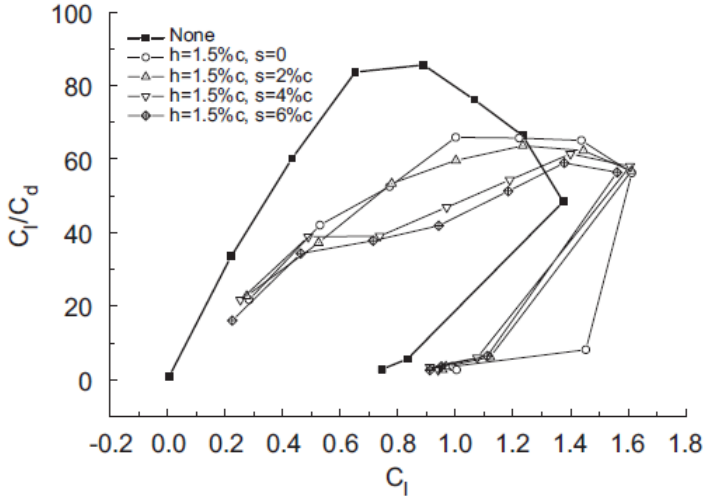

Figure 1.8: Lift-to-drag ratio vs. lift coefficient for different flap locations.[4]

Pressure distributions over an the same airfoil mentioned before with same height are shown in Fig.1.9. Increased suction with the GF is evident over the upper surface while the lower surface experiences an increase in pressure, giving rise to a substantial increase in the lift coefficient. Note that there is an adverse pressure gradient in front of the flap as a result of a recirculating region on the lower airfoil surface just upstream of the flap as shown in Fig.1.10.

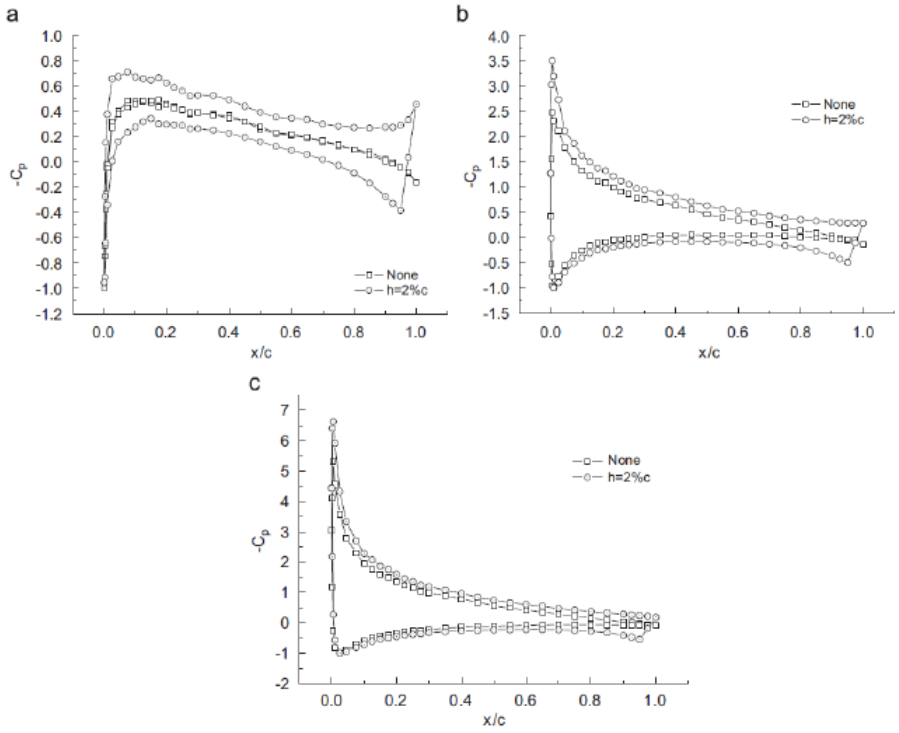

Figure 1.9: Pressure distributions over an airfoil with the Gurney flap: (a) $\alpha = 0°$, (b) $\alpha = 6°$ and (c) $\alpha = 10°$. [4]

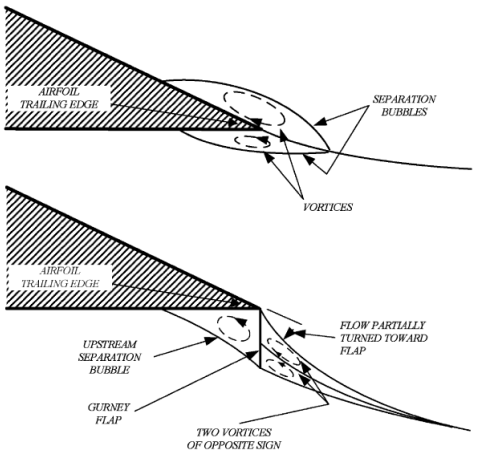

Figure 1.10: Flow patterns without and with the Gurney flap depicted by [1]

When there are no Gurney Flaps installed, the streamlines are in general very smooth and there seem to be no observable vortices in the wake region. When a 2%C GF is fitted to the airfoil, however, the streamlines suggest the existence of a vortex in the wake of the flap, with a 6%C shows a pair of counter-rotating vortices in the wake region behind the flap presented by Fig.1.11.

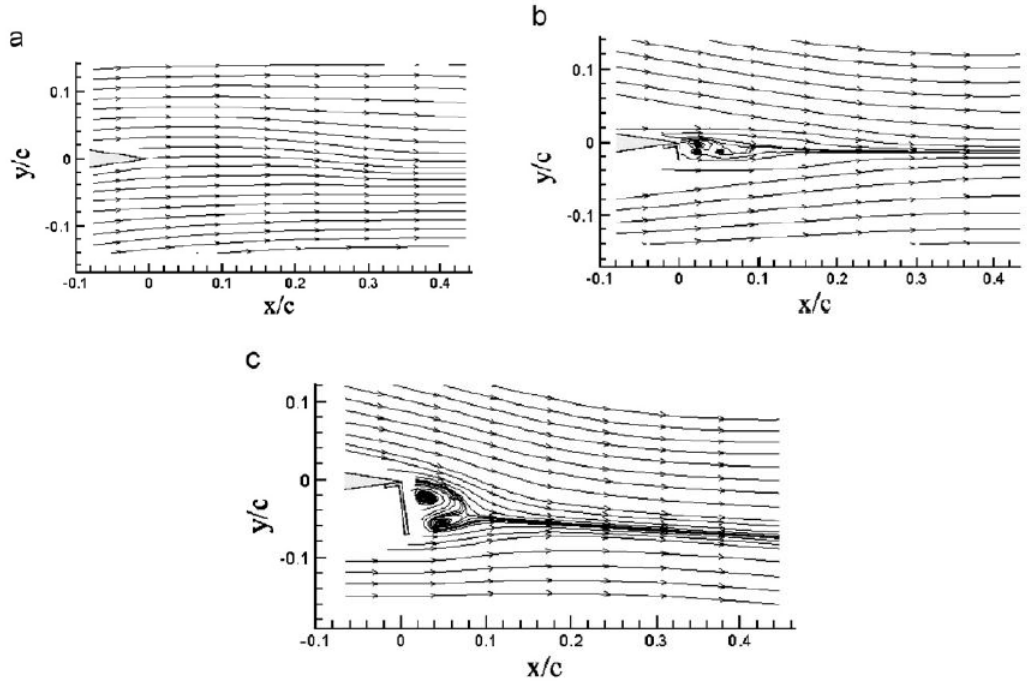

Figure 1.11: Time-averaged streamlines at $\alpha = 0°$ with and without the Gurney flap: (a) clean airfoil, (b) 2%C Gurney flap and (c) 6%C Gurney flap.[6]

A GF with h=6%C was mounted at different positions with an angle of attack of 2.5° shown in Fig.1.12.

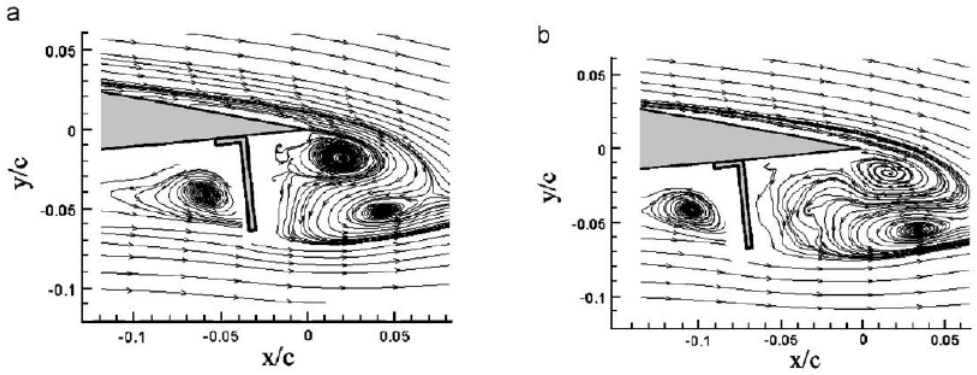

Figure 1.12: Time-averaged streamlines around an airfoil at $\alpha = 2.5°$ with a Gurney flap of h = 6%C mounted at s = 4%C (a) and s = 8%C (b).[6]

When the flap is mounted forwards, a flow separation occurs over the upper surface as the velocity is decelerated and the pressure recovered leading to a loss of rear lift, thus the total lift of the airfoil is reduced.

Miniature Trailing-Edge Effectors introduced by [7], or MiTEs, presented if Fig.1.13 are as effective as plain flaps, and high frequency deployments are achievable due to their small size. Experiments showed success with their use in flutter stabilization with an effective deployment at frequencies exceeding 125 Hz used also to for rotor-blade control provides aerodynamic control at the outboard stations of the rotor blades reducing the high loading at the root of the blade.

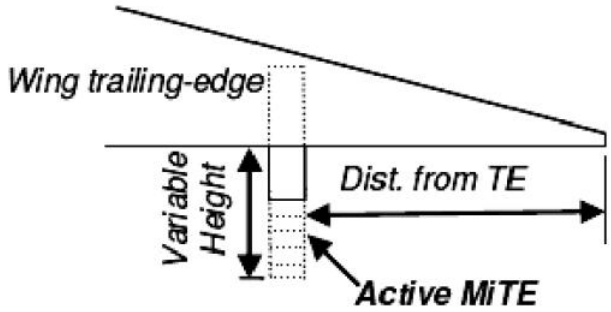

Figure 1.13: Concept of MiTE. [7]

The frequency of these oscillations was observed to depend on the height of the Gurney flap and boundary layer thickness.
MiTEs has been used for vibration control on rotorcraft, the major concern is their ability to achieve increments in the lift and pitching moment at high frequencies. [7] studied a helicopter model with Gurney flap showing an increases in the rotor performance at high thrusts and in forward flight but that at lower thrusts and hover, the Gurney flaps decrease this performance. His study included the increasing of the maximum flight speed, achievable rotor thrusts, thrusting performance, maneuver performance and payload capabilities. These gains would indirectly increase the cruise performance showed to be very effective for transonic airfoils, as they provide a more efficient configuration for high-speed flows, while still providing high lift when needed. Fig.1.14 shows the increase in the maximum forward speed of a MiTE-equipped helicopter.

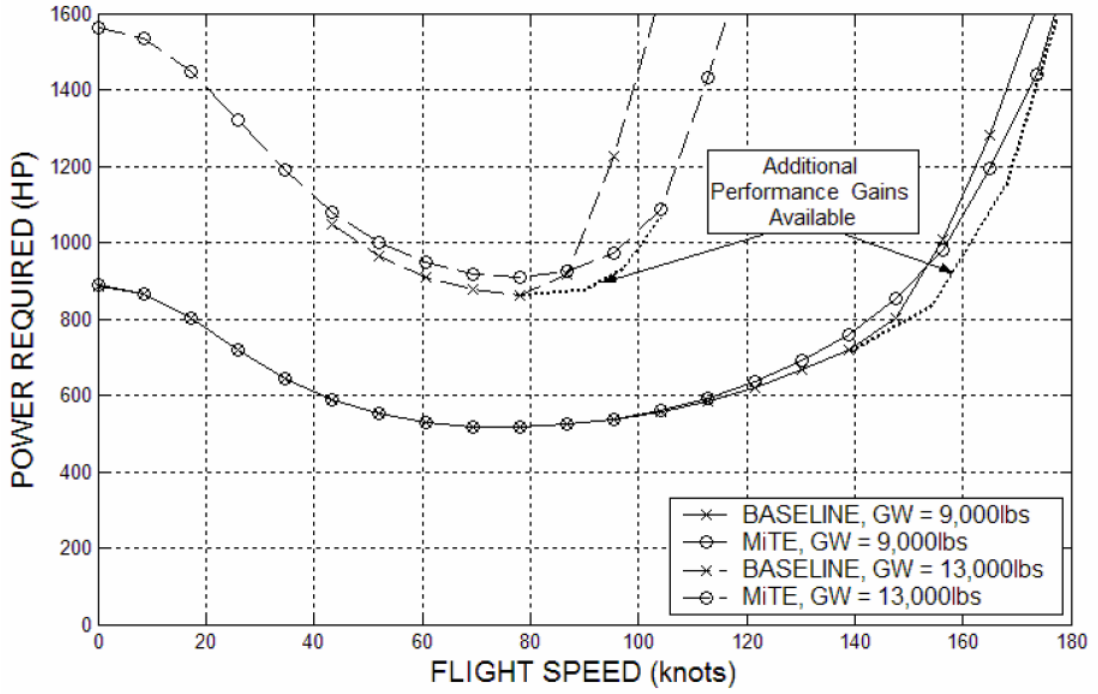

Figure 1.14: Comparison between baseline and MiTE rotor performance in level forward flight with variations in the gross weight calculated using the dynamic stall model and without an optimal MiTE deployment schedule.[7]

Adaptive Gurney Flap for Rotor Blades

The rotor performance enhancements due to MiTEs was investigated by [8] using a modified version of ROTOR, a rotor performance analysis code based on blade-element theory predicting the required power for hover and level forward flight with a trimmed rotor state. To model the aerodynamics during the rotor analyses, the models were separated into two categories. The first category was the modeling of the baseline airfoil without a MiTE and the second category is one that pertains to the modelling of MiTEs. The program was set up to use a separate set of data that represents the same airfoil with the specific Gurney flap being used attached to the airfoil providing the needed $\triangle cl_{GF}$ and $\triangle cd_{GF}$ as a function of angle of attack and Mach number. The objective was initially to have the MiTE retracted at lower angles of attack when additional lift is not needed. When the lift requirements increase, MiTEs deploy to achieve higher lift without a stall drag penalty shown by Fig.1.15.

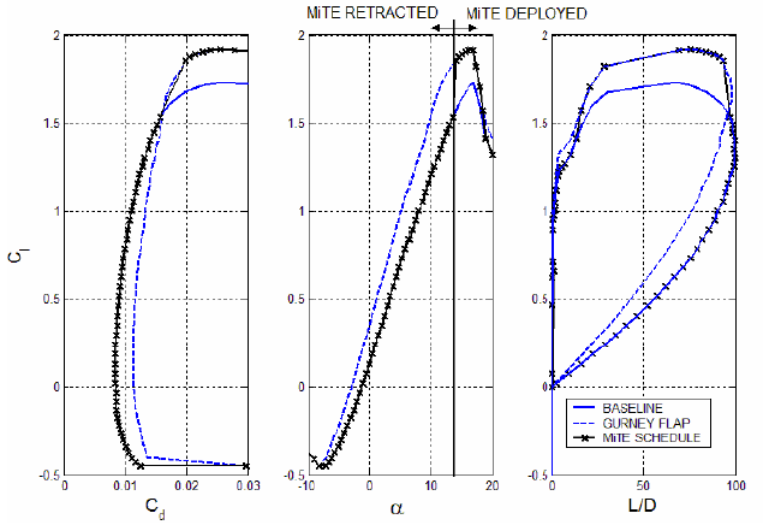

Figure 1.15: Deployment schedule of MiTEs. [8]

[8] demonstrated that MiTEs are capable of increasing the maximum speed of the rotorcraft. This is consequence of a MiTEs ability to delay stall on the retreating blade. This reduced drag and increased the lift-to-drag ratio allows greater speeds. The author also demonstrated that the greatest effect is due to the increased its maximum lift on the transonic airfoil.

A study made by [9] with a NACA 4412 airfoil was tested, in a boundary layer wind tunnel, with the aim to study the effect of a Gurney flap, as an active and passive flow control device submitted to a turbulent flow field with the objective of determination of flow pattern characteristics downstream the airfoil in the near wake. A movable up-down Gurney Flap mechanism located on lower surface at a distance of 8%c from the trailing edge in order to appreciate an increment of c_l when the excitation frequency increases, in comparison with the clean airfoil.
The author observed that the c_l values of the model with the Gurney flap fixed are something greater than the corresponding values for the movable Gurney condition. Regarding the c_d behavior, it diminishes when the frequency increases, but its minimum value is something greater than the case for the clean airfoil. An example of the mechanism used can be seen by Fig.1.16.

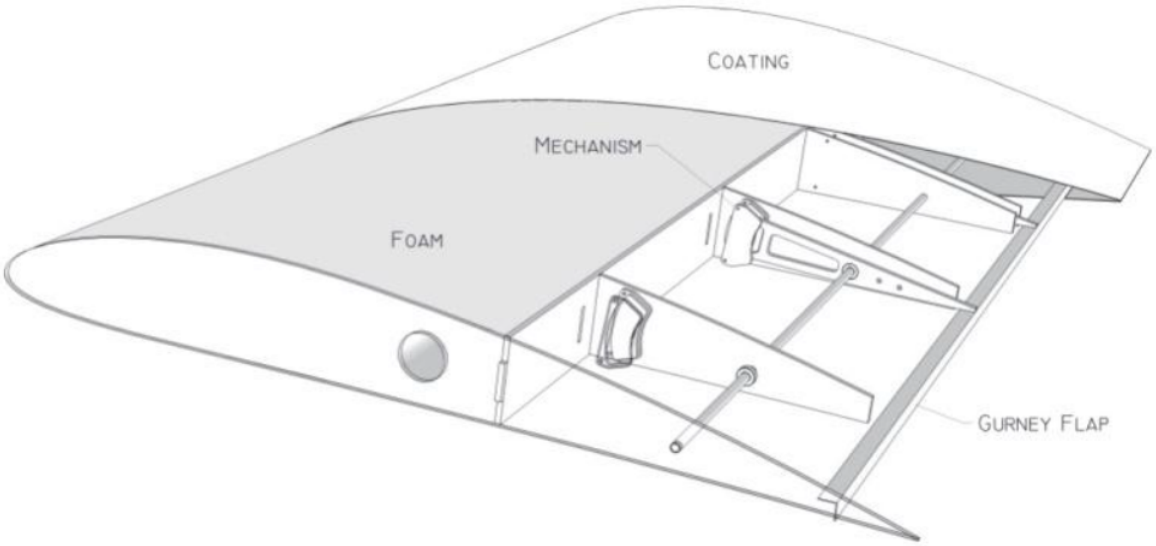

Figure 1.16: Tested wing model.[9]

The Gurney flap was a movable plate of 5mm height (1%c), corresponding to its maximum vertical displacement, and 1mm width with a wingspan length.

The aerodynamic loads were measured, in a first instance, for two angles of attack, 0° and 8°, with the movable flap at 5, 10 and 15Hz frequencies, with the motivation to obtain preliminary results about the device behaviour shown by Fig.1.17.

Frecuency	α	C_l	C_d
5 Hz	0°	0,499	0,084
	8°	1,423	0,173
10 Hz	0°	0,523	0,049
	8°	1,435	0,160
15 Hz	0°	0,524	0,033
	8°	1,479	0,150

Figure 1.17: Aerodynamic coefficients, for 0° and 8° at 5, 10 and 15 Hz. [9]

The author, [9], concluded then for frequencies up to 15Hz, the section lift coefficient grows meanwhile the section drag decreases. According other works [1], the vortex wake close to the trailing edge, had clockwise and counter-clockwise vortices. If the movable (vertical) Gurney flap oscillates outside and inside the wing, with a frequency that allows moving down the rear stagnation point of the airfoil, the lift will grow. So, according the flap frequency, it will promote an increase or decrease of the lift.

1.2.2 Actuation Mechanism of a Gurney flap

The aim of the Gurney Flap is to be able to actuate such a flap as the rotor blade goes around the helicopter to improve the lift on the retrieving side while not affecting the characteristics of the blade on the advancing side. This will enhance the lift and maximum performance of the rotorcraft. [6] [10].

A study about Piezo-Actuators in order to find the suitable actuator for a Gurney Flap mechanism was conducted by [11], stating that the requirements should be:

- The mechanical energy developed needs to be sufficient to actuate the flap in the worst aerodynamic case.
- The actuator needs to be sufficiently fast to execute one full cycle within one blade revolution.
- The weight and space taken by the actuators must be as small as possible.
- The actuators need to be embedded within the rotor blades and therefore need to sustain the high g-forces generated.
- The reliability should be as high as possible to meet the time between maintenance checks.

Piezo-stack actuators are the most efficient piezoelectric actuators due to the high strain constants in the direction of the applied voltage and various types are commercially available. The linear actuator solution is much lighter than the stack actuator alternative, but the devices are already at its maximum capabilities in terms of speed, whereas the stack actuators bandwidth would allow not only to deploy the Gurney flaps as the blade goes around but also to perform active vibration reduction at frequencies that are at least four times the revolution.
The stack actuator solution presents some interesting possible multi-purpose usage. The flap can be divided into multiple sections and the operating frequencies can be much more important, it would allow to modify quickly the envelope of the helicopter not only to increase the lift for the retrieving blade, but also for damping high frequency vibrations and twisting the blade. Furthermore, stack actuators have already been successfully integrated into demonstrators for active vibration damping.

An initial study by [2] into the actuation of a Gurney flap using a piezoelectric bender was conducted to determine if the necessary displacements and actuation frequencies could be achieved. A finite element model was developed to predict the deflection and natural frequencies of the system. A full-scale prototype was built and the schematic can be seen in Fig.1.18, along with the fabricated design in Fig.1.19.

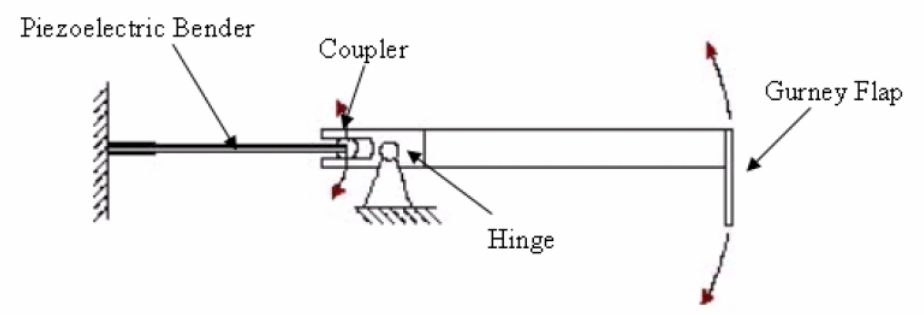

Figure 1.18: Schematic of Gurney flap concept by [2]

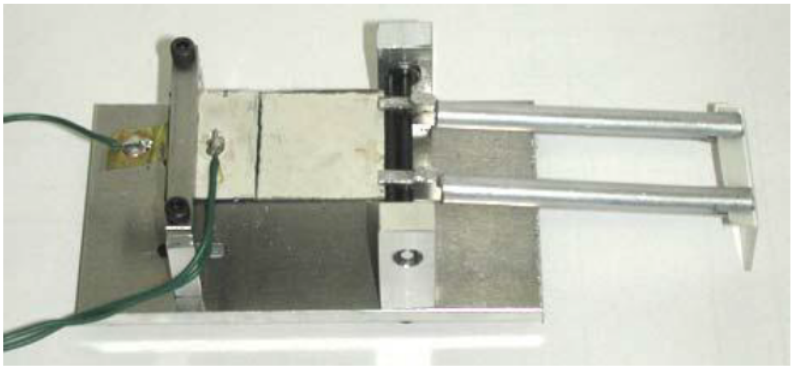

Figure 1.19: Fabricated active Gurney flap developed by [2]

This design was tested and proven to meet the required displacements and actuation frequencies. For the case studied, a deflection of 0.36 in was required based on a 0.02c-high Gurney flap located at 0.9c. The airfoil considered was the S903. The design achieved a maximum displacement of approximately 0.80 inches at the desired operating frequency of 18.5 Hz. This work showed that a Gurney flap could be actuated on the scale required in rotorcraft applications.
A different mechanism using a voice coil as actuator was conducted by [12], shown by Figs.1.20 and 1.21

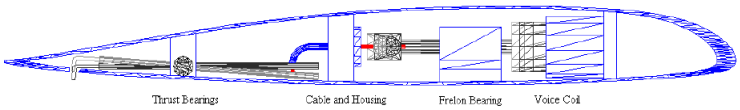

Figure 1.20: Initial design concept-profile. [12]

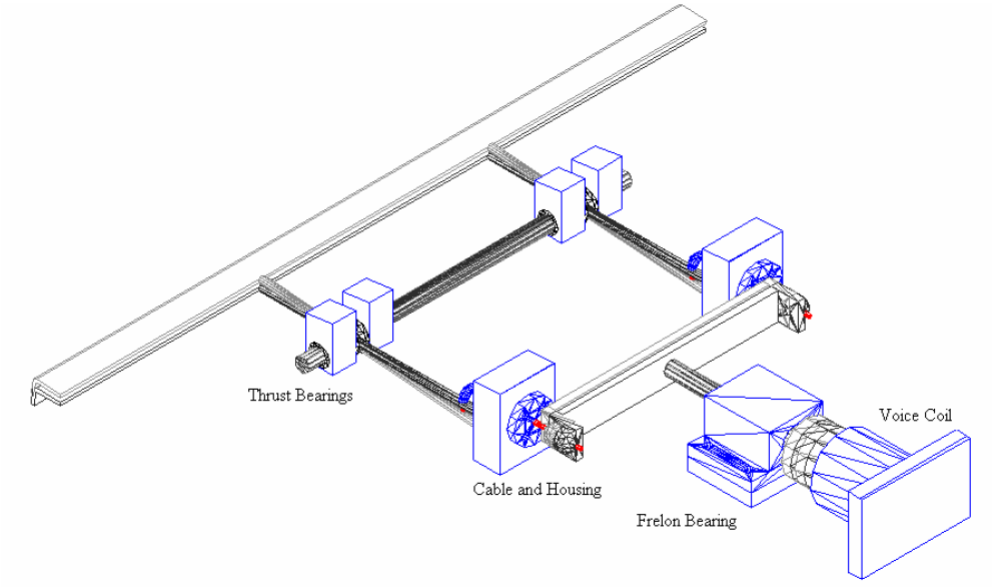

Figure 1.21: Initial design concept-perspective. [12]

The voice coil is placed as far forward in the cross-section as possible to locate the center of

gravity of the assembly close to the aerodynamic center (for aeroelastic stability).
The author developed a linear state-space model of the design to simulate the response of the flap/actuator system with the objective of predicting the the rotation and corresponding flap deflection given an arbitrary input signal. The fully deployed flap corresponded to a deflection of approximately 3.5 millimeters identical to an angle of 3 degrees. Fig.1.22 shows the actuator's simulated response to a sine wave input with a peak voltage of 5 and a frequency of 4 Hz.

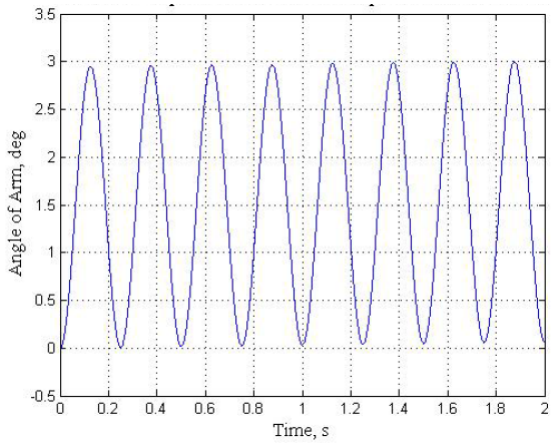

Figure 1.22: Simulated response of the actuator. [12]

Due to centrifugal loadings during the blade rotation which the mechanism was subjected [12] analysed the displacement and stress in arm/cable housing combination shown in Fig.1.21, the results presented in Fig.1.23 where the deflection is less than one millimeter and the stresses are bellow the yield strength of aluminum[1].

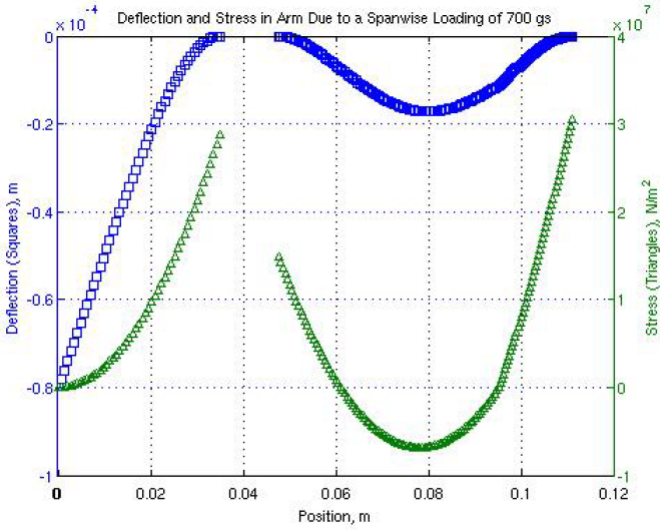

Figure 1.23: Results for CF loading of arm/housing combination. [12]

The fabricated initial concept is shown by Fig.1.24. Fig.1.25 shows a sample data set which includes the input signal used to drive the coil and the velocity, position, and angular deflection of the flap itself. The data revealed some non-linearities which made the initial design inconsistent

[1]The discontinuity represents the thrust bearing

mainly due the fraying and eventual failure of the cables, which would result in have to realign the arms and bracket.

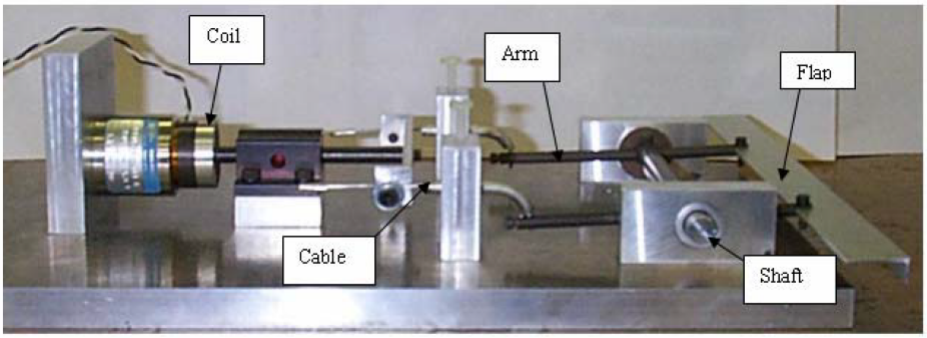

Figure 1.24: Side view of the fabricated, initial concept.[12]

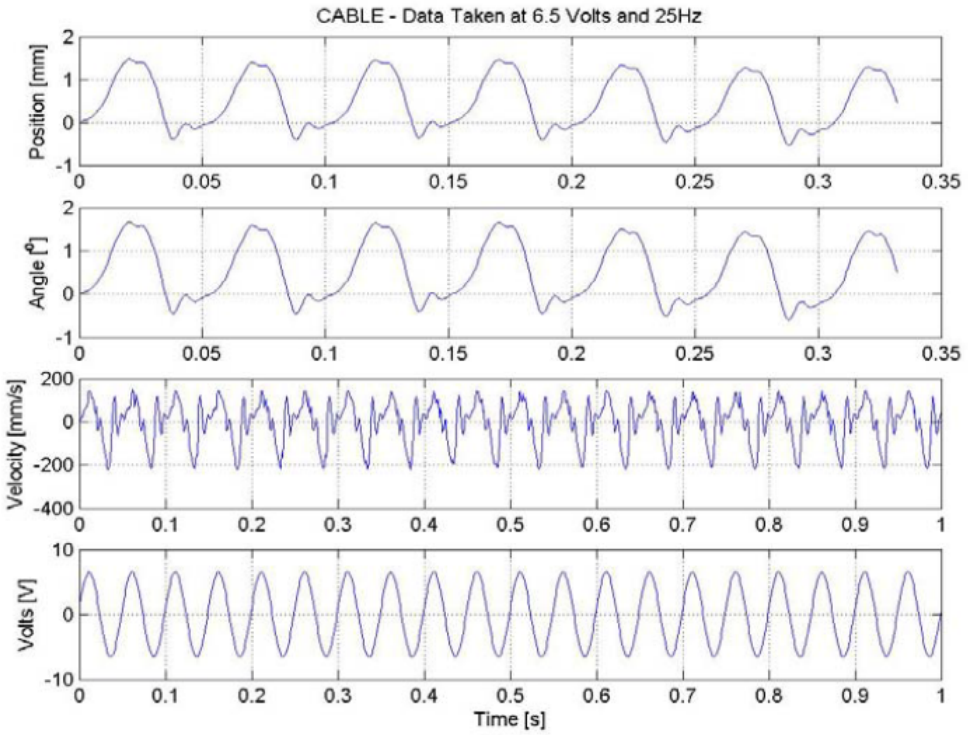

Figure 1.25: Sample data set from initial prototype. [12]

A second mechanism, Fig.1.26, was build replacing the cable and housing by a rigid link.

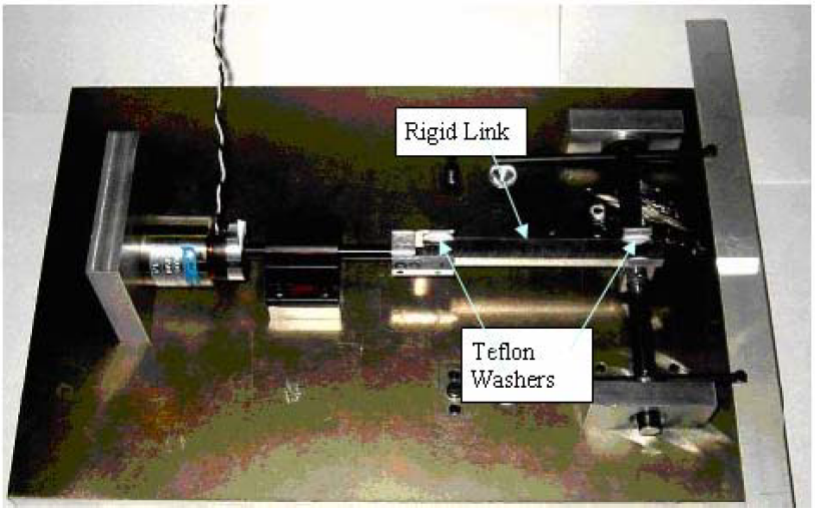

Figure 1.26: Fabricated second generation concept. [12]

Similar results from Fig.1.25 are presented in Fig.1.27. Although the results resembled to a linear system the operation as fairly inconsistent at lower frequencies/lower velocities due the initial friction created by Teflon bearings harder to overcome than at higher frequencies.

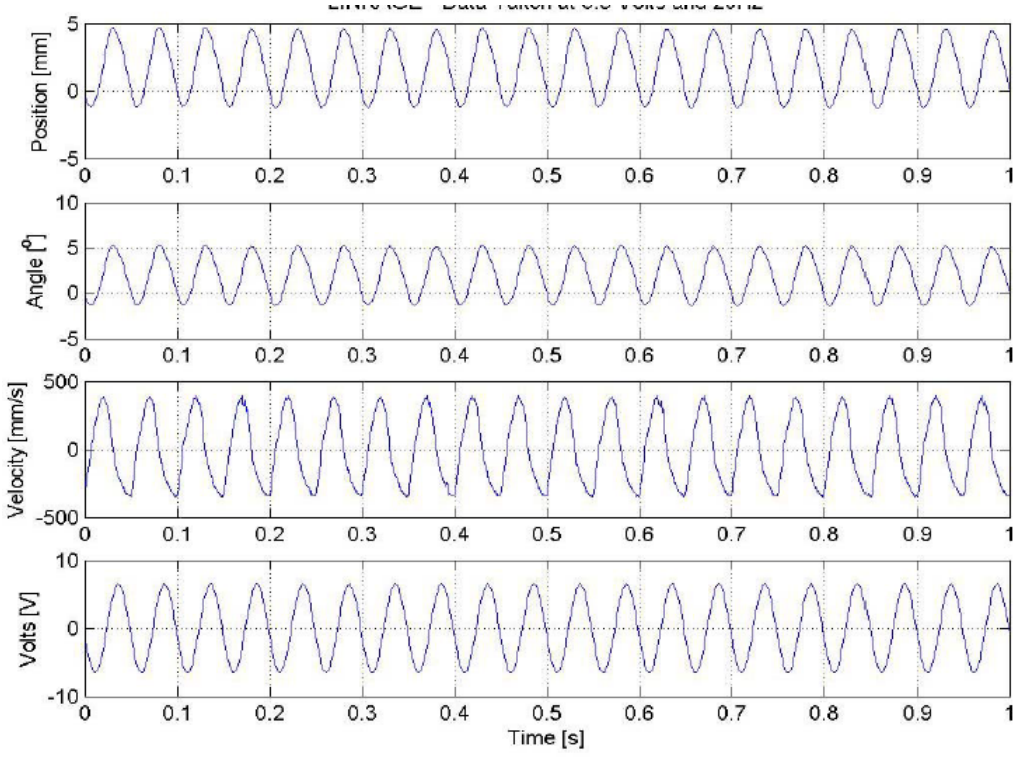

Figure 1.27: Sample data from the 2nd generation prototype. [12]

1.3 Structure of the work

This report is divided in 5 chapters.
In the first and present chapter, a small introduction about the Gurney Flap is referred as well

the main objectives of this project. Is also presented a review about previous works conducted by several authors mainly in the Aerodynamic point of view of the Flap.
In the second chapter is introduced a preliminary design of the study in question and the main requirements that have to be complied. It is mentioned important aspects, such as, the review of several actuators and some important parts of the mechanism that are not studied in the structural analysis.
In the third chapter the description of the numerical code is presented. It contains some important equations that characterize the motion of the mechanisms and also a small introduction to all structural analyses performed by Ansis software.
The chapter 4 is intended for the presentation of the final results. In this phase the results of the static, modal, kinematic and dynamics analyses are presented. Is also presented an optimization of the mechanism structure and the necessary technical features of the actuator in order to drive the system at 150 Hz.
In the fifth and final chapter the conclusion and some recommendations are discussed.

Chapter 2

Description of the Mechanism

2.1 Preliminary Design

The preliminary design of the mechanism was provided by the AST, shown by Fig.2.1, where the GF is attached to the support by a rotating axle. The Support is bonded to the spar and it has as identical curvature with the top and bottom skins, see Figs. 2.2 and 2.3.

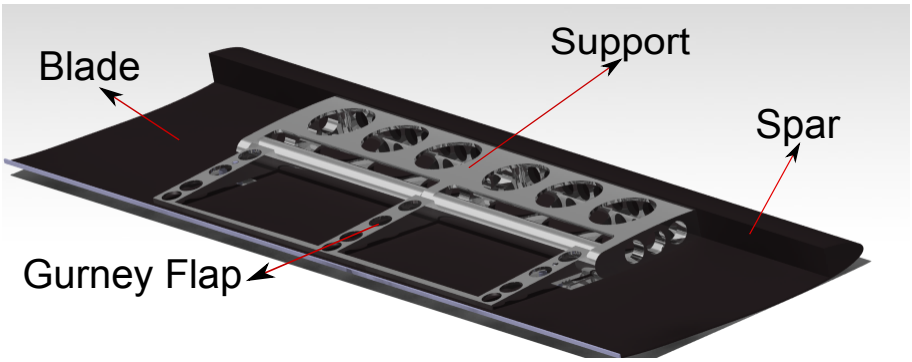

Figure 2.1: Preliminary Design Project

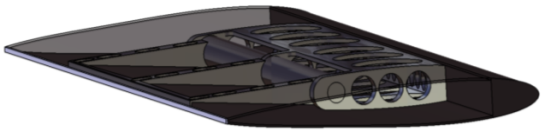

Figure 2.2: Preliminary Design Project Isometric View

Figure 2.3: Preliminary Design Project Side View

The actuation system can be inserted inside the support acting in the chord wise direction or under the GF acting in the flap wise direction.[1] In the following chapters the position of the actuators will have a thorough explanation.
The list of the requirements, mentioned in the chapter 1.1, for the conception of the mechanism are:

- The complete Gurney flap structure shall sustain the blade accelerations of $19.500 m/s^2$ span wise, $1500 m/s^2$ chord wise, $100 m/s^2$ flap wise and aerodynamic loads of $31 N/m$ chord wise and -4.03N/m flap wise (positive upwards).
- The maximum flap wise displacement of the Gurney flap structure due to the deformations imposed by the blade accelerations shall be less than 0.1mm.

[1] Hereafter the chord wise direction would be treated as X axis and Flap wise direction as Z Axis, being the same nomenclature used in Ansys. For the Matlab Code different nomenclature of the Axis is used which will be explained in the following chapters.

- The mass of the Gurney flap structure shall be maintained to a minimum.
- The minimum fully deployed AGF height shall be 1.1% of the chord length, with a preferred capability of reaching 1.5% of the chord length (chord length = 90mm).
- The chord wise location of the deployed AGF surface shall be at 95% of the chord length or more.
- The AGF shall be deployed with a vertical orientation from the blade's lower surface.
- The complete actuation cycle shall be performed at frequencies up to 60 Hz minimum, and 150 Hz would be an asset.

  The chosen material for the support and the Gurney Flap is Aluminium Alloy 6061 T-6 80 HF where some properties can be found in Appendix C and in [13].
  All the sensors inherent to the mechanism will not be taken into account for the structural analysis.
  The combined weight of the structure and the flap of this preliminary design is 0.0049 kg.

2.2 Review of the Actuators

2.2.1 Piezoelectric

Piezoelectric ceramic, or PZT (lead zirconic titanate), has the ability to convert mechanical energy to electrical energy through the piezoelectric effect. For actuators, the reverse piezoelectric effect converts electrical energy (voltage) into mechanical energy (strain). [14].

2.2.1.1 Piezo-stack

The Piezo-stack is shown in Fig.2.4. These actuators are very efficient and several types are available commercially. They can actuate at high Frequencies and can also generate high pull and push forces. On the other hand they are very heavy and sometimes they need an amplified motion system due to the fact that the stroke is in order of μm.

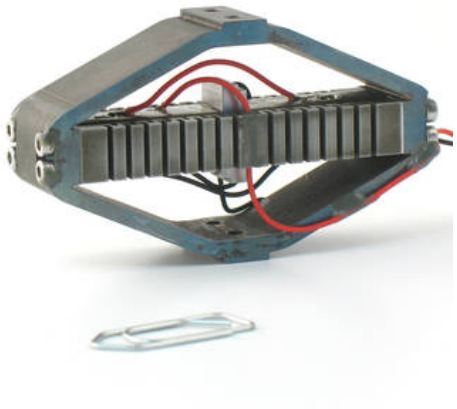

Figure 2.4: Piezo-Stack

2.2.1.2 Piezo-Linear

These actuators, Fig.2.5 are lighter than Piezo-Stack, they are able to operate at low Voltage, they can operate at high Frequencies and also they have a full stroke much higher than the piezo actuators mentioned above. A disadvantage is the fact that can not produce high pull and push forces.

Figure 2.5: Piezo-Linear

Several Piezo Actuators can be found in [15] and some properties are shown in D. The most promising actuators are APA 100M, APA 150M, APA 200M and FPA-0085E-S-0518, although their size is just too close from our physical limitations of available room and might require a slight adaptation on the blade structure or on the actuator itself.

2.2.2 Voice Coil

Voice Coil Actuators are the simplest type of electric motors. These motors consist of two separate parts; the magnetic housing and the coil, Fig.2.6

Figure 2.6: Voice Coil

They have the ability to operate at high frequencies with a large full stroke. They can provide necessary pull and push forces without an amplifying system but these forces are smaller when compared to the Piezo-Stacks. One big disadvantage is their size; the electric motors found in the market to fulfill the requirements of this project are too big for the available space.

2.2.3 Electromagnetic Actuators

An electromagnetic actuator is a special design of electromagnet that consists in a coil and a movable iron core called the armature. When current flows through a wire, a magnetic field is set up around the wire.

Figure 2.7: Electromagnetic Actuators

They can generate high force and large displacements at lower voltage. The size of these actuators is also a concern.

2.3 Rotating Axles

The rotating axles is the joint between the support and the GF, allowing the flap to rotate around the span wise axis[2], therefore, is important to choose an interface between these two pieces. This joint can be bearings, bushings or even flexible hinges.
For this study the flexible hinges, similar to Fig.2.8, were chosen.

Figure 2.8: Flexible Hinges

The choice of the flexible hinges is due to several reasons, for instance:

- They are frictionless, therefore, do not create a an additional friction force in the contact between the GF and the support;[3]
- Low hysteresis;
- Lubrication and maintenance are not required;
- Infinite cycle life ;
- They can operate at very low and high temperatures;

[2] Y axis in Ansys nomenclature
[3] An important feature allowing the actuator to operate with lower pull and push forces

- Very easy installation;

They also have some disadvantage such as:

- Only operate with low angles of rotation, less than 10°;[4];
- Structural issues and potential buckling effects;
- Complex manufacturing;

More information about the characteristics and dimensions can be found in [16]. During the structural analysis the pivots are neglected.

[4] In the project the rotation angle of the flap is between 1° and 2°

Chapter 3

Description of the Numerical Simulation

3.1 Static Analisys

The basis of the finite element method is the representation of a body or a structure by an assemblage of subdivisions called finite elements. The Finite Element Method translates partial differential equation problems into a set of linear algebraic equations

$$[K]\{u\} = \{F\} \tag{3.1}$$

where K is the stiffness matrix, u nodal displacement vector and F nodal vector force.
The objective of the static analysis is to calculate the deformation and stress of the Gurney flap without considering the inertial forces inherent to the rotation of the GF and the Support using Ansys Software. The inertial forces due the blade accelerations mentioned in Chapt.2.1 are taken into account.

3.2 Kinematic Analysis

The kinematics of the mechanisms were modelled in a small routine using the software Matlab. Figs.3.1 and 3.2 illustrate the mechanisms in 2 dimensions.[1] It is important to state that the Y axis in Matlab corresponds to the Z axis in Ansys, or, as mentioned before, the flap wise direction and the X axis, or chord wise direction, is the same in both nomenclatures. The span wise direction corresponds to Y axis in Ansys and it is neglected in Matlab for the reasons mentioned above.

The study of the kinematics was separated in three points, Fig.3.1. The Point 1 corresponds to kinematics of the actuator, ——; the Point 2 corresponds to kinematics in the link between the arm of the Flap, represented by the ——, and the Gurney Flap, ——, and the Point 3 is the bottom of the Gurney Flap.
This kinematic study is afterwards compared with kinematic simulations done by Ansys software which equations are not shown in the present chapter.

[1] The third dimension for this particularly study was neglected, thus, the centrifugal forces are not taken into account

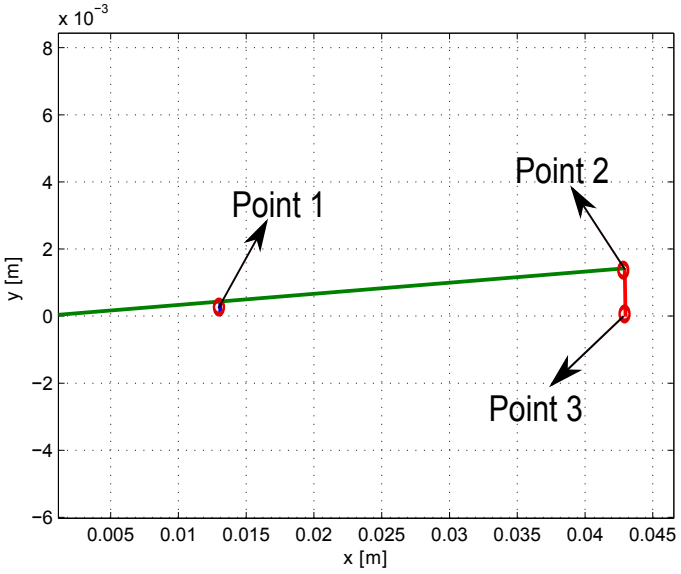

Figure 3.1: Mechanism 1 Modulated in Matlab

The only difference between Mechanism 1, from Fig.3.1, and Mechanism 2, Fig.3.2 is the position and the direction in which the actuator is working, thus, the kinematics in Point 1 is different for both mechanisms but for the rest of the points the equations remain the same. In chapter 2.1 the direction of the actuators was mentioned. For the Mechanism 1 the system is actuated in the Y direction and in the Mechanism 2 the system is actuated in X direction. These two different directions in which the system is actuated it is important for the calculation of the kinematics and the dynamics of the actuator.

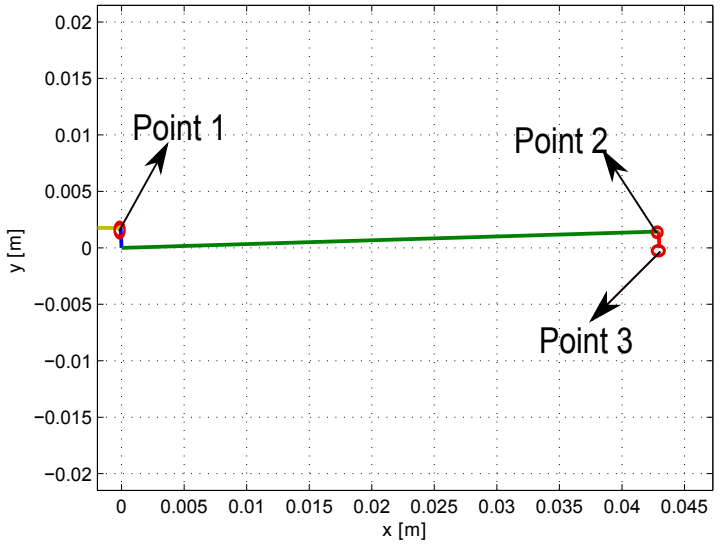

Figure 3.2: Mechanism 2 Modulated in Matlab

In order to have smooth displacement of the Gurney Flap a sinusoidal function of the actuator's velocity was modelled to serve as an input in the numerical code. In Fig.3.3 it is possible to see an example of the velocity function also represented by Eq. 3.6.

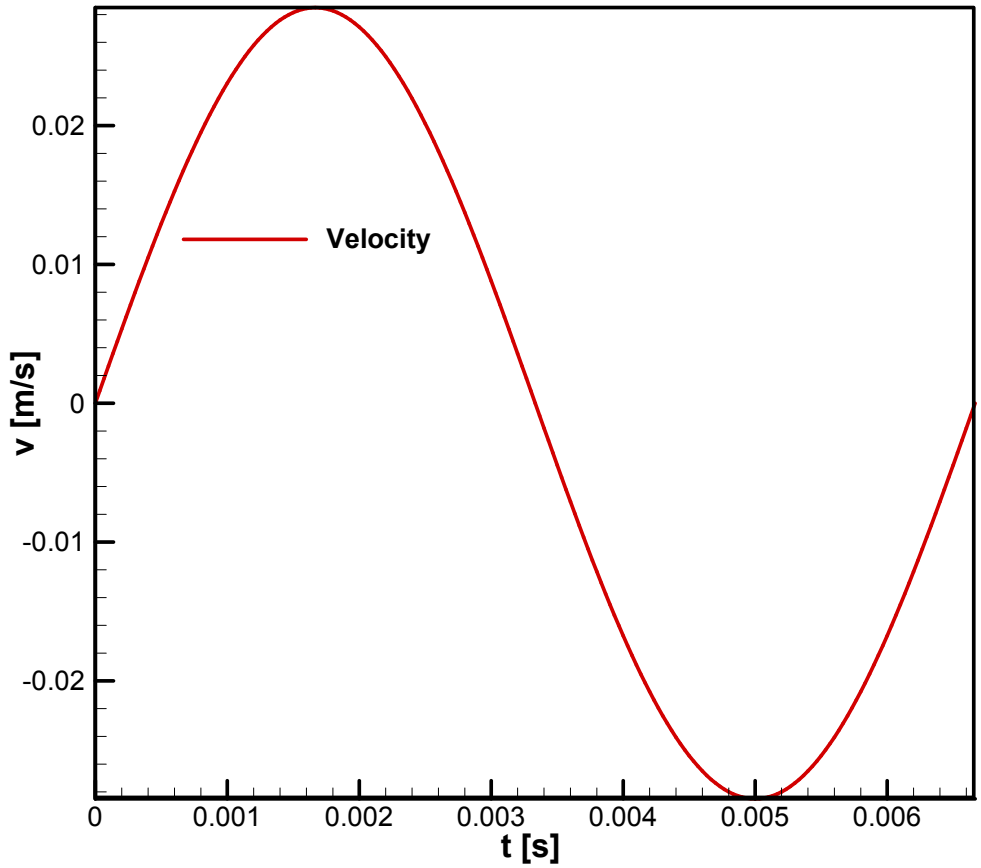

Figure 3.3: Velocity of the actuator model

Eq.3.2 represents the frequency chosen to be 150 Hz in this project, thus, the period is 0.0067 seconds.

$$f = \frac{1}{T} \tag{3.2}$$

A schematic of the mechanism is shown by fig.3.5 where the displacement and velocity vectors are represented for each point. The calculation of this parameters are represented in the following equations.

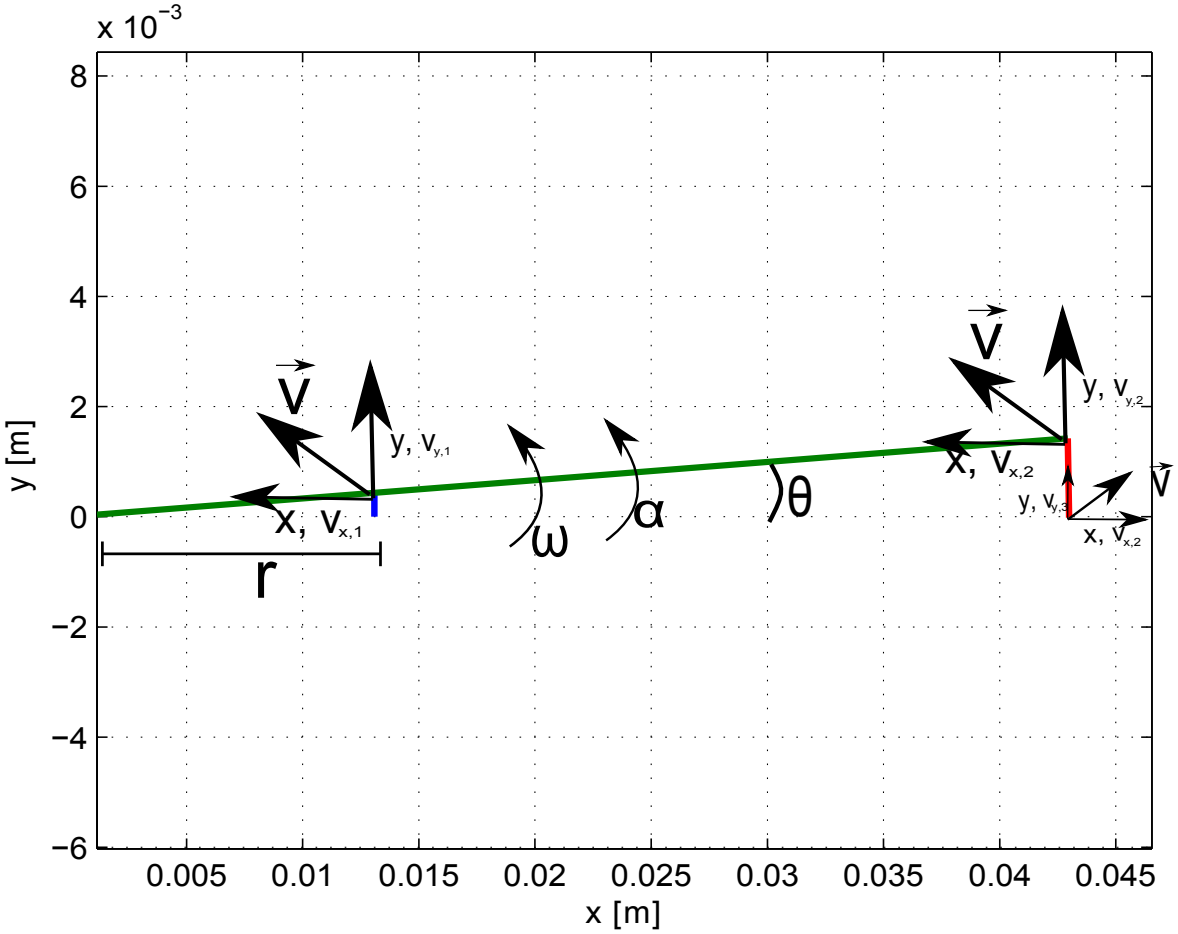

Figure 3.4: Schematic of the mechanism with kinematic parameters

Mechanism 2

Point 1

Eqs.3.3 to 3.9 represent the displacement, velocity and acceleration of Point 1 in X and Y direction. The displacement is obtained by simple trigonometric equations, the velocity is dependent on the actuator's velocity and the acceleration is obtained by derivation of the velocity. The procedure it is an iterative method, where the time is discrete and not continuous. The angle θ is obtained by integrating the angular velocity represented by Eq.3.10.

$$y_1 = r \times cos(\theta) \tag{3.3}$$

$$x_1 = r \times -sin(\theta) \tag{3.4}$$

$$\vec{v_1} = v_{x,1} \times cos(\theta) \tag{3.5}$$

$$v_{x,1} = v_{act} \times sin\left(\frac{2\pi}{T}t\right) \tag{3.6}$$

$$v_{y,1} = \vec{v_1} \times sin(\theta) \tag{3.7}$$

$$a_{y,1} = \frac{dv_{y,1}}{dt} \tag{3.8}$$

$$a_{x,1} = \frac{dv_{y,1}}{dt} \tag{3.9}$$

Angular Velocity and Acceleration

The Eq. 3.10 and 3.11 are respectively the angular velocity and the angular acceleration. As it is possible to see the the angular velocity is dependent of the actuator's velocity.

$$\omega = \vec{v_1} \times r \tag{3.10}$$

$$\alpha = \frac{d\omega}{dt} \tag{3.11}$$

where r represents the distance from the actuator to the rotating axle.

Point 2

The next equations represent the kinematics of Point 2 following the same procedure explained in chapter 3.2.

$$y_2 = cos\left(\frac{\pi}{2} - \theta\right) \times b \tag{3.12}$$

$$x_2 = cos(\theta) \times b \tag{3.13}$$

$$\vec{v_2} = \omega \times b \tag{3.14}$$

$$v_{y,2} = \vec{v_2} \times cos(\theta) \tag{3.15}$$

$$v_{x,2} = \vec{v_2} \times sin(\theta) \tag{3.16}$$

$$a_{y,2} = \frac{dv_{y,2}}{dt} \tag{3.17}$$

$$a_{x,2} = \frac{dv_{x,2}}{dt} \tag{3.18}$$

Point 3

The kinematics in Point 3 are represented by the next equations:

$$y_3 = -cos(\theta) \times Flap + cos\left(\frac{\pi}{2} - \theta\right) \times b \tag{3.19}$$

$$x_3 = sin(\theta) \times Flap + cos(\theta) \times b \tag{3.20}$$

$$v_{y,3} = v_{y,2} + Flap \times \omega \tag{3.21}$$

$$v_{x,3} = v_{x,2} + Flap \times \omega \tag{3.22}$$

$$a_{y,3} = \frac{dv_{y,3}}{dt} \tag{3.23}$$

$$a_{x,3} = \frac{dv_{x,3}}{dt} \tag{3.24}$$

Mechanism 1

In the beginning of this sub chapter it was referred that the only difference between Mechanism 1 and Mechanism 2 is the kinematics of Point 1, therefore, the following equations represent the kinematics in that point for this mechanism. The kinematic of the other points remains the same, as explained above.

Point 1

$$y_1 = r \times sin(\theta) \tag{3.25}$$

$$x_1 = 0 \tag{3.26}$$

$$\vec{v_1} = v_{y,1} \times cos(\theta) \tag{3.27}$$

$$v_{y,1} = v_{act} \times sin\left(\frac{2\pi}{T}t\right) \tag{3.28}$$

$$v_{x,1} = 0 \tag{3.29}$$

$$a_{y,1} = \frac{dv_{y,1}}{dt} \tag{3.30}$$

$$a_{x,1} = \frac{dv_{y,1}}{dt} \tag{3.31}$$

3.3 Dynamic Analysis

After the kinematic analysis,it is important to make a dynamic study of the mechanisms in order to calculate the stress and deformation of the structure, using Ansys. The calculation of the necessary force which the actuator has to provide to the system are modulated by basic dynamic equations are using the Matlab numerical code.

3.3.1 Dynamic Modelled by Ansys

The way that the dynamic or transient analysis is modulated by Ansys software is shown by Eq.3.32.

$$[M^e]\{\ddot{u}\} + [C^e]\{\dot{u}\} + [K^e]\{u\} = \{Q^e\} \tag{3.32}$$

Being $[M^e], [C^e]$ e $[K^e]$ respectively the matrices of mass, damping and stiffness.

Fig.3.5 represents the angular velocity chosen as input of the system in the transient analysis. One of the requirements in chapter 2.1 is the aerodynamic force which the flap is subjected to The aerodynamic force in the X direction is represented in the Fig.3.6 following a sinusoidal function due to fact that when the Flap is completely retracted the aerodynamic force is null. The Aerodynamic force in the flap wise direction[2] is considered to be -4.03N/m constant in time.

[2] Z direction in Ansys and Y direction in Matlab

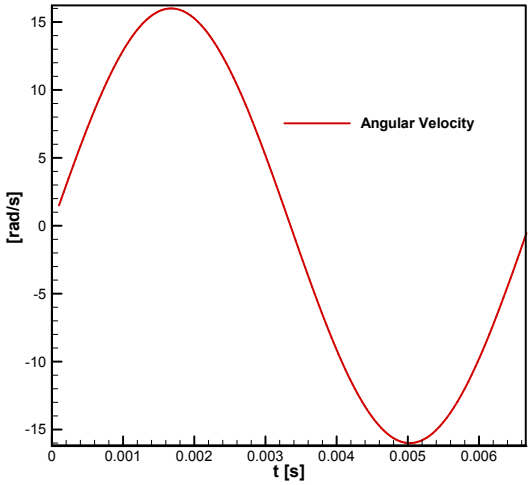

Figure 3.5: Angular Velocity Model

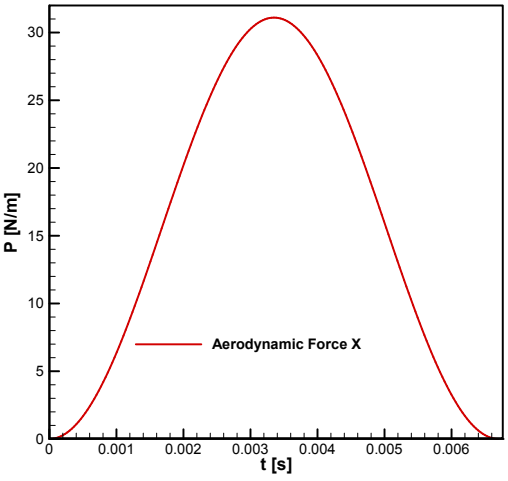

Figure 3.6: Aerodynamic Force model

3.3.2 Dynamics modelled with Matlab

The following equations represent the modelling of the necessary forces that the actuator needs to provide to produce the rotation of the GF. Only two dimensions are considered because the centrifugal forces are neglected. The mass of the flap supporting structure is neglected in the Matlab study.

Forces

Eq.3.33 represents the inertial force induced by the blade accelerations in the Y axis, mentioned in chapter 2.1.

$$F_{ext,y} = a_{ext,y} \int m \tag{3.33}$$

Similar to the above equation, the following expression represents the inertial force resulting from a blade acceleration of -1500 m/s^2

$$F_{ext,x} = a_{ext,x} \int m \tag{3.34}$$

The next equation represents the sum of the inertial forces from Eq.3.33 and the inertial force due the rotation of the Gurney Flap.

$$F_{I,y} = F_{ext,y} + \alpha \int m \times x \tag{3.35}$$

Eq.3.36 is similar to the above equation but in the X direction.

$$F_{I,x} = F_{ext,x} + \alpha \int m \times y \tag{3.36}$$

The next equation represents the weight of the gurney flap.

$$P = g \int m \tag{3.37}$$

Moments

The moment due the weight is shown in the equation.

$$M_P = g \int m \times x \tag{3.38}$$

The Eq.3.39 and 3.40 are the moments due to the inertial forces created by the blade accelerations.

$$M_{ext,y} = a_{ext,y} \int mx \tag{3.39}$$

$$M_{ext,x} = a_{ext,x} \int my \tag{3.40}$$

Eq.3.41 represents the sum of the moments of the inertial forces.

$$M_I = M_{ext,y} + M_{ext,x} + \alpha \times I_{zz} \tag{3.41}$$

Solving the system of equations from Eq3.42 with he sum of all forces and moments it is possible to calculate the force of the actuator, F_{actua} and the reaction forces in the support, $F_{y,support}$ and $F_{x,support}$.

$$\begin{cases} F_{y,support} + F_{a,y} + P = F_{I,y} \\ F_{x,support} + F_{a,x} + F_{actua} = F_{I,x} \\ F_{a,y} \times b + F_{a,x} \times Flap + F_{actua} \times r - M_P = M_I \end{cases} \tag{3.42}$$

3.4 Modal Analysis

For the modal analysis cases, damping does not exist therefore the dynamic equation, Eq. 3.32, can be reduced to:

$$[M^e]\{\ddot{u}\} + [K^e]\{u\} = \{Q^e\} \tag{3.43}$$

The equation of motion can be given by:

$$\left[-\omega^2[M^e] + [K^e]\right]\chi e^{i\omega t} = 0 \tag{3.44}$$

$$\left[-\omega^2[M^e] + [K^e]\right]\chi = 0 \tag{3.45}$$

As $\omega^2 = \lambda$:

$$[[K^e] - [M^e]]\,\chi = 0 \tag{3.46}$$

$$\lambda = -\omega^2 \tag{3.47}$$

From the equation above λ represents the eigenvalues, ω the natural frequencies, χ corresponds to an eigenvector that defines the modes of vibration of the system.
Using Ansys software it is possible to compute the natural frequencies of the flap.

Chapter 4

Results and Discussion

4.1 Static Analysis

4.1.1 Mesh Discretization

The elements chosen for meshing the flap are tetrahedral solid elements shown by Fig.4.1. The choice of these elements is due to the complex geometry.

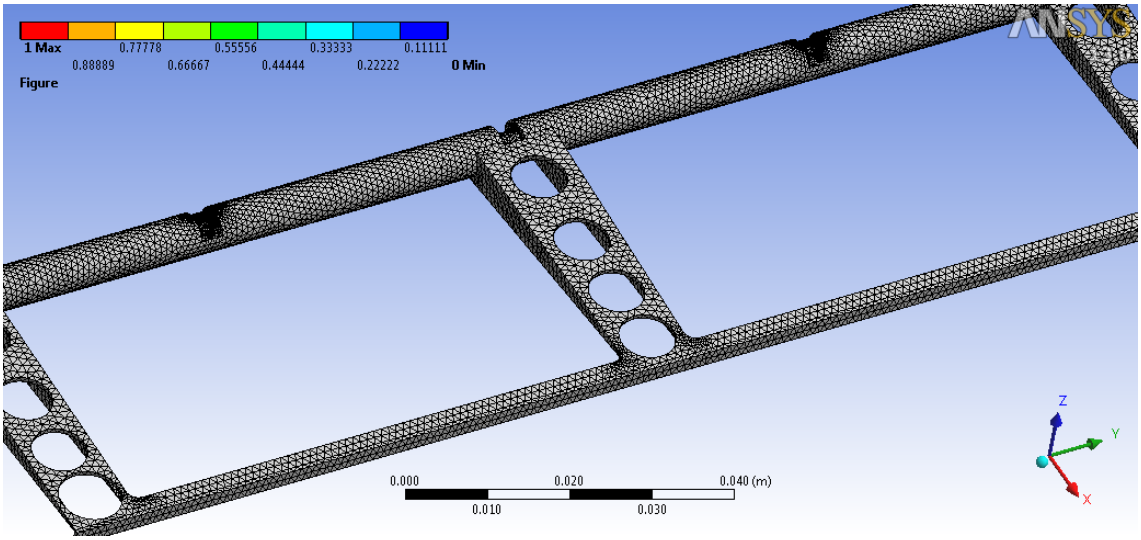

Figure 4.1: Static Analysis Mesh

Fig.4.2 represent the mesh quality from the structural analysis represented by the Number of elements vs quality coefficient, being 0 considered bad quality and 1 good quality. As is possible to visualize in the Fig.4.2 most of the elements are in the good quality region, therefore, the mesh is considered to be good.

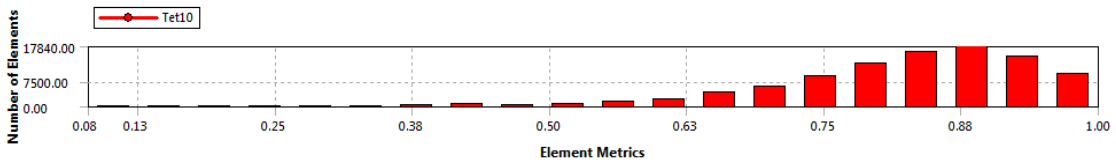

Figure 4.2: Static Analysis Mesh Quality

The next figure represents the mesh convergence in function of the maximum stress vs number of elements. After 90000 elements the solution starts to converge.

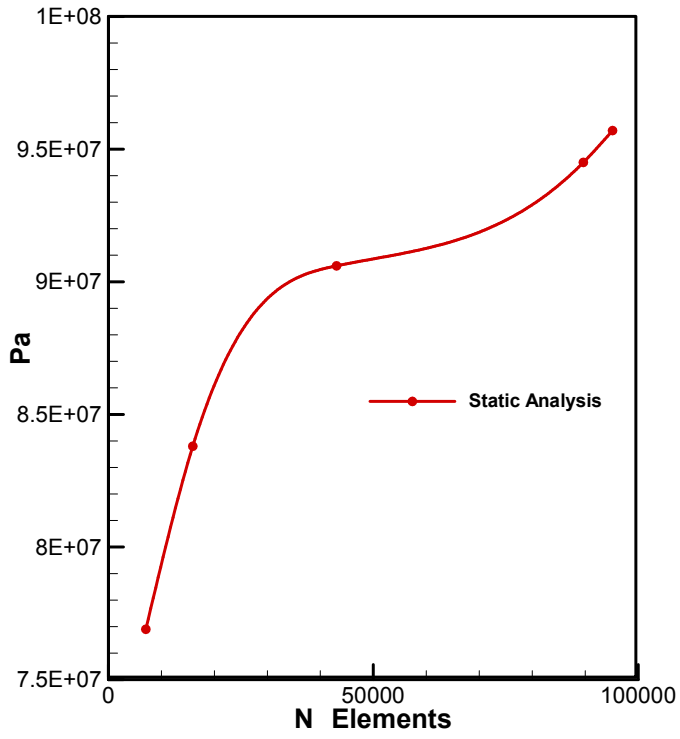

Figure 4.3: Static Analysis Mesh Convergence

4.1.2 Parametric Study Optimization

In order to reduce the mass a parametric study of the radius size, presented in Fig.4.4, was conducted. In Chapter E it is possible to see from table E.1 the parametric study, regarding different radius dimensions, calculating the maximum stress, the maximum directional deformation[1] and the mass.

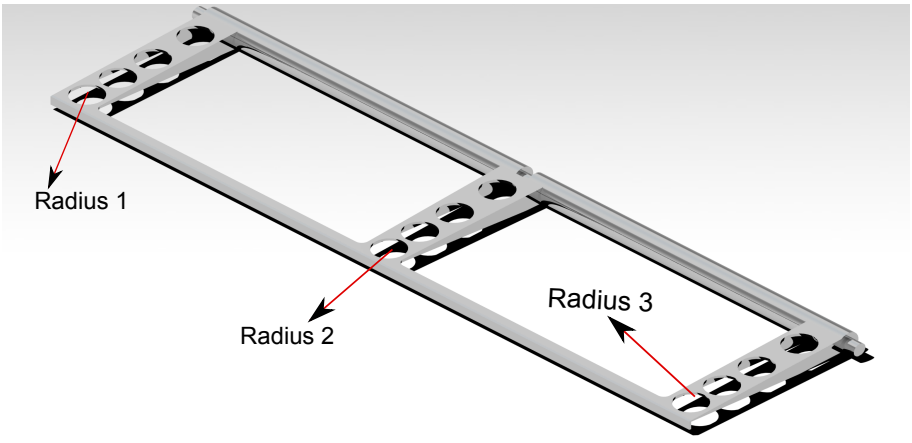

Figure 4.4: Gurney Flap Optimization

Figure 4.5 represent the Maximum Directional Deformation vs Radius 2 vs Radius 3 where is possible to view that increasing the radius of these two parameters the maximum deformation is higher than 0.1 mm. From Fig.4.5 is also possible to conclude that increasing the radius of this

[1] In Chapter2.1 it is refereed that the maximum deformation it has to be less than 0.1 mm

two parameters the mass reduces.

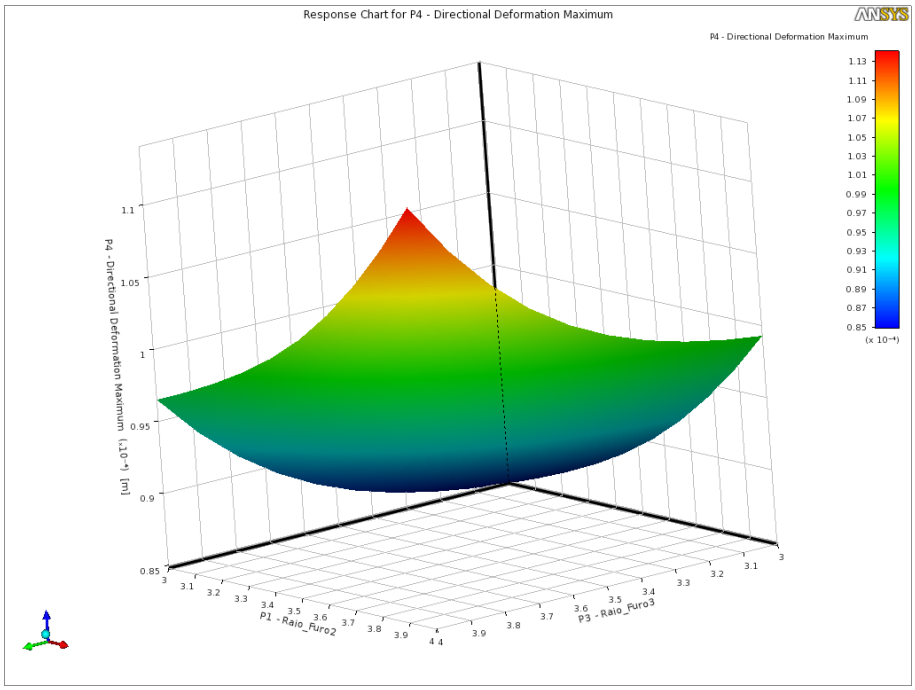

Figure 4.5: Maximum Directional Deformation

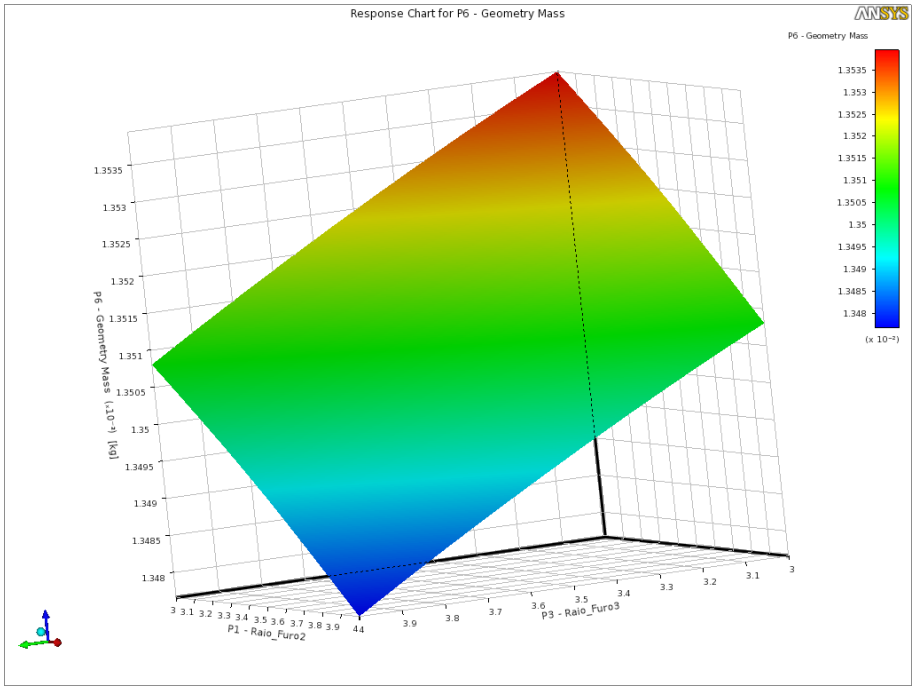

Figure 4.6: Geometry Mass

Fig.4.7 represent the maximum stress, it is noticeable that the radius 2 is more sensible two higher stress, also shown by Fig.4.8 representing the local sensitivity of each parameter in the three calculated properties mentioned before. From the figure 4.8 it is also obvious that radius 2 is more sensible to higher deformations and stress, followed by radius 3.

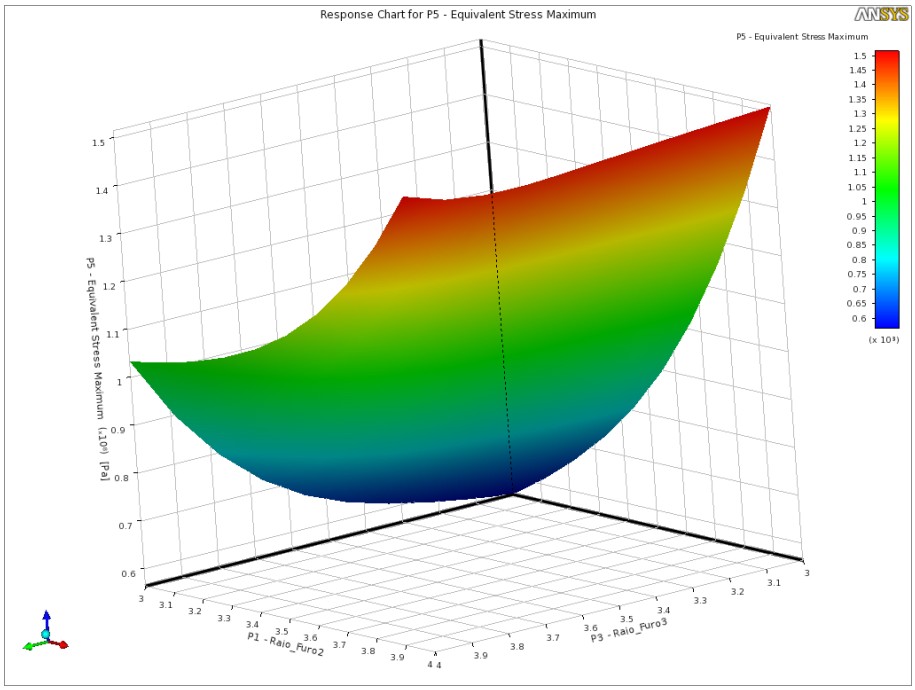

Figure 4.7: Maximum Stress

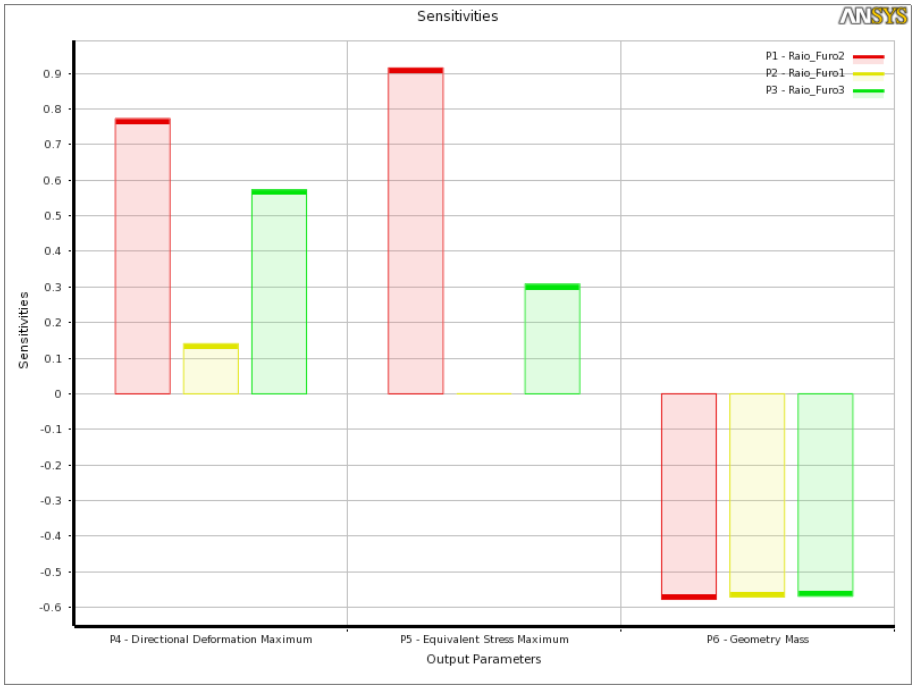

Figure 4.8: Local Sensitivity

Having these results it was important to find the best values in order to reduce the mass, maintain the maximum deformation bellow 0.1 mm and reduce the maximum stress. With the aid of Optimization module of Ansys software it was possible to find a suitable candidate resulting in $Radius1 = 3.9775mm$, $Radius2 = 3.546398438mm$ and $Radius3 = 3.7801067mm$.

4.1.3 Deformation

Fig.4.9 represents the total deformation or the module of the directional deformations. In the figure the shaded region represents the Gurney Flap without any load, it is noticeable a large deformation due to the centrifugal force[2]. The Flap is subjected to torsion around the Z axis.

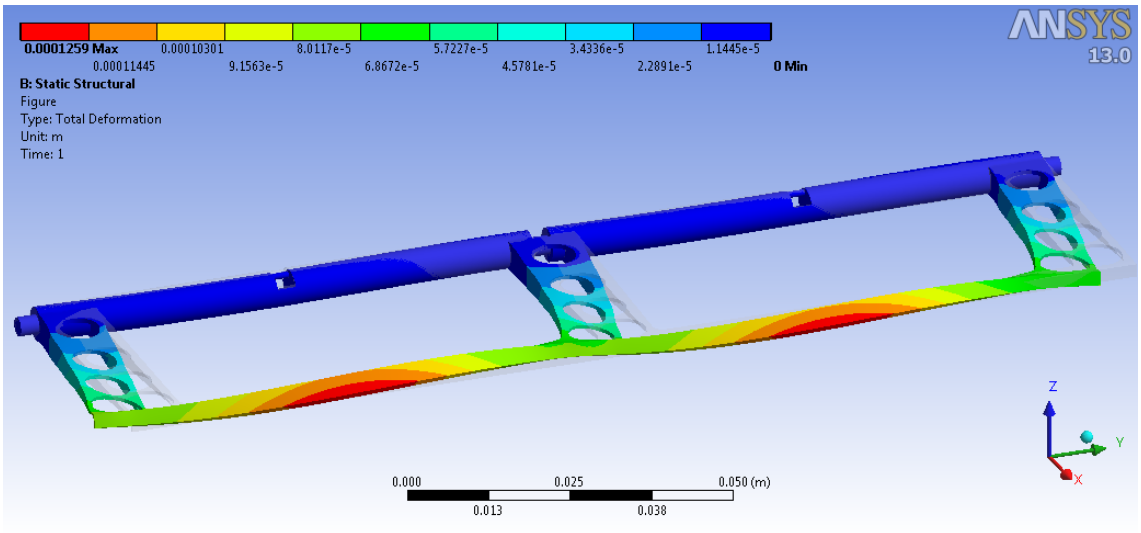

Figure 4.9: Total Deformation

Figure4.10 represents the Deformation in the X direction, being the maximum deformation represented by the red color in Gurney region. This maximum deformation is 9.7785e-005 m, remaining bellow 0.1 mm.

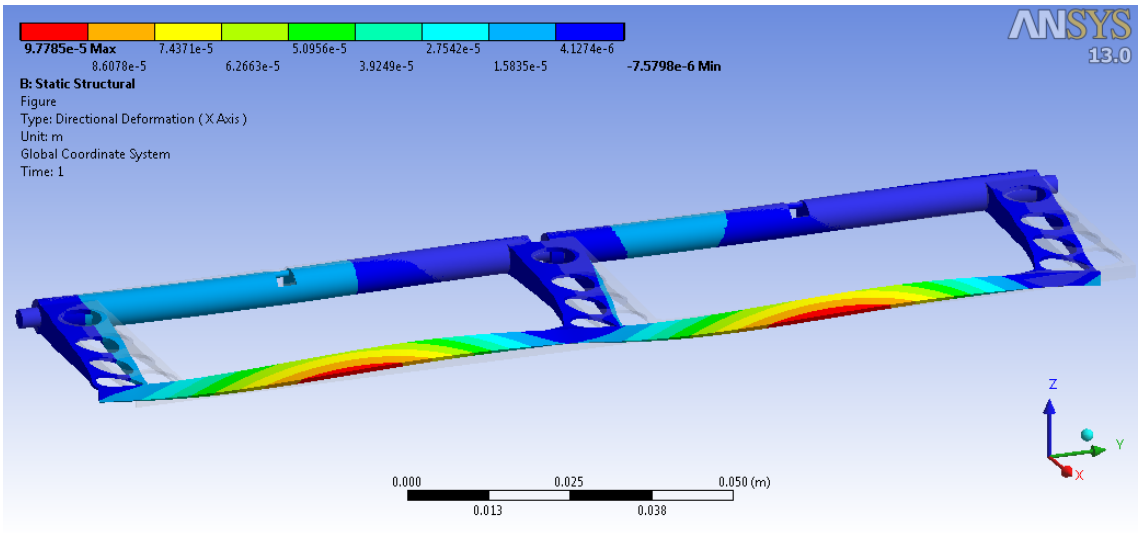

Figure 4.10: Deformation X Axis

The Deformation in Y direction is represented by Fig.4.11 being the maximum deformation of -7.1271e-005 m, represented by the blue color.

[2]Force due to the centrifugal acceleration of $19500 m/s^2$ positive in Y direction, caused by the rotation of the blade

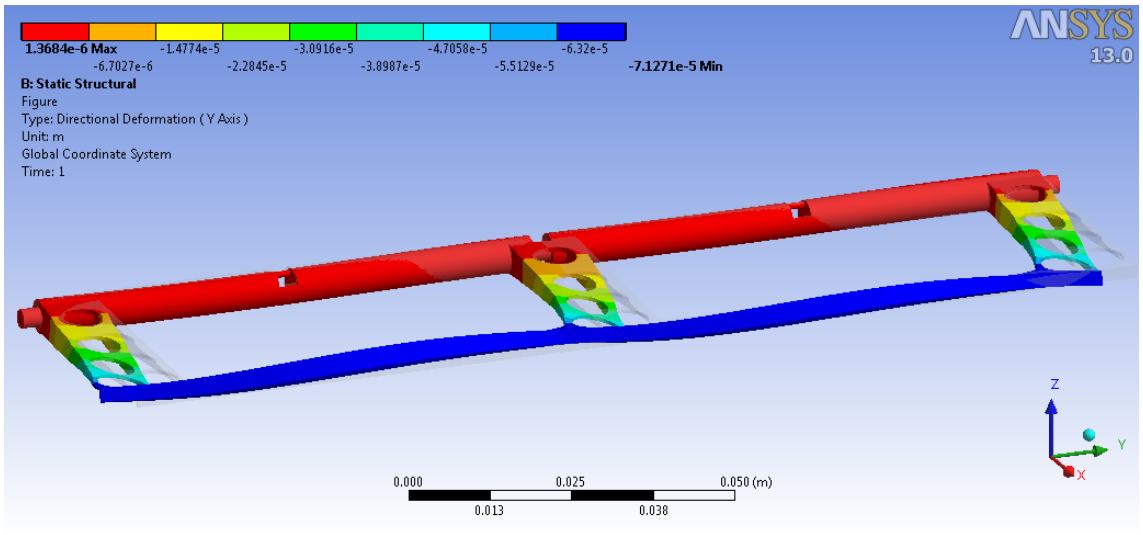

Figure 4.11: Deformation Y Axis

The next figure represents the deformation in Z axis, where the maximum deformation is 5.2297e-005 m represented by the red color. Is also visible a small torsion in the trapezoidal arms of the flap.

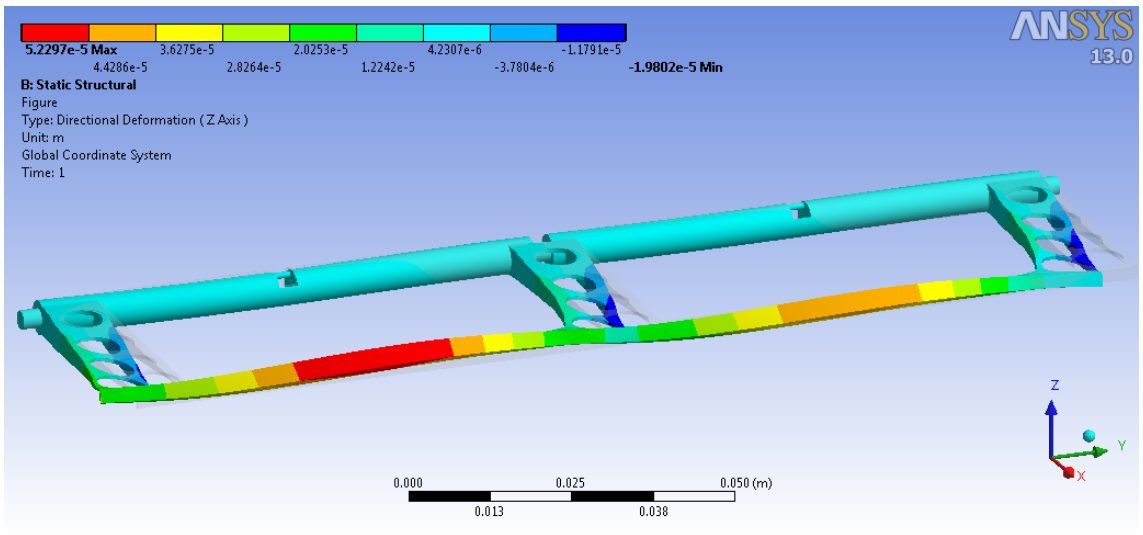

Figure 4.12: Deformation Z Axis

4.1.4 Stress

Fig.4.13 represents the Von Mises Stress of the Flap. The location of the maximum stress is in radius 2, how was mentioned before, this region is more sensible to higher stress. The maximum equivalent stress is 9.1279e+007 Pa.

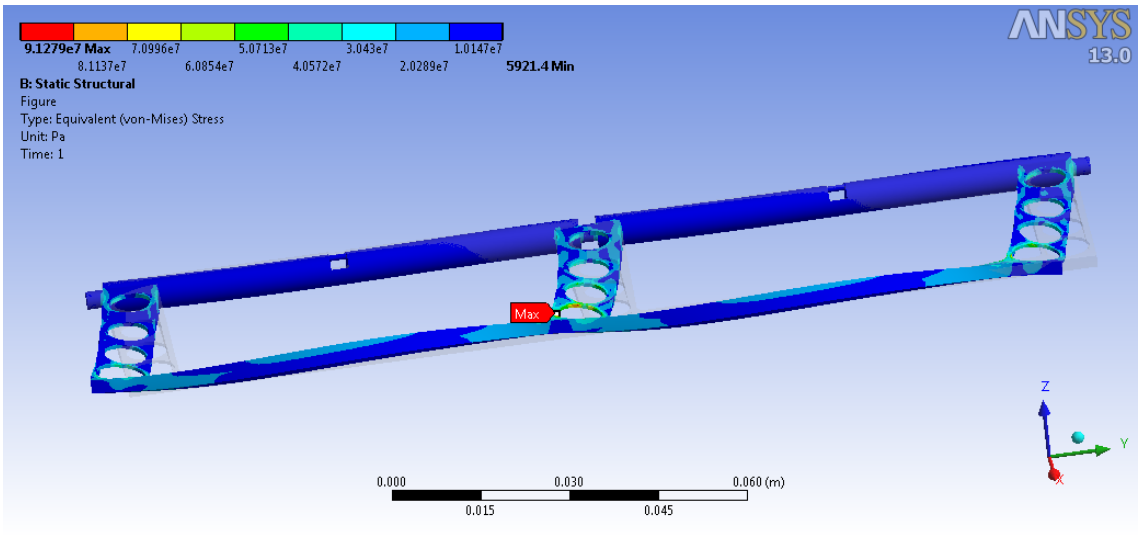

Figure 4.13: Stress Von Mises

Figure 4.14: Stress Von Mises

The next figure represents the Safety Factor, around 3.2866 in the region where the stress is higher. This safety factor is considerably big; the normal safety factor for projects similar to this is around 1.5.

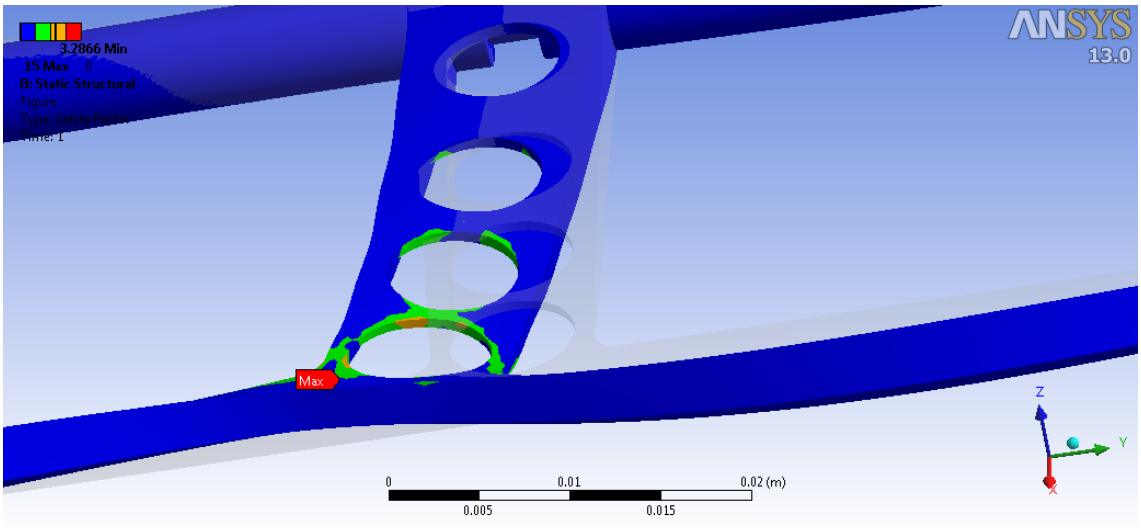

Figure 4.15: Safety Factor

4.2 Kinematic Analysis

In this sub-chapter the kinematic results of both mechanisms are presented. The comparison between the Matlab code and the Ansys rigid body module is conducted in order to validate both results. The equations used in the Ansys module are unknown but is important to refer that several joints[3] were chosen in order to module the kinematics of the mechanism to have one degree

[3]This joints can be found in [17]

of freedom which the Gurney Flap is subjected.[4]
Since this is a rigid body analysis the stress and deformation are not taken into account[5] as also the blade accelerations are neglected for both numerical analysis.

4.2.1 Kinematics Matlab

In chapter 3.2 the equations of kinematics in three points are described for both mechanisms. The solution of as displacement, velocity and acceleration are here described.

4.2.1.1 Mechanism 1

Fig.4.19 represents the displacement, velocity and acceleration of Point 1, corresponding to the actuator as mentioned before. The first graphic corresponds to the actuator displacement in Y direction being 4.60e-004 m. The X displacement is zero due to fact of the direction of which the actuator is driven already mentioned before. The velocity in the Y direction is 0.216816 m/s and the homologous acceleration is around $256 m/s^2$. These are important results for the choice of a suitable mechanism.

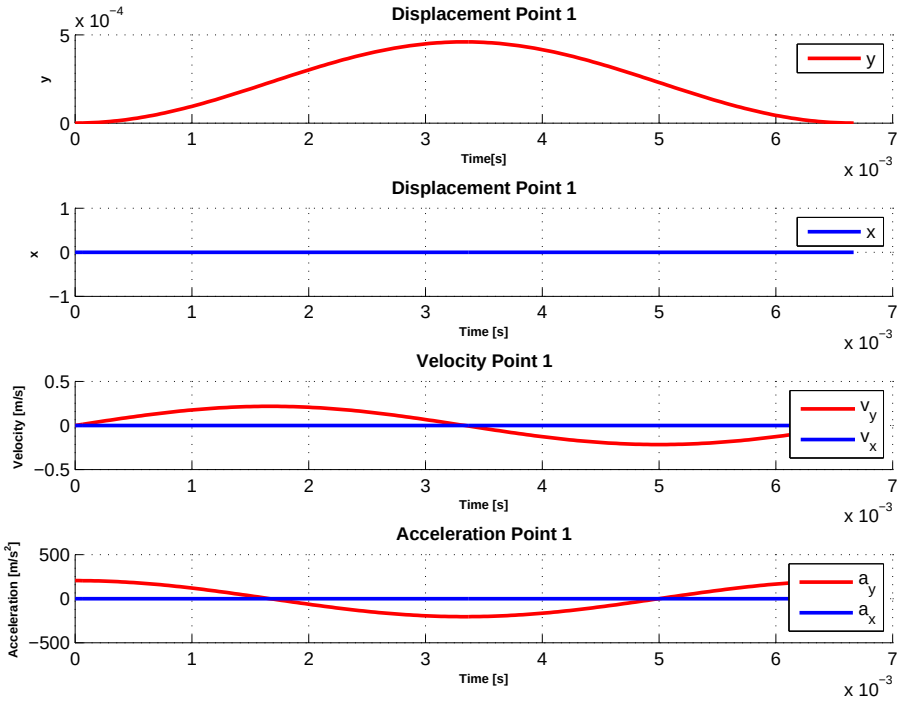

Figure 4.16: Kinematics Point 1

Similar results from above are shown by Fig.4.21 for Point 2. There is big change in Y displacement but the same does not occur in X displacement. It is also remarkable the value of the a_y increase to around $850 m/s^2$ due to big angular accelerations which the is subjected.

[4]Rotation along the Y Axis.
[5]Therefore no mesh is needed.

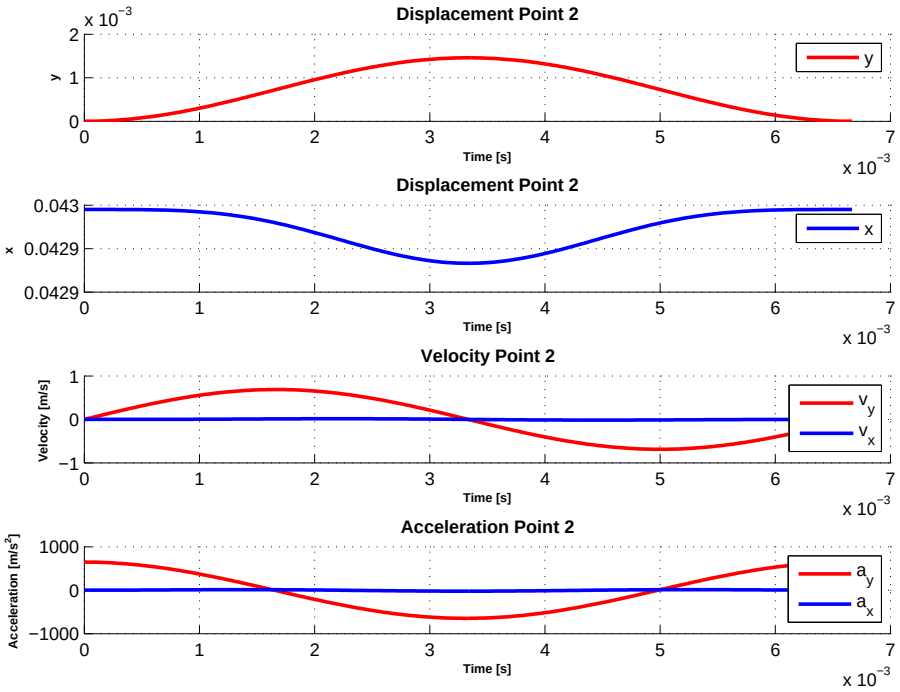

Figure 4.17: Kinematics Point 2

The kinematics of Point 3 is presented in Fig.4.18. In the $t = 0s$ the flap is fully deployed, retracting for $T/2$ and being again deployed showing a periodic shape.

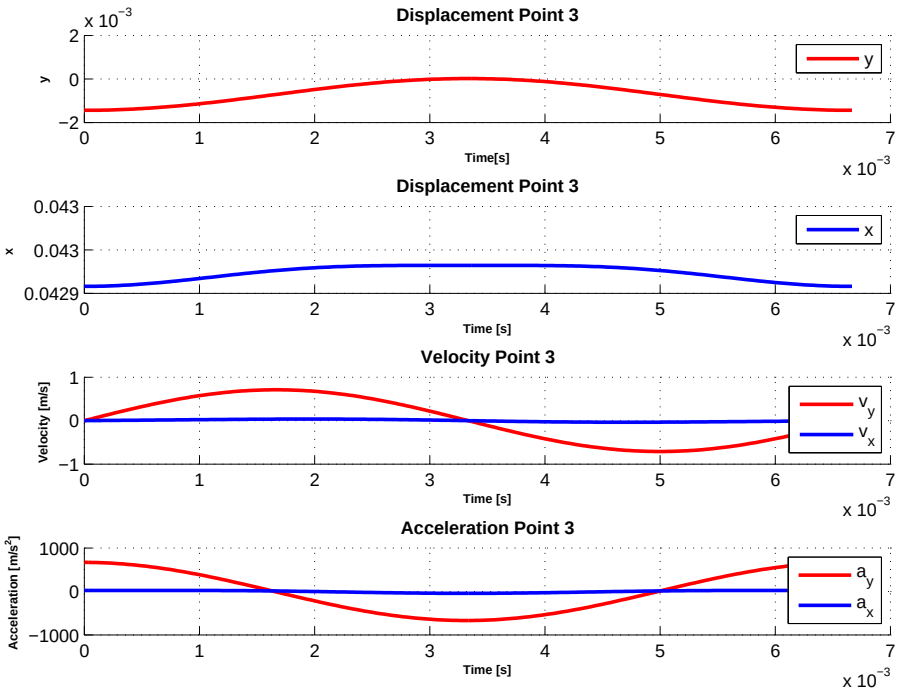

Figure 4.18: Kinematics Point 3

4.2.1.2 Mechanism 2

The same methodology stated above is now explained for mechanism 2. As mentioned in 3.2 the only difference between mechanism 1 and mechanism 2 is the position and the direction in which the mechanism is driven, therefore, only the equations in Point 1 are different.
Similar to mechanism 1, in the beginning the flap is fully deployed and since the system is actuated in X direction it is possible to see a displacement of -6.04669e-005 m and a velocity of -2.85e-002 m/s^2. It is important to emphasize the choice of the actuator depends on the displacement and velocity[6] that needs provide to the system.

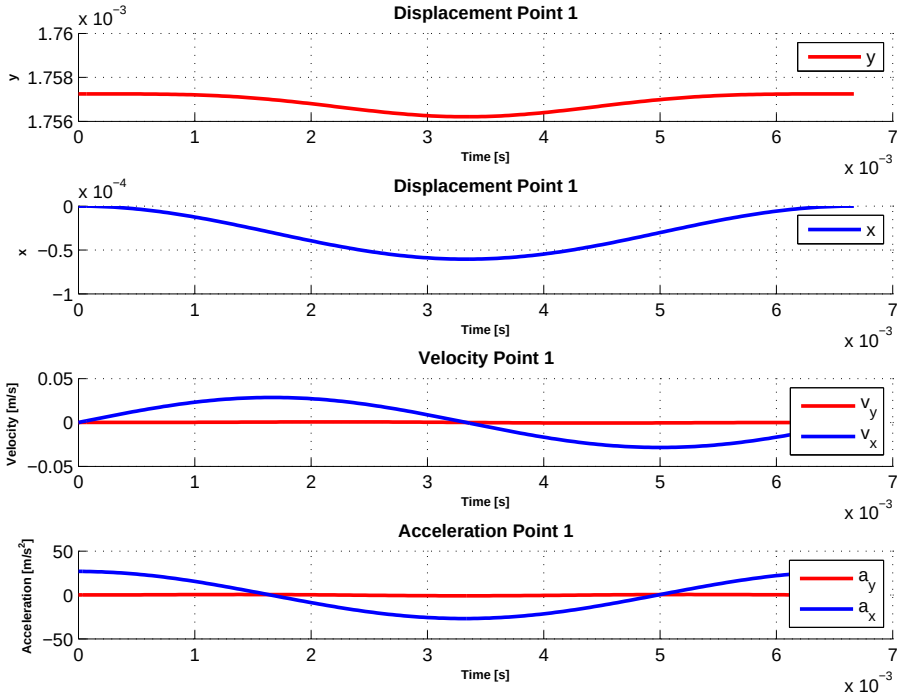

Figure 4.19: Kinematics Point 1

Since the kinematic equations of the both mechanisms are the same for Point 2 and Point 3 the results are equivalent from the ones shown above as is possible to see in Figs.4.21 and 4.21.

[6] Among other properties that will stated afterwards

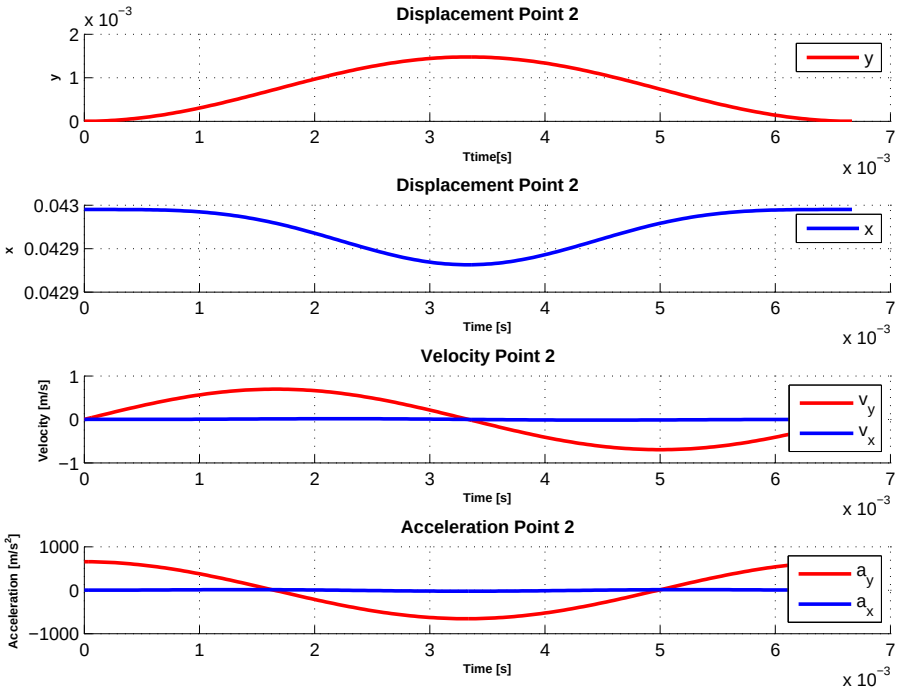

Figure 4.20: Kinematics Point 2

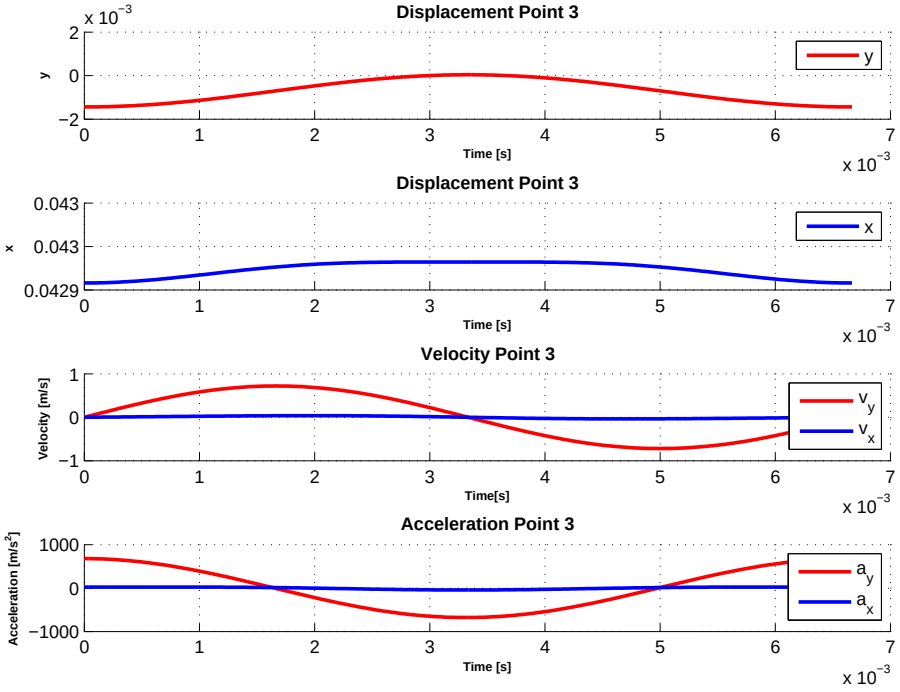

Figure 4.21: Kinematics Point 3

4.2.2 Kinematics of the Actuator

Since the actuator is an important feature of the mechanism it was conducted a study to compare the kinematics properties, such as displacement, velocity and acceleration, between the numerical code in Matlab, the rigid body module of Ansys and also the transient/dynamic analysis, using the

same software, involving all the inertia force which the system is subjected. The angular speed is an initial condition for the kinematic and dynamic analysis in Ansys. From Fig.4.22 and Fig.4.23 is shown respectively the angular velocity and the angular acceleration which is exactly the same in the three analyses.

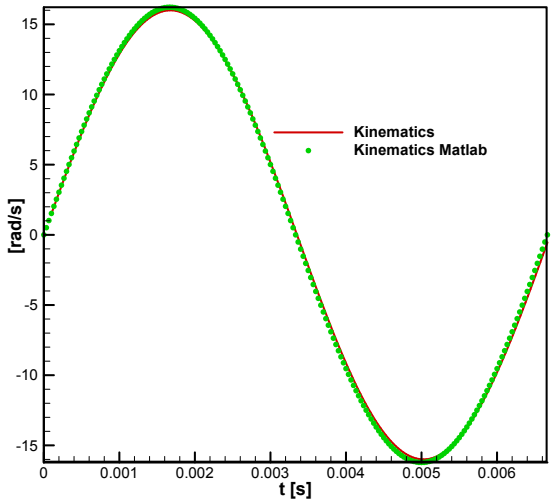

Figure 4.22: Angular Velocity

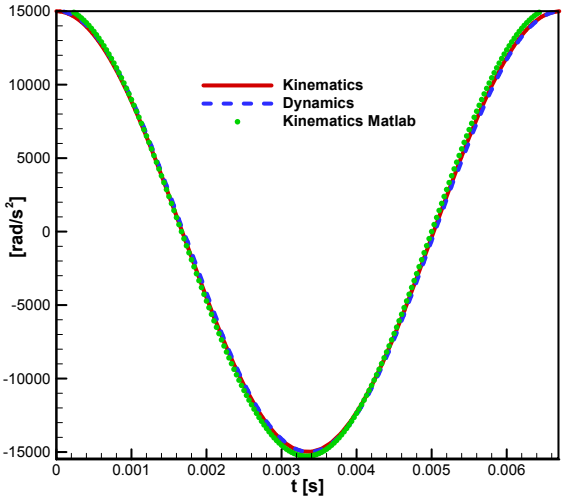

Figure 4.23: Angular Acceleration

4.2.2.1 Mechanism 1

Concerning the mechanism 1, Fig.4.24 represents the displacement of the actuator. The results are similar for both analysis with a small difference between the Matlab displacement and Ansys kinematic and transient studies, most probably because of the equations of the kinematics are not exactly the same.

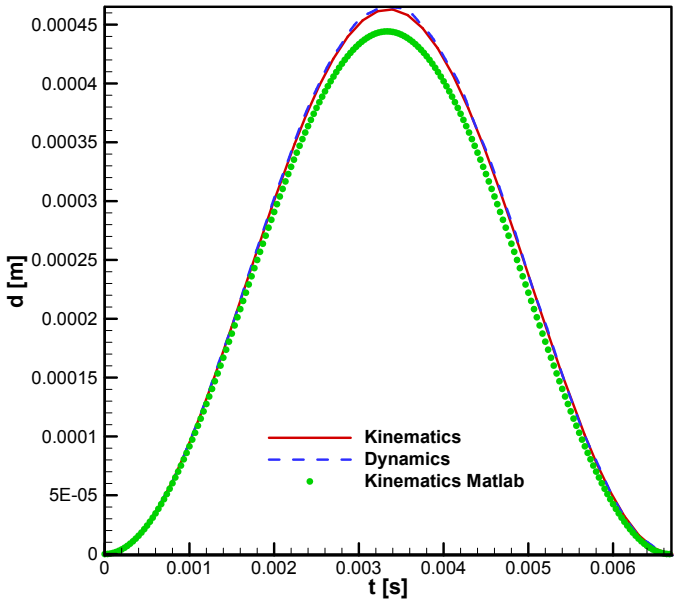

Figure 4.24: Displacement Actuator

The velocity of actuator is represented by Fig.4.25 where is possible to see some differences in velocity calculated by the dynamic analysis. In Fig.4.26 this differences are amplified due to the

fact that the acceleration is the derivative of the speed. These large deviations can be cause by non linearities provoked by the blade accelerations in Z[7] direction.

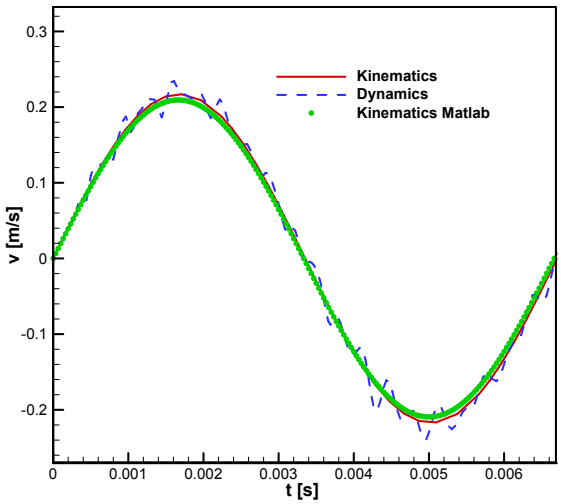

Figure 4.25: Velocity Actuator

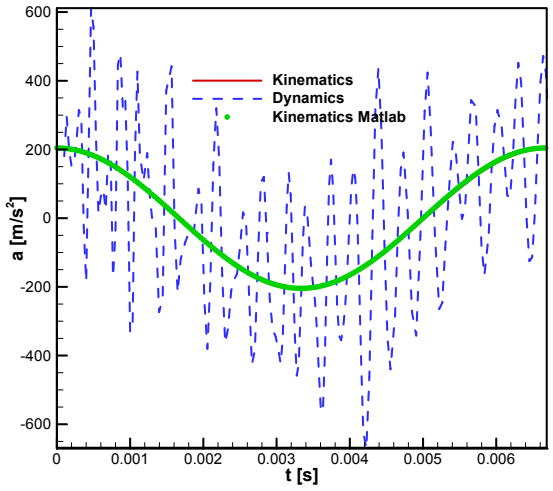

Figure 4.26: Acceleration Actuator

4.2.2.2 Mechanism 2

In the displacement of the actuator in mechanism 2 the non linearities mentioned above are stronger mostly to the blade acceleration in the X direction it is much bigger.

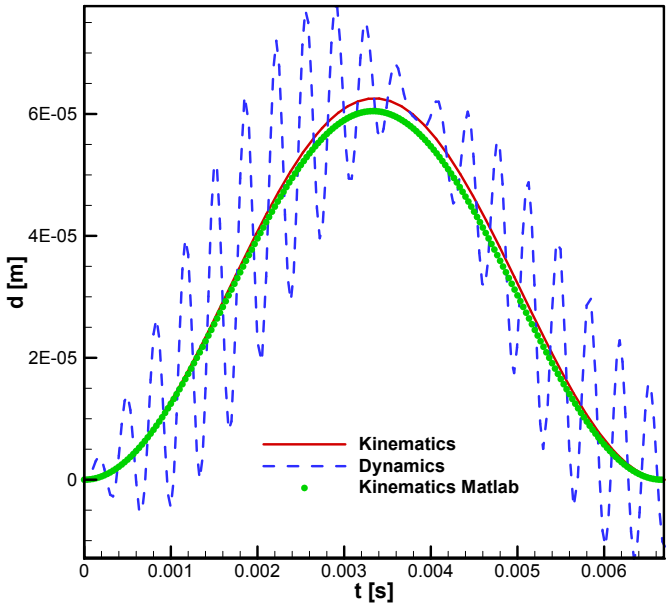

Figure 4.27: Displacement Actuator

A huge deviation between the kinematics and the dynamics is seen, the velocity and acceleration are amplified due the external accelerations possible to see in Figs.4.28 and 4.29, therefore, the analyses of kinematics is not enough to have a proper choice of the actuator.

[7]In Ansys Nomenclature or Y direction in Matlab.

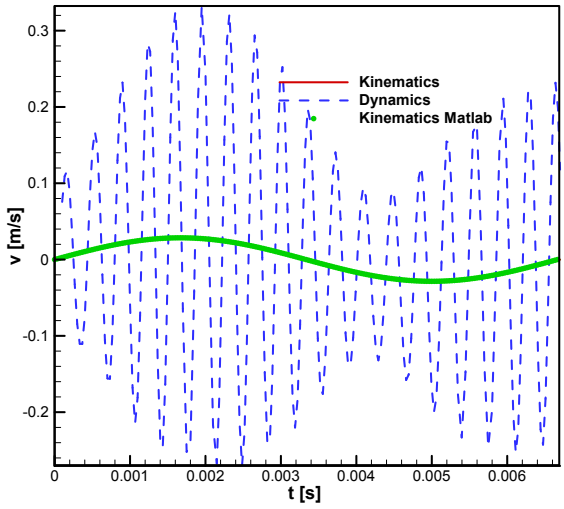

Figure 4.28: Velocity Actuator

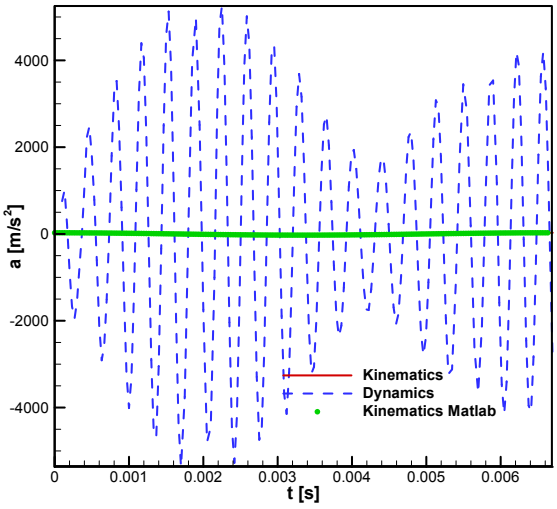

Figure 4.29: Acceleration Actuator

4.3 Modal Analysis

The modal analysis is very important in this study due to the fact that the mechanism is subjected to a certain frequency in order to be actuated; therefore, the study of the natural frequencies is rather important.

4.3.1 Gurney Flap

4.3.1.1 Mesh Discretization

For the modal analysis is important to define a mesh to be possible to obtain the natural frequencies and the deformations associated to that frequencies, therefore, a mesh similar to the static analysis was chosen but more refined in the region of the Gurney Flap as it is possible to in Fig.4.30.

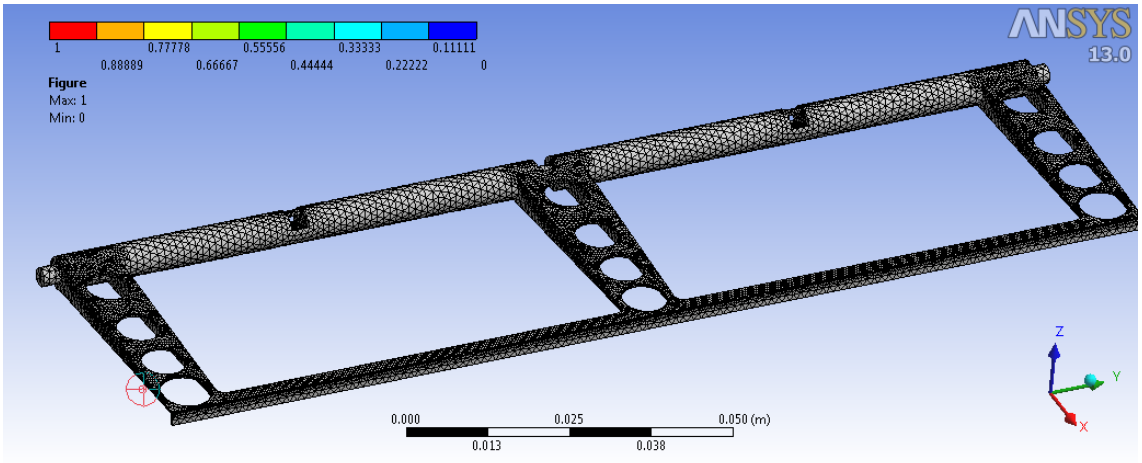

Figure 4.30: Mesh Modal Analysis Gurney Flap

The mesh quality is shown by Fig.4.31 and it is considered a good mesh for the same reasons mentioned before.

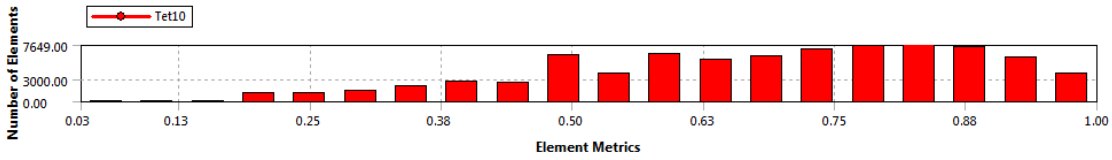

Figure 4.31: Mesh Quality Modal Analysis Gurney Flap

Fig.4.33 represents the mesh dependency of the 3° mode, which is a mode more stable for the convergence study. As is possible to see in the following figure, a mesh with about 95000 elements it is enough to have a good solution.

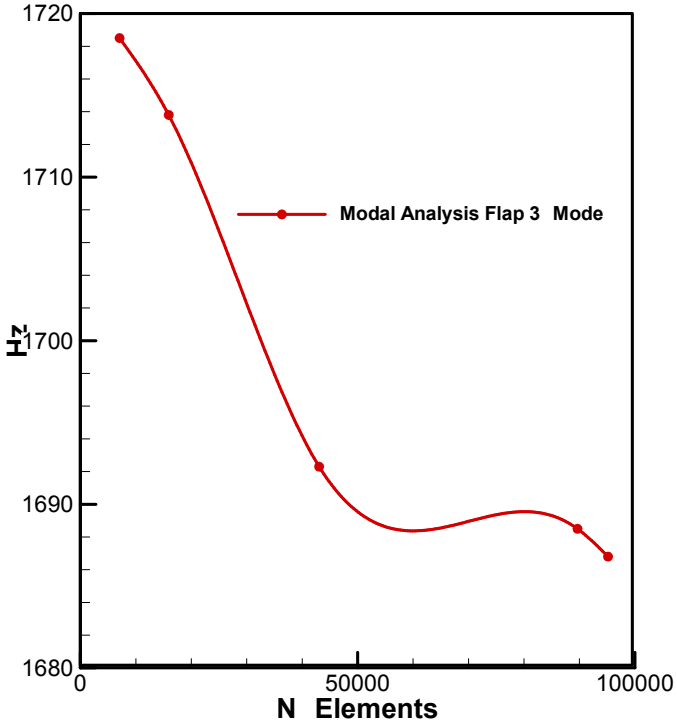

Figure 4.32: Mesh Convergence Modal Analysis Gurney Flap

4.3.1.2 Frequency Modes

The natural frequencies are represented by Fig.4.33 and the 1° mode is 834.4 Hz, much higher to the 150 Hz that actuators provide to the system given a high margin of safety.

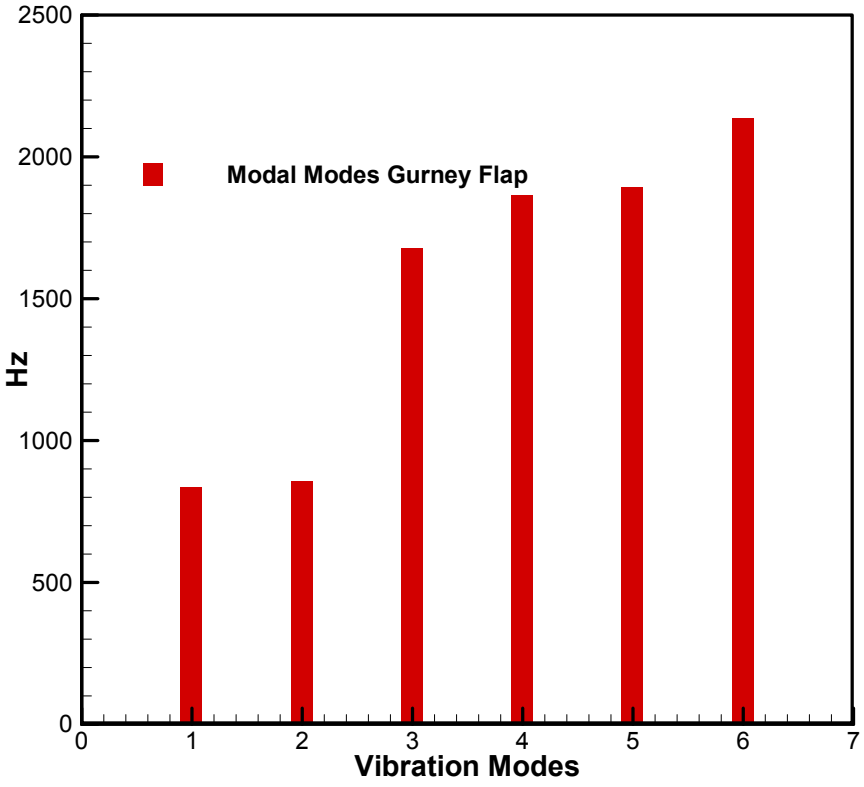

Figure 4.33: Frequency Modes Gurney Flap

Figs.4.34 to 4.39 represents the deformation associated to the 6 modes.

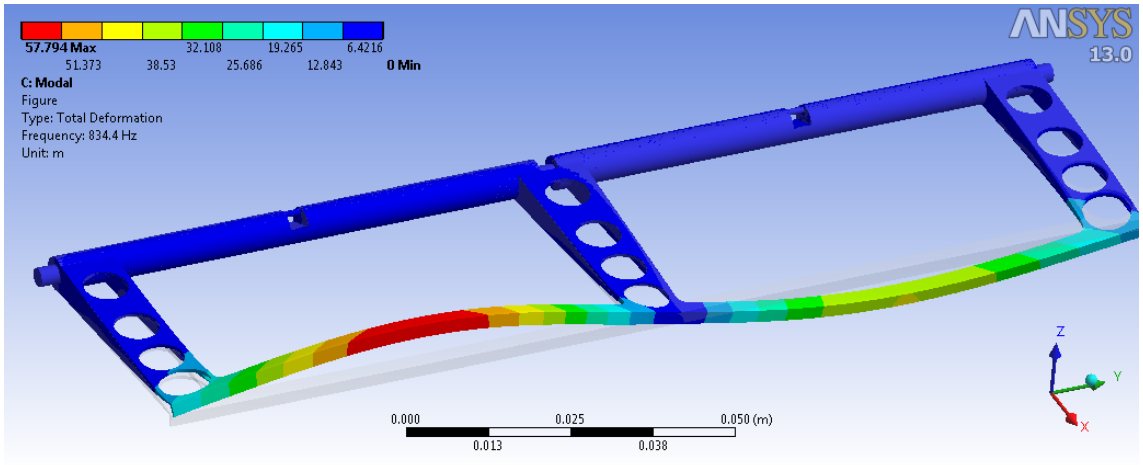

Figure 4.34: 1° Mode

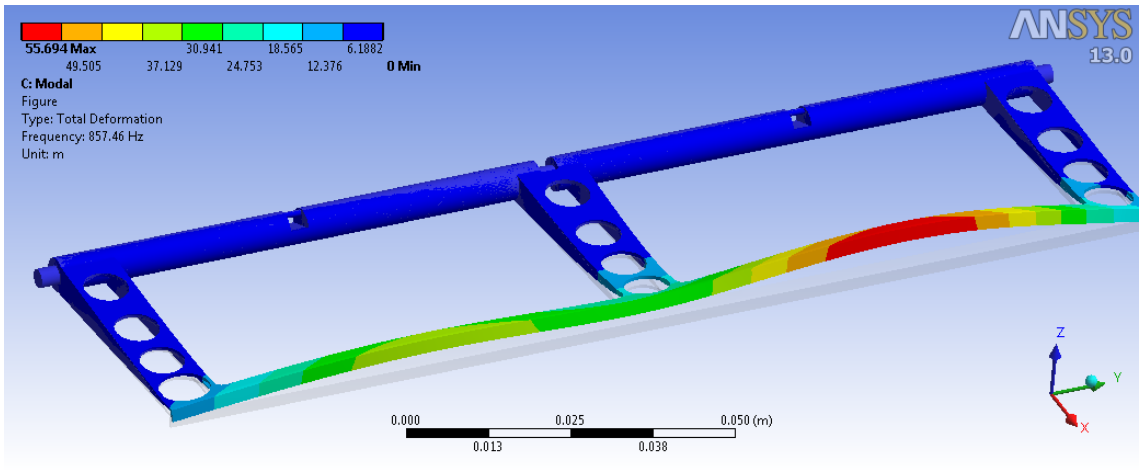

Figure 4.35: 2° Mode

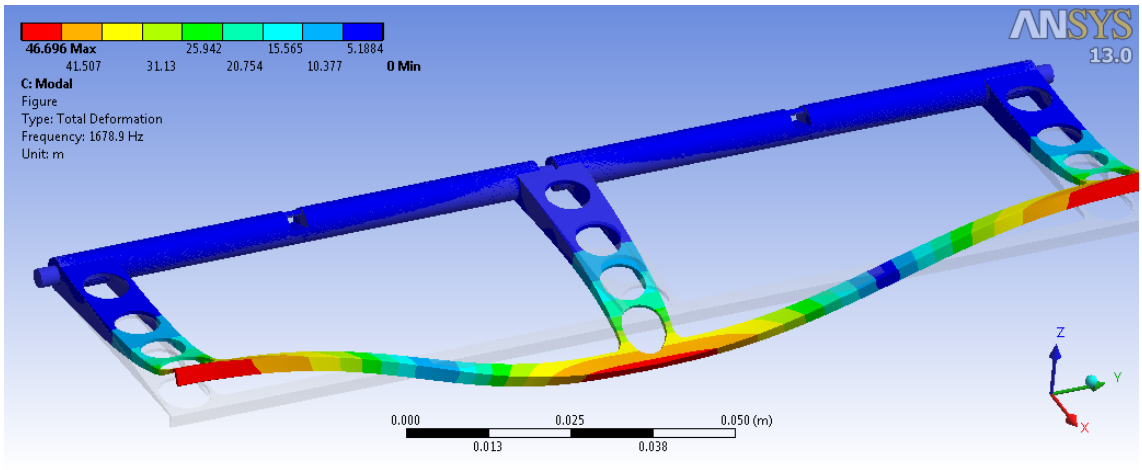

Figure 4.36: 3° Mode

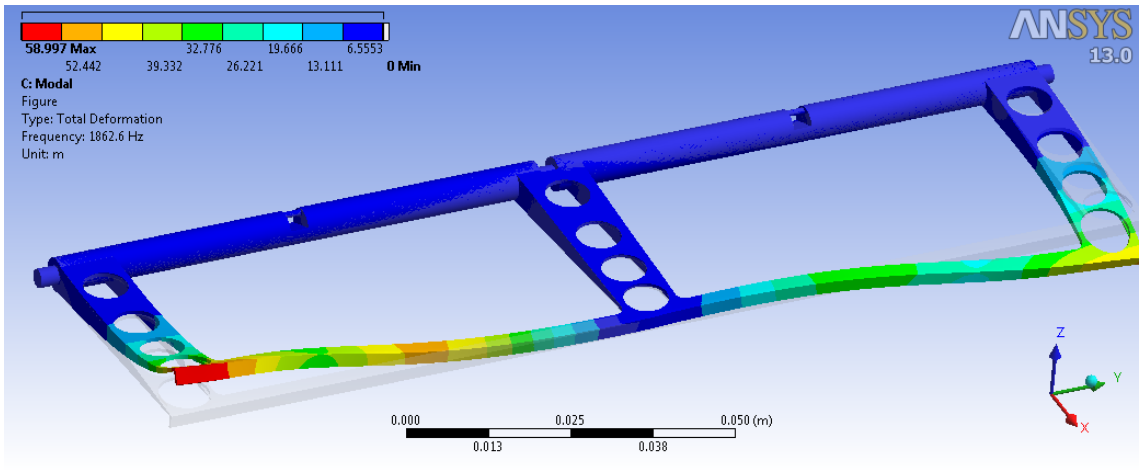

Figure 4.37: 4° Mode

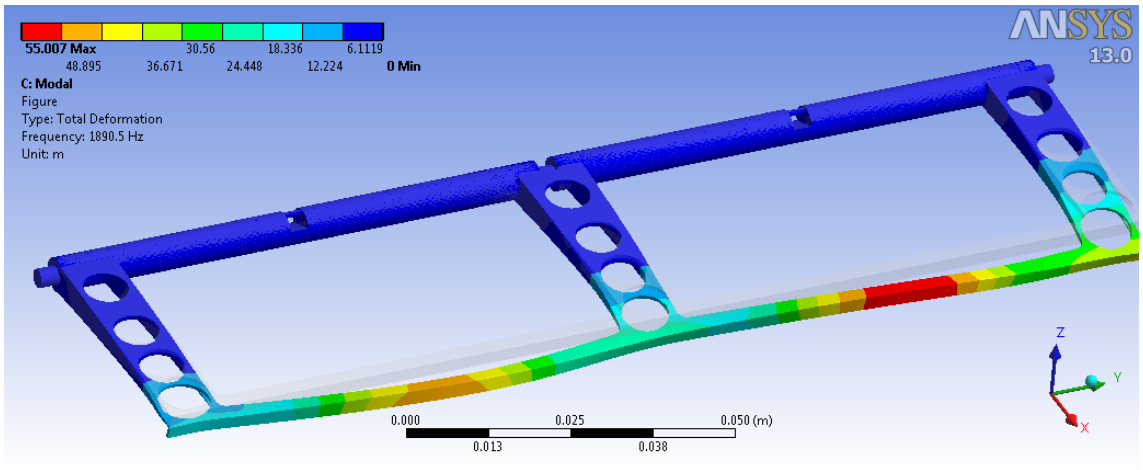

Figure 4.38: 5° Mode

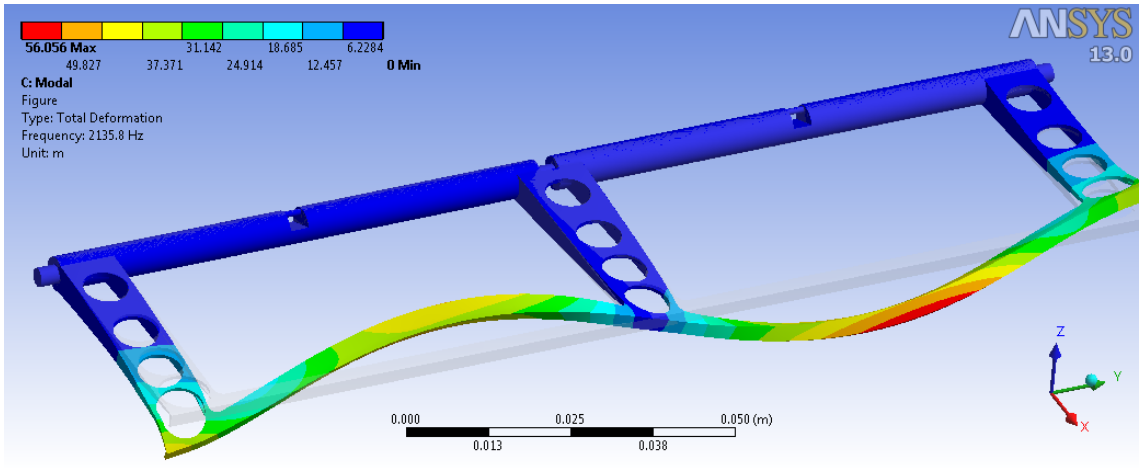

Figure 4.39: 6° Mode

4.3.2 Mechanism 2

After the modal analysis in the Gurney Flap it is important to make an analysis to all system, Support and GF[8]. Since it is almost impossible to simulate the actuators due to its complexity, it was chosen to replace the actuation system by a cylinder inside another, shown by Fig.4.40, imposed by a translation joint. This replacement of the actuation system was also made in the rigid body and transient analysis. The support was bonded to the spar, bottom part and top part of the blade to simulate the reality.

[8] After imposed all joint properties mentioned in 4.2

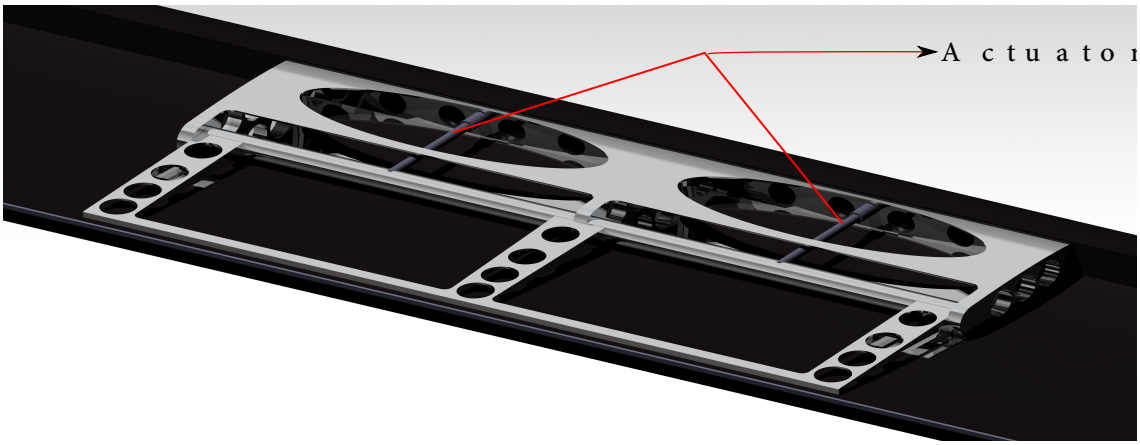

Figure 4.40: Design of Mechanism 2

4.3.2.1 Mesh Discretization

A mesh with tetrahedral solid elements was chosen, as shown in Fig.4.41, where the biggest difference of analysis above is the inclusion and meshing of the support and the "actuators". The mesh is refined in the region of the flap is more susceptible to larger deformations. The blade was not meshed because is not the scope of this project to study the natural frequencies of the rotor blade.

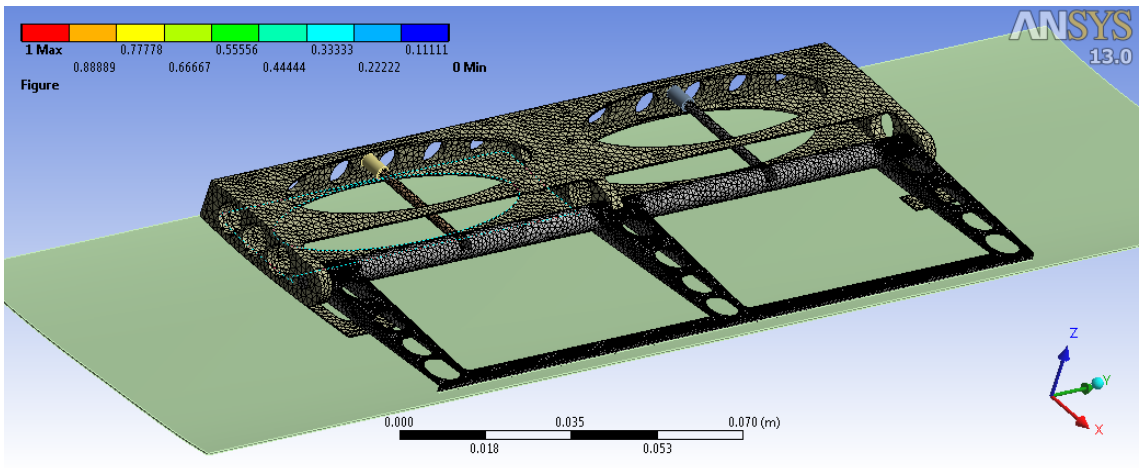

Figure 4.41: Mesh Modal Analysis Mechanism 2

The mesh quality, from the next figure, is not as good as previous analysis but the bad elements are situated in the support and in the actuator which are not subjects to large deformations as the Gurney Flap, therefore, refining them it would take to high computation time without changing the solution as is possible to see in Fig.4.43.

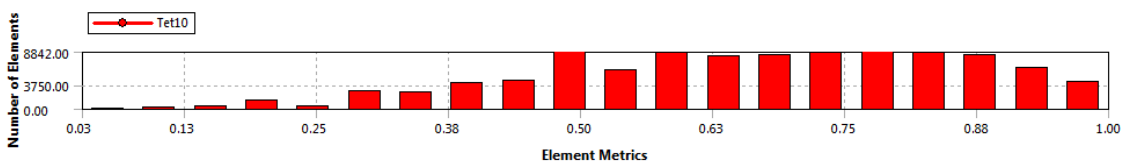

Figure 4.42: Mesh Quality Modal Analysis Mechanism 2

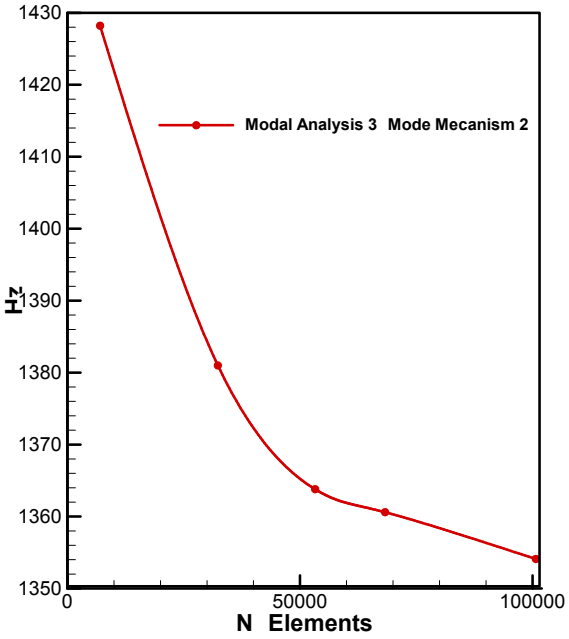

Figure 4.43: Mesh Convergence Modal Analysis Mechanism 2

4.3.2.2 Frequency Modes

Fig.4.44 represents the natural frequencies of the assembly. The first natural frequency is 836.3 Hz, very similar to the one obtained by the modal analysis of the Gurney Flap in Chapt.A.2.

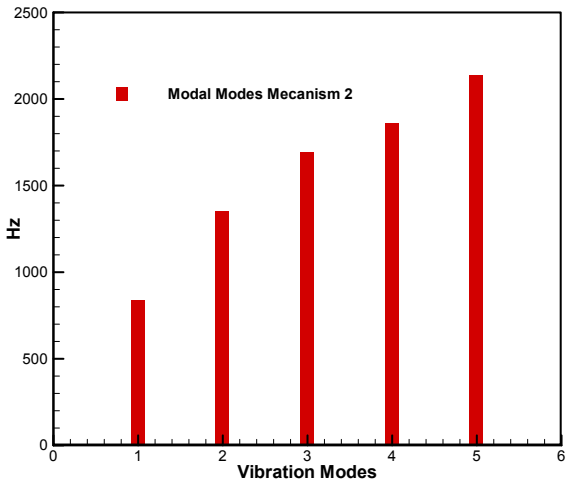

Figure 4.44: Frequency Modes Mechanism 2

The next figures represents the deformation associated to the 5 frequency modes.

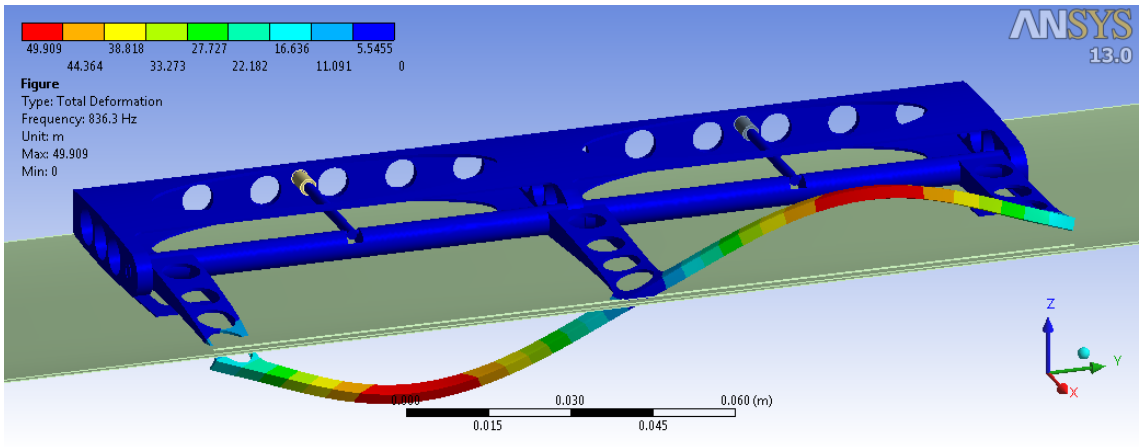

Figure 4.45: 1° Mode

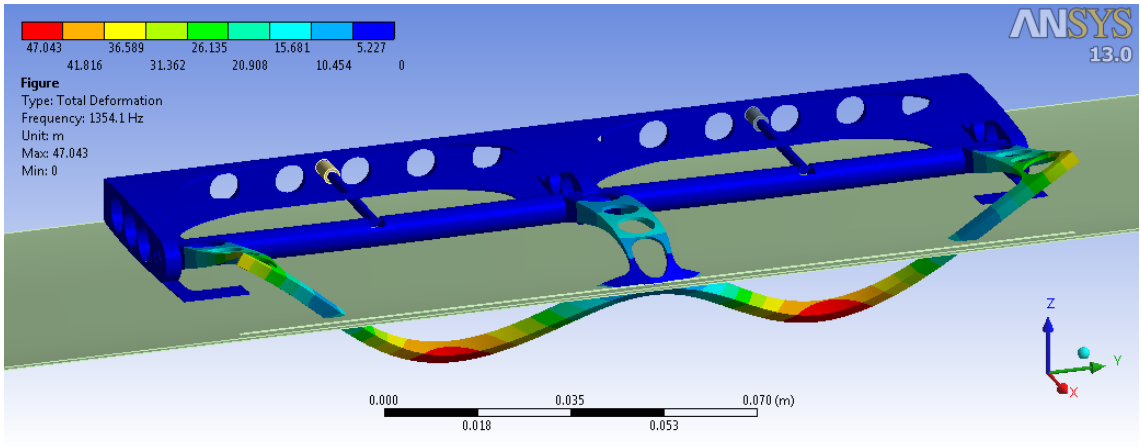

Figure 4.46: 2° Mode

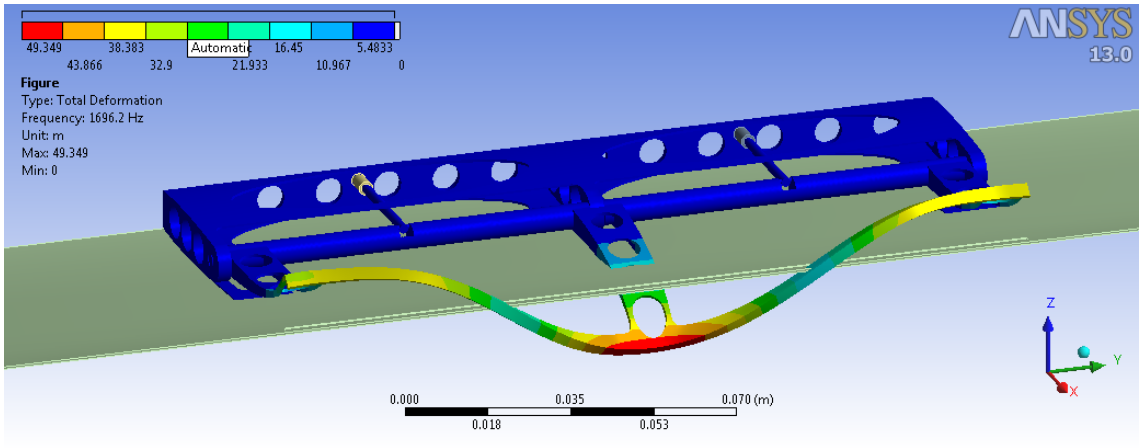

Figure 4.47: 3° Mode

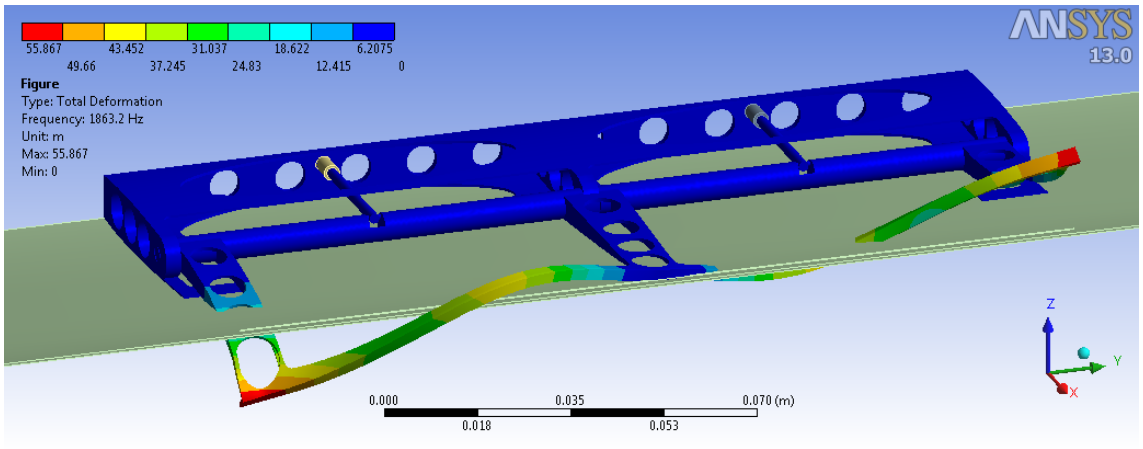

Figure 4.48: 4° Mode

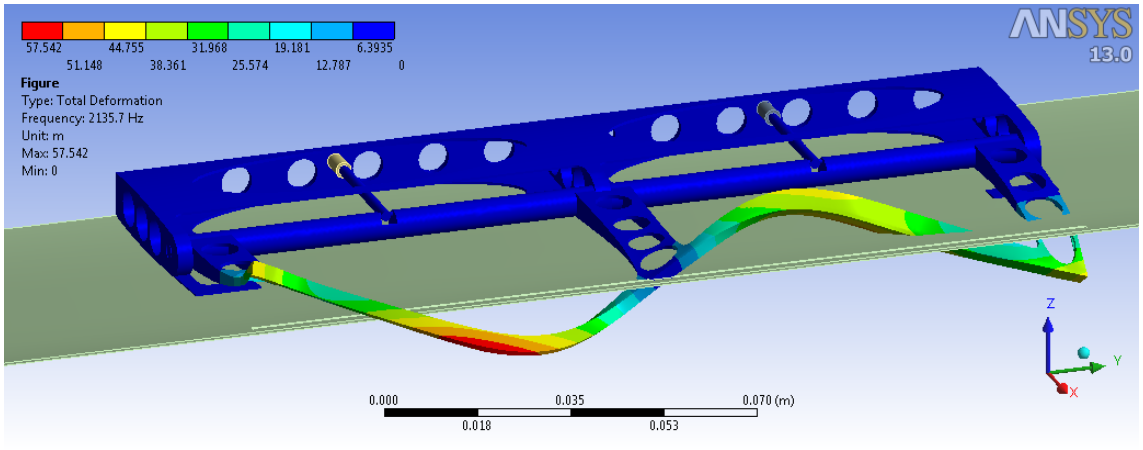

Figure 4.49: 5° Mode

The 1° natural frequency of the mechanism 1 is 773.03 Hz being lower from analysis above but considerably higher to the 150 Hz frequency which the system is subjected. This result can be due to position of the actuator.
All results related to mechanism 1 relative the modal analysis can be found in Chapt.A having exactly explanation mentioned above.

4.4 Dynamic Analysis

The dynamics analysis or transient was the most important study of this project. It allowed calculating the stress and the displacement of the Gurney Flap. It also allowed calculating the displacement, velocity and acceleration of the actuator which the results were shown in Chapt.4.2.2. The computation of the transient analysis is extremely heavy and time consuming.

4.4.1 Mesh Discretization

The properties of the mesh used are identical to the modal analysis mentioned above. The Gurney Flap region was refined exactly for the same reasons mentioned in Chapt.4.3.2, as shown in Fig.4.50.

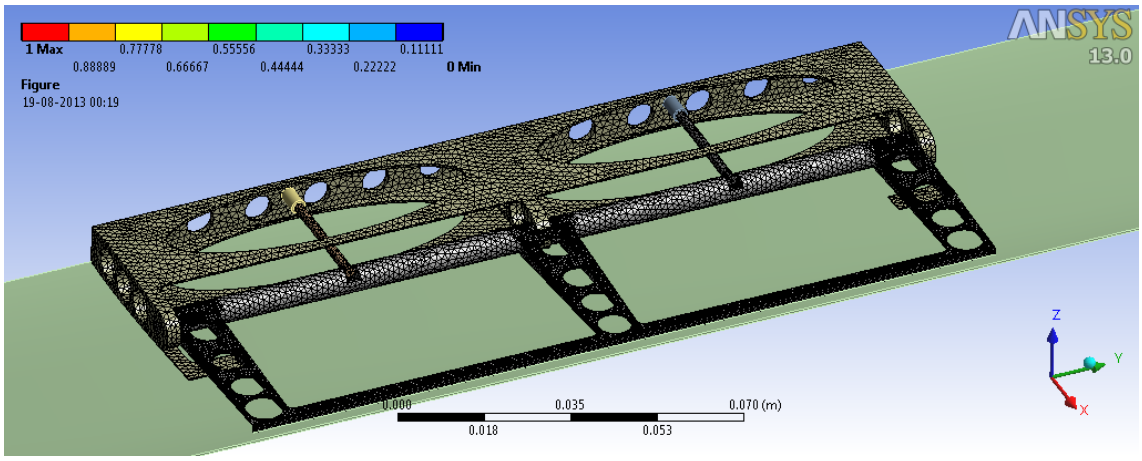

Figure 4.50: Mesh Dynamic Analysis Mechanism 2

As it is possible in figure 4.51 the quality of the mesh it not as good when compared with the previous analysis. Although in the region of flap the elements are considered good elements.

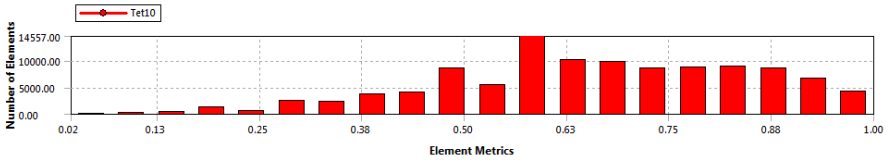

Figure 4.51: Mesh Quality Dynamic Analysis Mechanism 2

In the study of mesh dependency the solution started to converged at 100500 elements as shown in Fig.4.52.

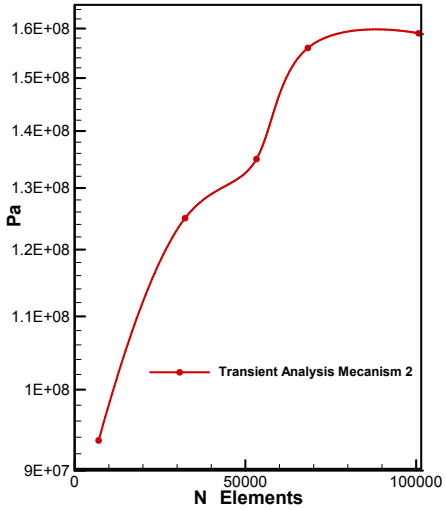

Figure 4.52: Mesh Convergence Modal Dynamic Analysis Mechanism 2

In the transient analysis the time is not continuous it is discrete, thus, the analysis is divided in several time steps represented in Fig.4.53, all substeps had a convergence in this analysis.

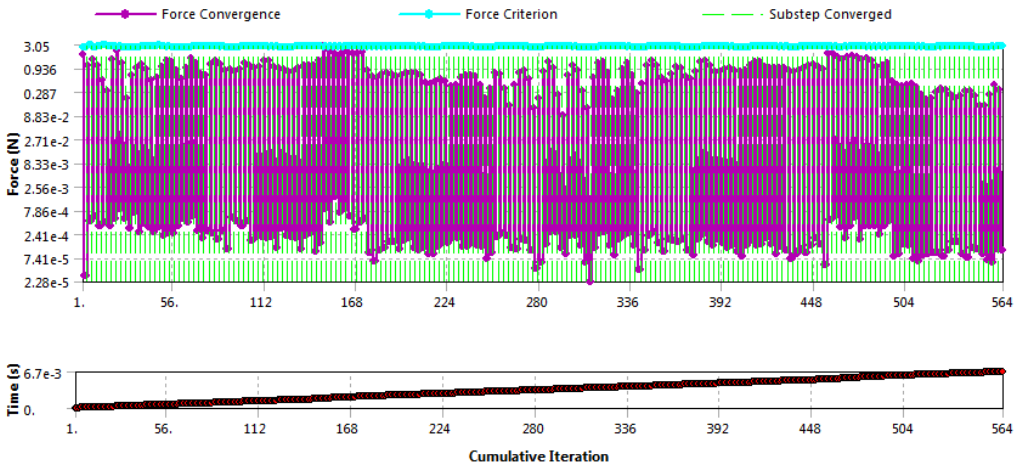

Figure 4.53: System Convergence Modal Dynamic Analysis Mechanism 2

4.4.2 Displcement

One requirement is that area exposed of the GF when fully deployed should be bigger than 1.1% of the chord preferably 1.5%, as shown in Fig.4.54 the displacement of the flap represented by the blue color is -0.0012376 m which corresponds to 1.375% of the chord of the are exposed.

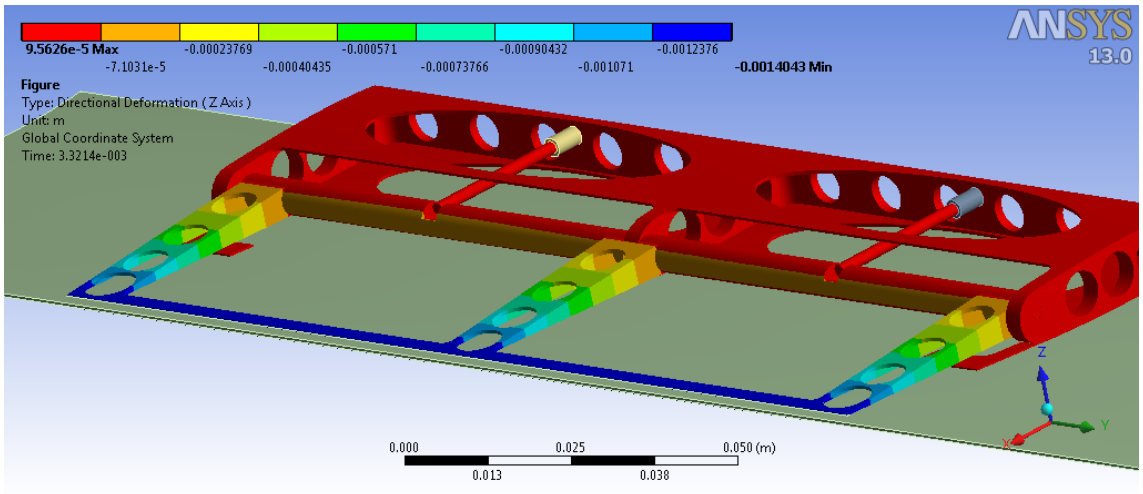

Figure 4.54: Deformation Z Axis Mechanism 2

4.4.3 Stress and Safety Facttor

Analysing the stress it is possible to see that the maximum equivalent stress is situated in the same region than the static analysis, in the radius 2, though the max. stress is 1.5644e8 Pa substantially bigger than the previous analysis. These increase of the max. stress is due to the inertial forces because the rotation of flap. The results are represented in Figs.4.55 and 4.57.

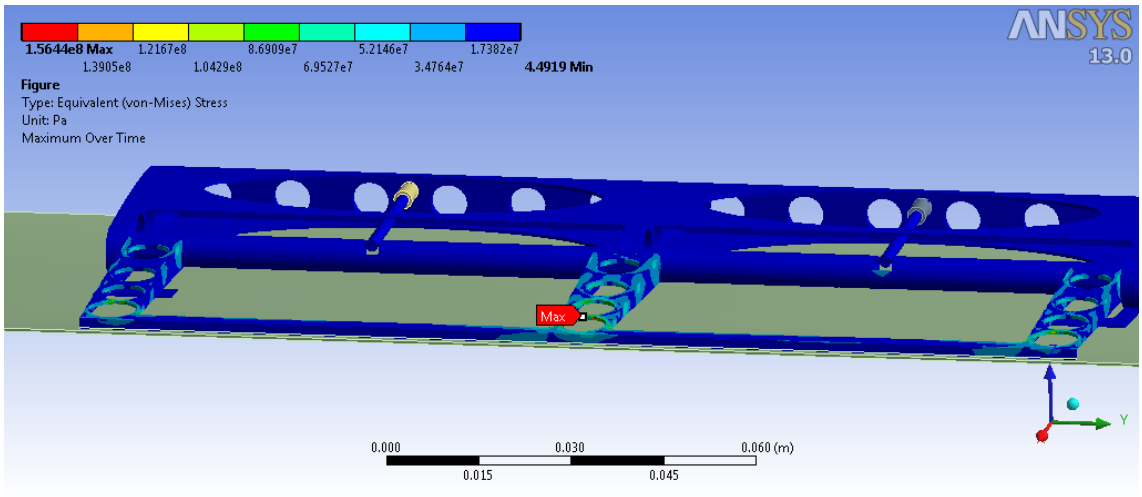

Figure 4.55: Maximum Stress Von Mises Mechanism 2

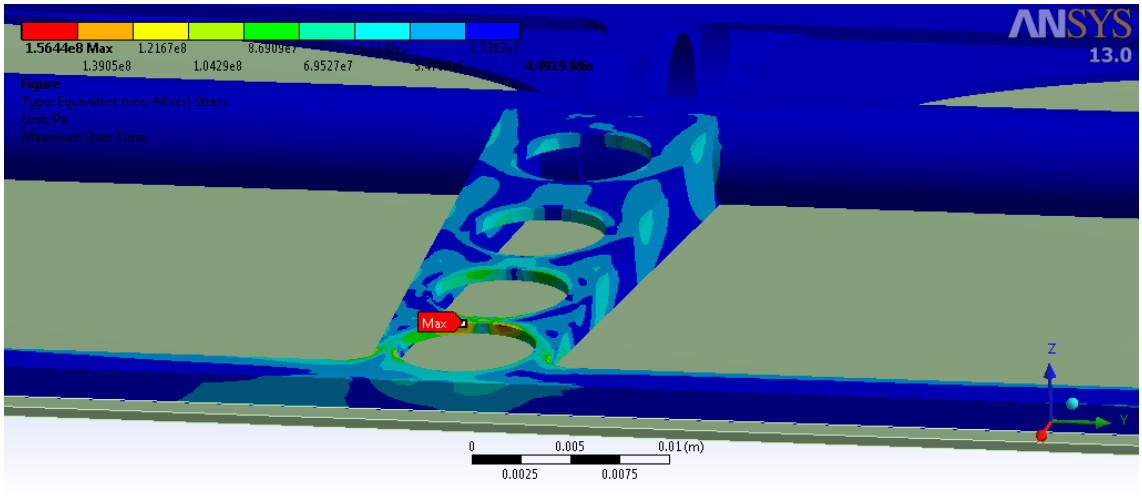

Figure 4.56: Maximum Stress Von Mises Zoom Mechanism 2

The stress in function of time is illustrated in Fig.4.57, where the stress changes between 3e7 Pa to the maximum stress mentioned above.

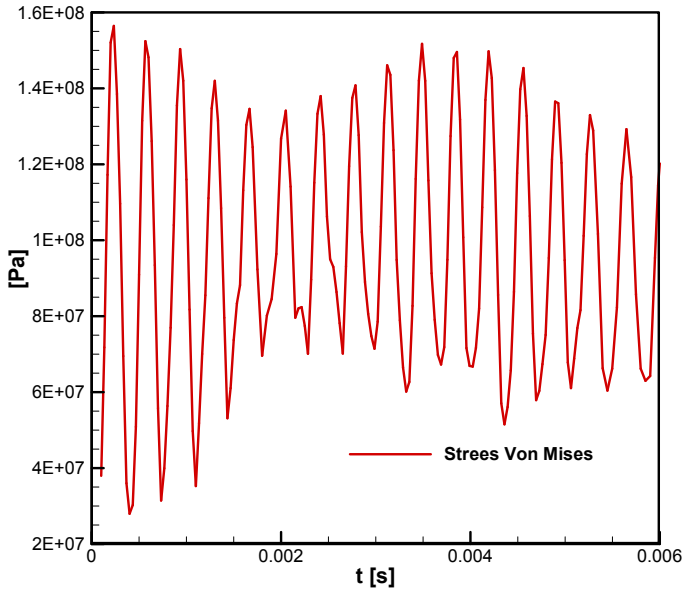

Figure 4.57: Stress Von Mises vs time Mechanism 2

Fig.4.58 exhibits the safety factor in function of time. The minimum value is around 1.9 which is higher than SF required for projects similar to this.

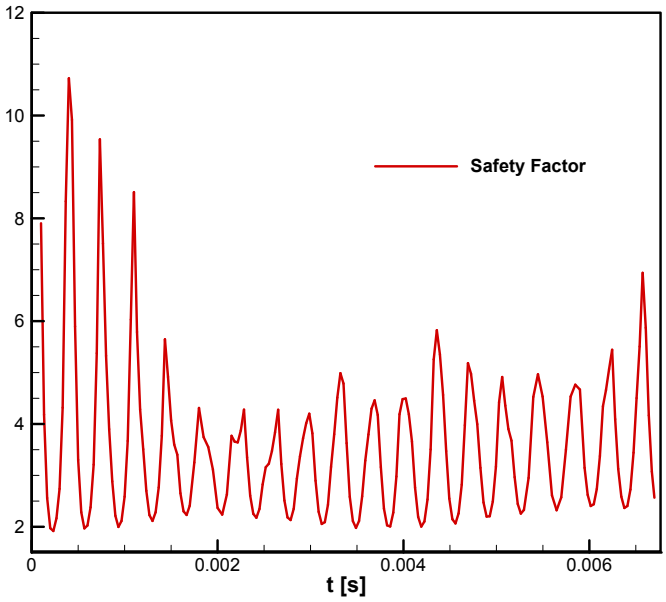

Figure 4.58: Safety Factor vs time Mechanism 2

4.4.4 Dynamics of the Actuator

The necessary force that the actuator needs to provide the to system is very complex to modulate in Ansys, therefore, it was calculated by a Matlab code using the equations indicated in Chapter3.3.2. The mass of the GF calculated by Matlab is 0.01470 kg and calculating the same property in Ansys is 0.01343 kg. The inertial moment is $I_{zz} = 1.704e - 006kgm^2$.
In Fig.4.59 the force of the actuator is shown, where the actuator is initially providing a push force and when the rotation changes in the anti-clockwise direction the actuator provides a pull force.

The push force is relatively smaller to the pull force mostly to the fact that the flap is under a great inertial force provoked by the acceleration of the blade in X direction(-1500 m/s^2). The reactions forces in the rotating axles are also represented by the first two graphics in Y and X direction.

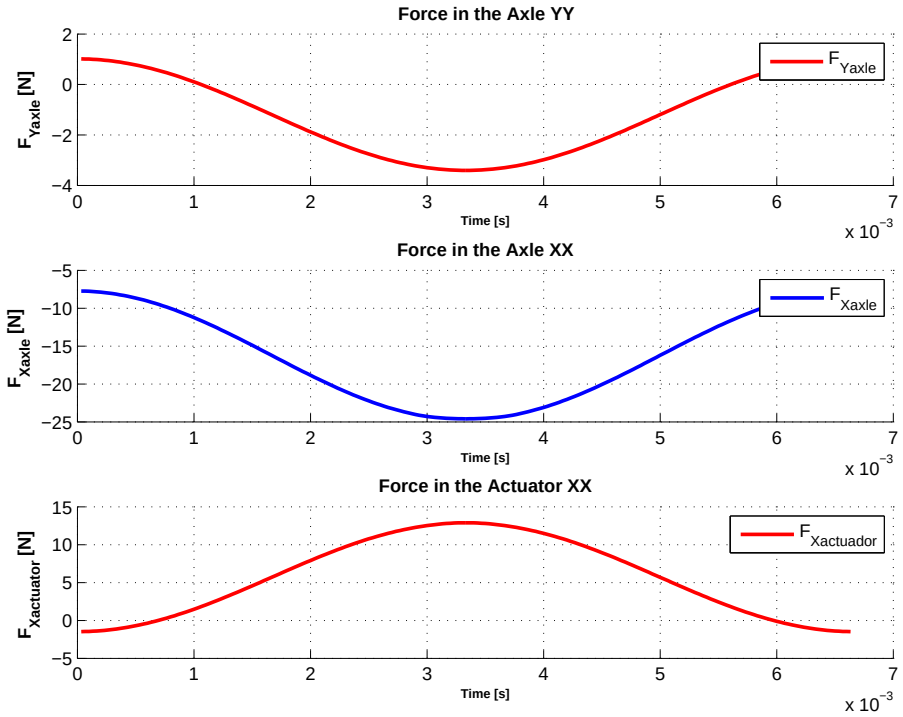

Figure 4.59: Necessary Force of the Actuator Mechanism 2

The necessary force showed in the graphic above represent the force of one actuator in a actuation system composed by two actuators.
It is important to refer that similar results related to the mechanism 1 are presented in Chapt.B. Since the shape of the Flap is the same, the maximum equivalent stress and displacement of the actuator are equivalent to the results mentioned above. The main difference is the force of the actuator because of the different formulation related to the dynamic of the actuation system.[9]

4.5 General results

In order to choose a suitable actuation system a parametric study was conducted with different positions of the actuators of both mechanism. The next graphics illustrates the distance of the the actuator to the rotating axle vs the necessary force of the actuator vs the displacement of the actuator.
Fig.4.60 corresponds to the mechanism 1 where is possible to visualize that increasing the distance from the actuator to the rotating axle, the necessary force decreases but the displacement of the actuator increases.

[9]The Actuator is driven in the Y direction in Matlab

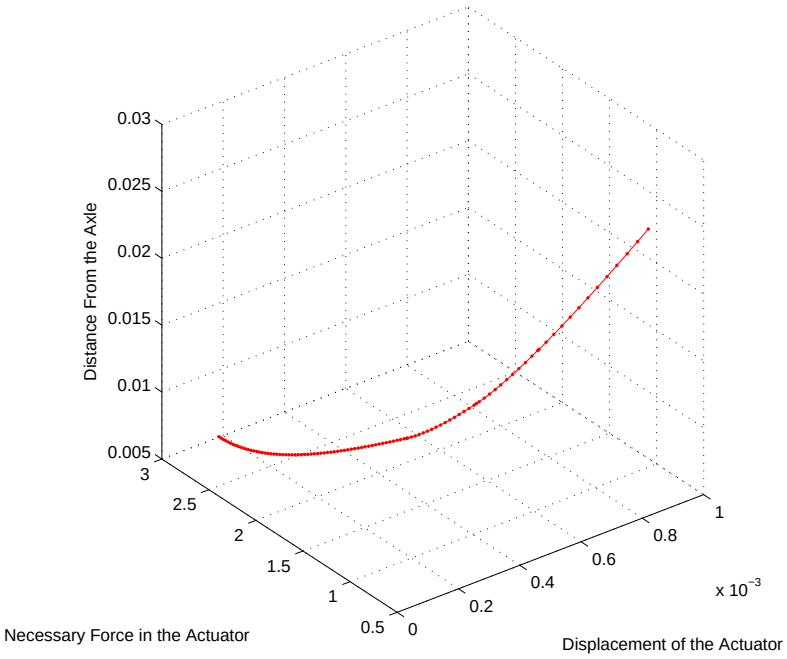

Figure 4.60: Position vs Force of the actuator vs Displacement Of Mechanism 1

The above explanation is suitable to next graphic which represents the mechanism 2, though the necessary F_{actua} is much more higher than the mechanism 1 but on the other hand the displacement of the actuator is smaller.

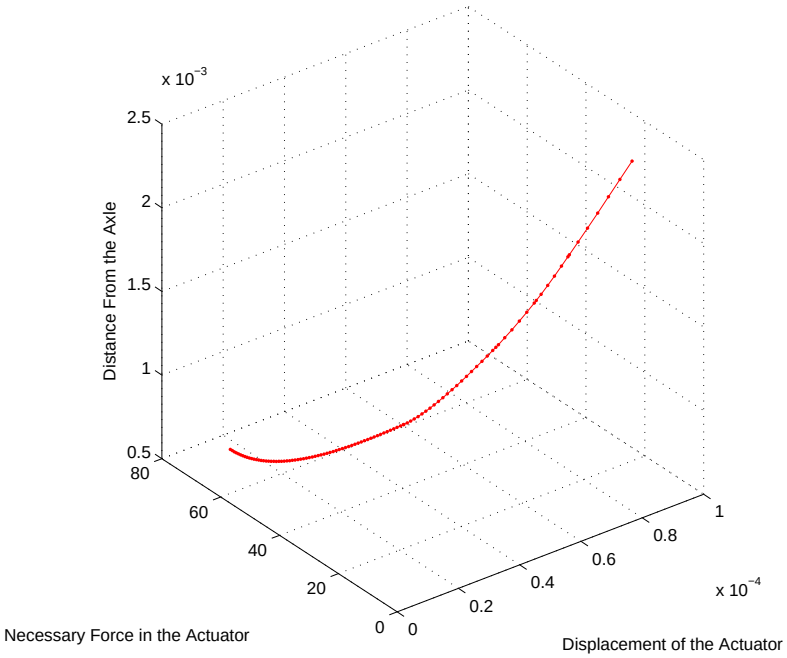

Figure 4.61: Position vs Force of the actuator vs Displacement Of Mechanism 2

The final weight of the assembly flap supporting and gurney flap is 0.0027 kg.

Chapter 5

Conclusion and Future Work

Conclusion

The Gurney Flap increases the lift coefficient of airfoils and hencethe aerodynamic performance of the rotor blades. The use of GF is especially useful during takeoff and landing of the aircrafts. For optimum aerodynamic performance, the GF should be mounted at the trailing edge perpendicular to the chord line of the airfoil or root chord line of the wing, where its height must be less than the local boundary layer thickness. The drag is increased by the Gurney Flap, but the lift-to-drag ratio can be greatly increased under certain conditions. With the increase of the frequencies in an actuated GF the lift coefficient increases and the drag coefficient decreases.
The aim of this project consist in designing a mechanism with an actuated Gurney Flap at high frequencies in order to enhance the aerodynamic characteristics. Respecting several structural requirements a optimization was done to reduce the mass of the system. Two different directions of the actuation system were studied to evaluate the best position of the actuator.

Kinematics Analysis

The kinematic analysis revealed good agreement between the Matlab analysis and the Ansys rigid body analysis, neglecting the inertial forces inherent to the system. This analysis demonstrated a high angular acceleration and a small angle, around 1.3°, which the flap is subjected in order to be fully deployed. It was also shown that the actuator needs to provide small displacements, O(10$^-$3) m for mechanism 1 and O(10$^-$4) m for mechanism 2, as also relative small velocity around 0.3 m/s. When these results were compared with the actuator's displacement, velocity and acceleration retrieved by the dynamic analysis some discrepancy's were found, with a large influence in the actuator's velocity and acceleration, mostly due to inertial forces provoked by the blade accelerations that the rotor is submitted such as centrifugal acceleration, normal acceleration and flapping accelerations of the blade.
Those discrepancies were higher in mechanism 2 mostly to fact that the actuator is under higher blade accelerations than mechanism 1. The influence of these non-linearities are almost negligible in the displacement of the actuator, thus, the normal kinematic equations are still valid to evaluate the necessary stroke that the actuation system needs to provide to the flap.

Static Analysis

This analysis was made mostly to evaluate the maximum directional deformation provoked by all inertial forces. It was possible to conclude that theses deformation were below the maximum required of 0.1 mm. It was also conducted an parametric optimization base in three radius, mentioned in Chapt.4.1.2, with the objective to reduce the mass of the Flap. The best candidates were found respecting the structural requirements.

Modal Analysis

In order to calculate the natural frequencies the Gurney Flap and the assembly Support/GF were subject to a modal analysis. The results retrieved showed that the natural frequencies are higher than 150 Hz which is the frequency of the actuation system.

Dynamic Analysis

Since the mechanism is subject to high inertial forces it was important to conduct a study where the stress and deformation were calculated simulating the real conditions, i.e. actuate the system to 150 Hz submitted the all aerodynamic and inertial forces. This analysis was the main scope of the project. The results showed a stress much lower than ultimate tensile stress of the material with a safety factor of 1.9. It was possible to analyse that when the Flap is fully deployed the the exposed height of the flap is around 1.3% of the chord.
For the necessary force of the actuator is possible to conclude that the actuator in mechanism 2 needs a much higher force than the actuation system in mechanism 1.

For some more general conclusion, the reduction of mass from the initial design is around 44% with all requirements respected.
The main difference from mechanism 1 and mechanism 2 is the position and direction in which the actuator is driven, influencing the actuators characteristics like displacement, velocity and acceleration. On the other hand the deformation, stress and natural frequencies are the same for both mechanisms. The necessary force that the actuator needs to driven the flap, in the mechanism 2 it is substantially higher than mechanism 1 but it is within the parameters of commercial PZT. It is always assumed that the actuation system is composed by two actuators with the objective to have a better control in the rotation the flap, otherwise, the actuator could deform under the centrifugal force.
An increase of the exposed area of the Flap when this is fully deployed is higher than the minimum required of 1.1%c. This design of the flap can resist to the all inertial forces, provoked by the motion of the blade and the 150 Hz actuation, and the aerodynamic forces fulfilling the requirements for the maximum deformation.
A parametric study was made in order to evaluate the best position of the actuator in function of necessary force to provide to the system and necessary stroke in order to have a fully deployment allowing a better choice of the actuator.
Finalizing, it was possible to design a mechanism inside a rotor blade actuating at very high frequencies with a very low mass fulfilling all requirements imposed.

Future Work

Here are some recommendations for a better design of the mechanism:

- A comparison between the numerical results and the experimental analysis in order to validate the results;
- Simulation of a structural analysis with different material, such as, carbon fibers for the flap and for the support to reduce the weight respecting all requirements of deformation;
- A proper choice of the actuation system based on the graphics shown in Chapt.4.5, which should be balanced by weight, cost, power consumption and life time of the actuator;

- Increase of the actuation frequency in order to enhance the aerodynamic properties of the blade to reduce the rotor fuel consumption;
- An numerical aerodynamic study of this mechanism and a experimental using wind tunnels the calculate the correct aerodynamic force which the flap is submitted;
- A fatigue study of the mechanism in order to calculate the number of cycles that the GF and the Support can operate;

Bibliography

[1] Liebeck. "Design of subsonic airfoils for high lift.". *Journal Aircraft*, 15(9):547–561, 1978. xiii, 2, 3, 6, 10

[2] S. Thepvongs. "Design and Testing of an Active Gurney Flap Actuator for Helicopter Rotor Blade Control.". Master's thesis, The Pennsylvania State University, 2002. xiii, 11, 12

[3] Zhang PF Li YC, Wang JJ. "Effect of Gurney flaps on a NACA0012 airfoil.". *Flow Turbulent Combustion*, 68(1):27–39, 2002. 2

[4] Pendergraft OC. Neuhart DH. *"A water tunnel study of Gurney flaps"*. NASA, TM-4071 edition, 1988. 3, 4, 5, 6

[5] Lemay J. Giguere P, Dumas G. "Gurney flap scaling for optimum lift-to-drag ratio.". *AIAA Journal*, 37(12):1888–90, 1997. 4

[6] K.-S. Choi J.J. Wang, Y.C. Li. "Gurney flap-Lift enhancement, mechanisms and applications". *Progress in Aerospace Sciences*, 44(1):22–47, 2008. 7, 11

[7] Michael Kinzel. "Miniature Trailing-Edge Effectors for Rotorcraft Performance Enhancements". *Journal of the American Helicopter Society*, 52(2):146–158, 2007. 7, 8

[8] Robert L. Roedts II. "Rotorcraft Perfomance Enhancements due to a Lower-Surface Miniture Effector". Master's thesis, The Pennsylvania State University, 2008. 9

[9] Colman J. Marañón Di Leo J. Boldes, U. and J.S. Delnero. "Low Speed Turbulent Boundary Layer Wind Tunnels". Technical report, National University of La Plata, Argentina. 9, 10

[10] Joo W. Lee D.-H. Yee, K. "Aerodynamic performance analysis of a gurney flap for rotorcraft application.". *Journal of Aircraft*, 44(3):1003–1014, 2007. 11

[11] R. Loedersloot A. de Boer R. Akkerman A. Paternoster, P. de Jong. "Actuator and Control System for Green Rotorcraft". In *University of Twente, Engineering Technology*, 2009. 11

[12] Michael Thiel. "Actuattion of an Active Gurney Flap for Rotorcraft Applications.". Master's thesis, The Pennsylvania State University, 2008. 12, 13, 14, 15

[13] W. Wong. "monotonic and Cyclic Fatigue Properties of Automotive Aluminum Alloys,". Technical report, SAE Technical Paper 840120, 1984. 18

[14] J.W. Waanders. Piezoelectric Ceramics. Technical report, Philips Components, Eindhoven, The Netherlands, 1991. 18

[15] CEDRAT TECHNOLOGIES. Compact dynamic precise. `http://www.cedrat-technologies.com/download/CEDRAT_TEC_Catalogue.pdf`. 19

[16] Riverhawk Company. Flexure pivots. `http://www.flexpivots.com/pdf/Riverhawk-FlexuralPivotCatalog.pdf`. 21

[17] Ansys Inc. *Multibody Analysis Guide*. Ansys Inc. 37

Appendix A

Modal Analyisis Mechanism 1

A.1 Mesh Discretization

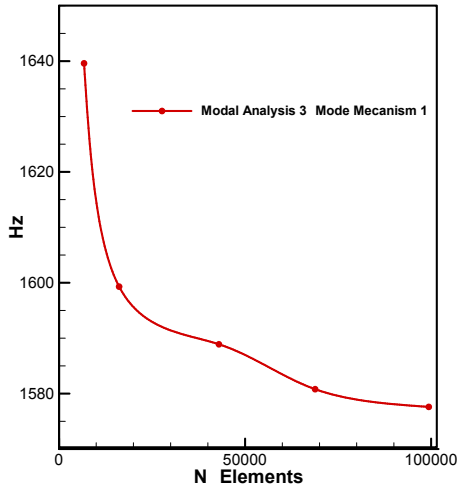

Figure A.1: Mesh Convergence Modal Analysis Mechanism 1

A.2 Frequency Modes

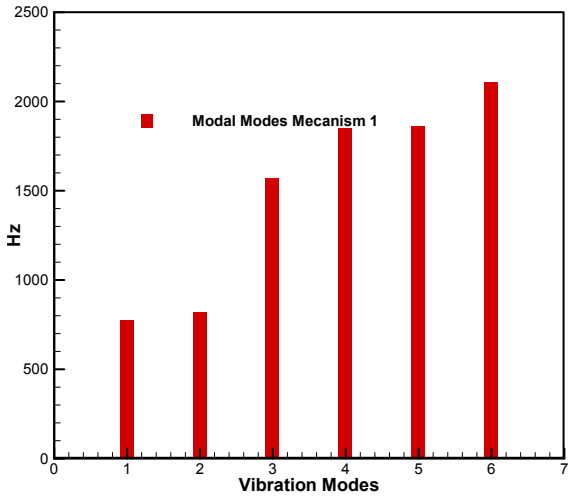

Figure A.2: Frequency Modes Mechanism 1

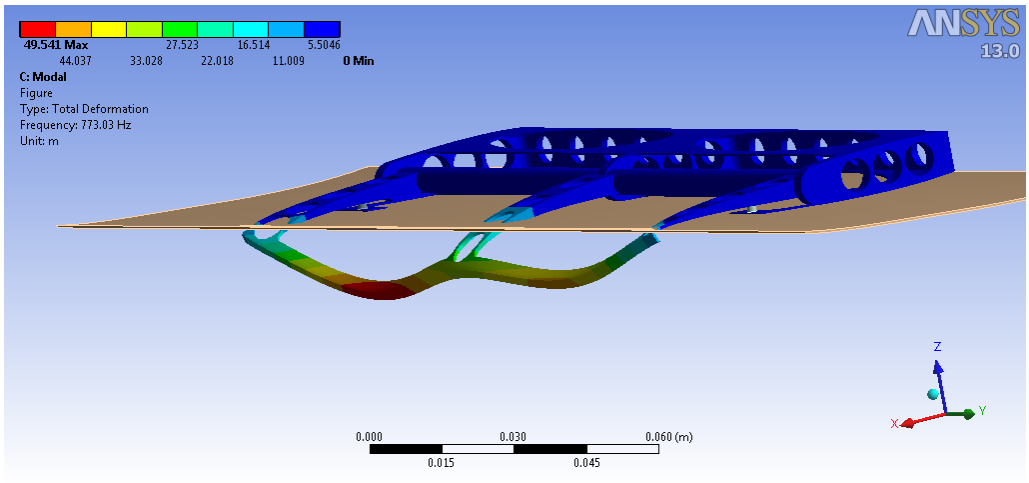

Figure A.3: 1° Mode

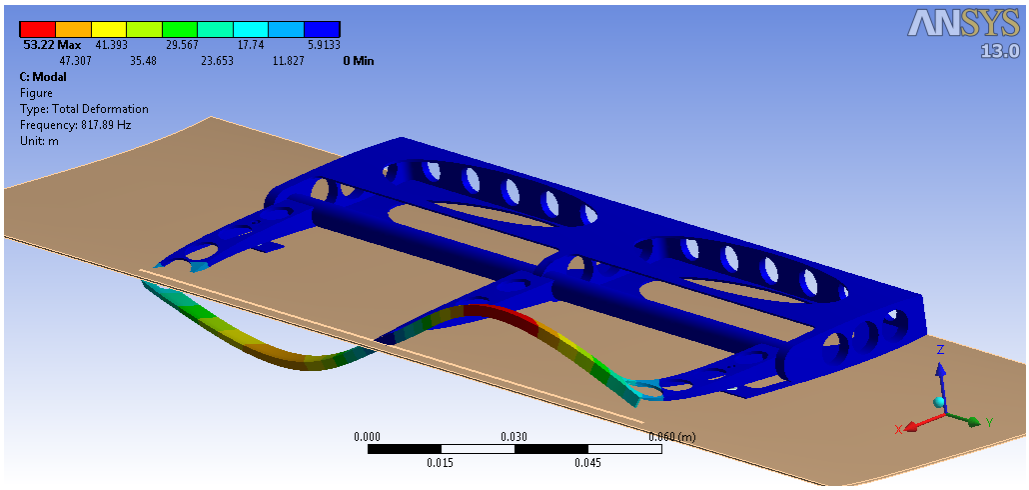

Figure A.4: 2° Mode

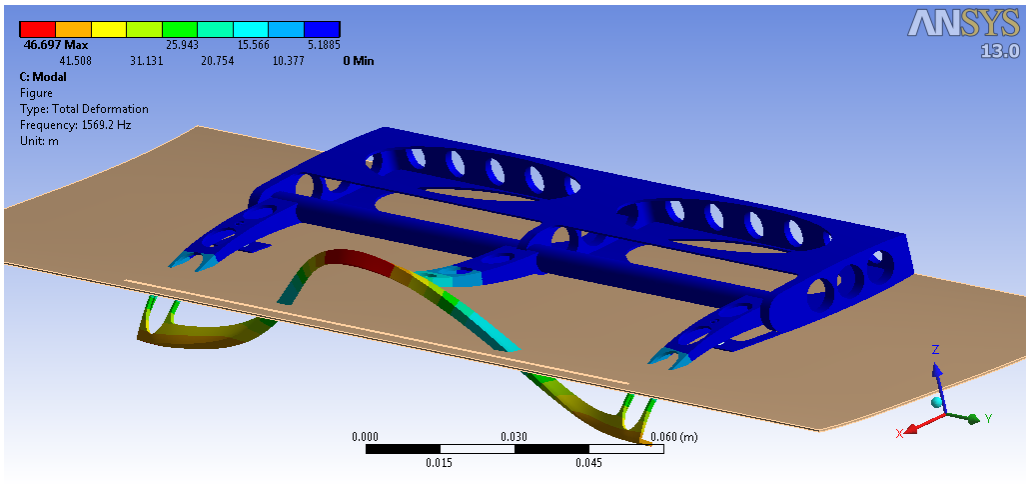

Figure A.5: 3° Mode

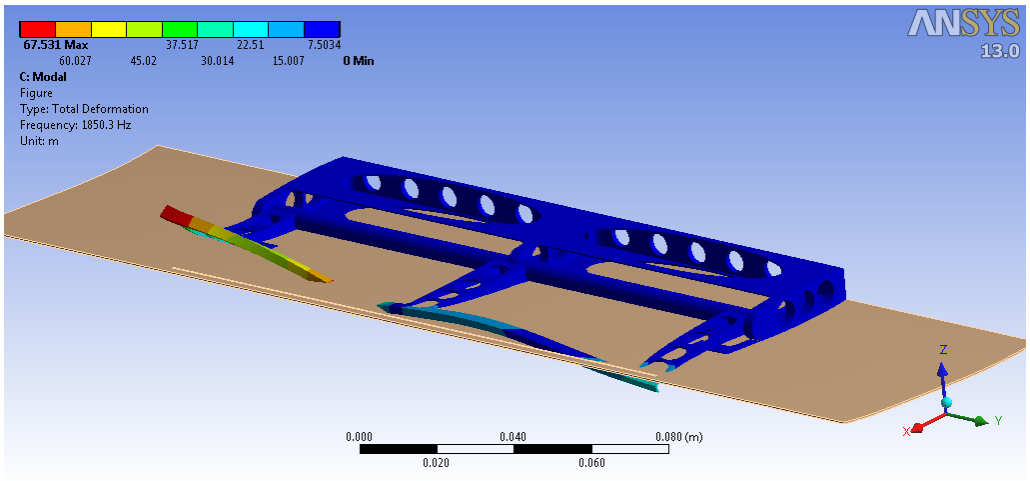

Figure A.6: 4° Mode

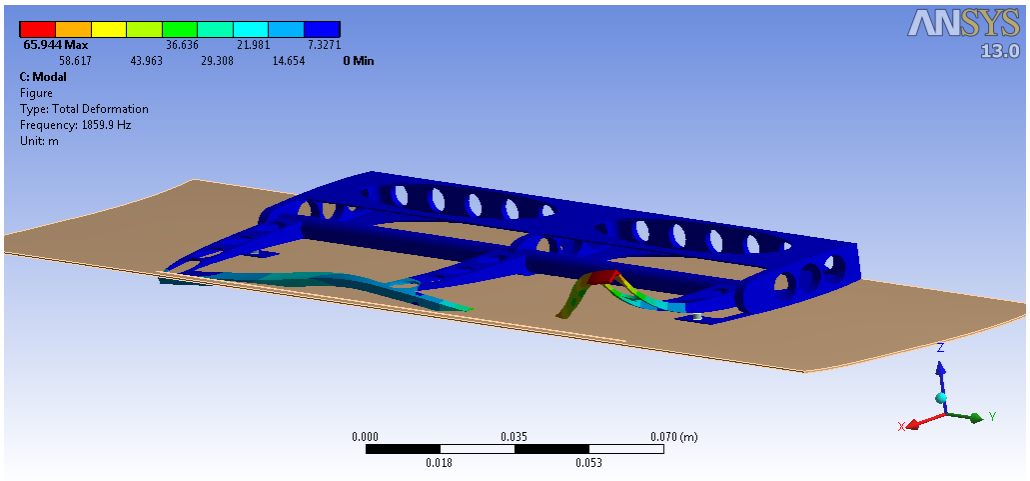

Figure A.7: 5° Mode

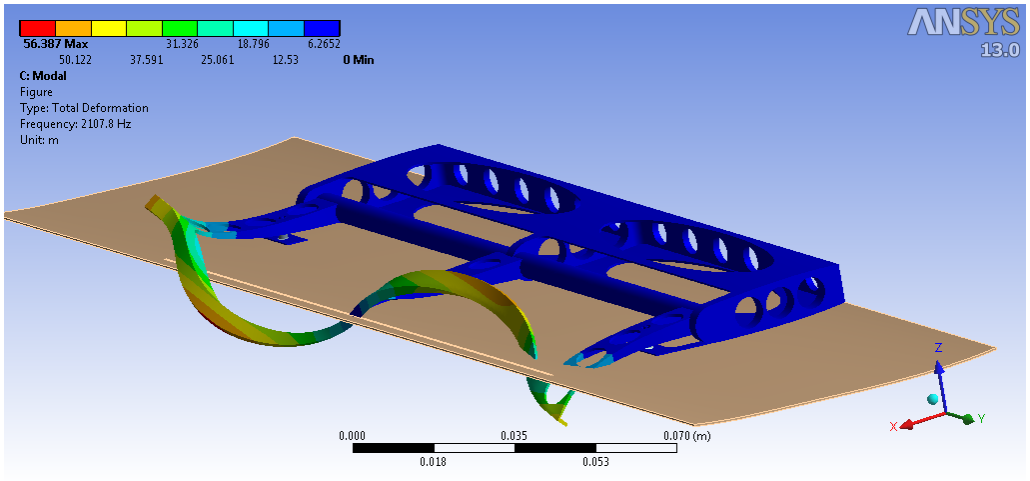

Figure A.8: 6° Mode

Appendix B

Dynamic Analysis Mechanism 1

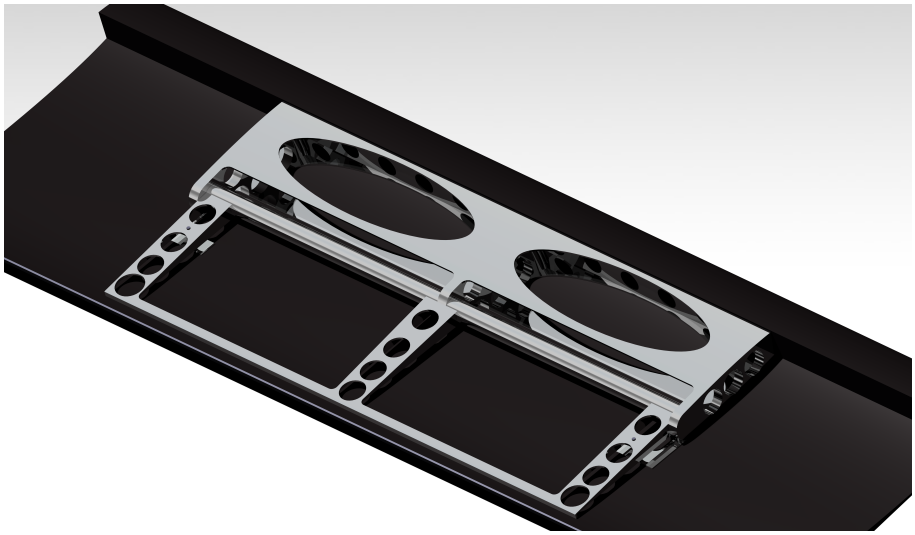

Figure B.1: Design of Mechanism 1

B.1 Mesh Discretization

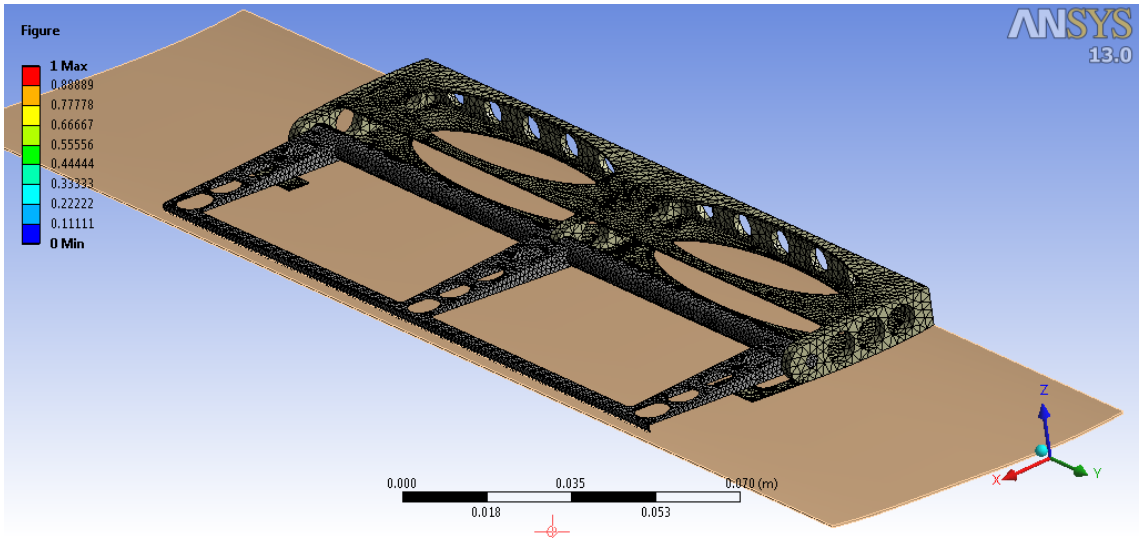

Figure B.2: Mesh Dynamic Analysis Mechanism 1

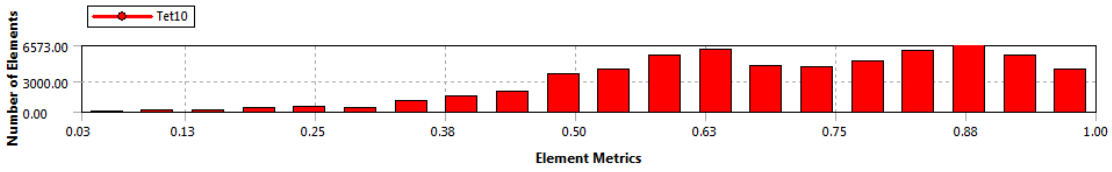

Figure B.3: Mesh Quality Dynamic Analysis Mechanism 1

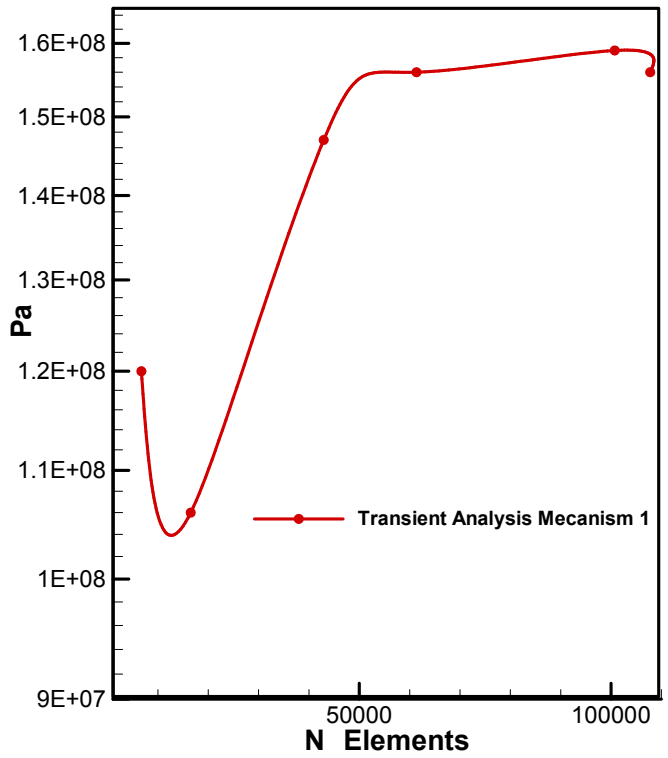

Figure B.4: Mesh Convergence Modal Dynamic Analysis Mechanism 1

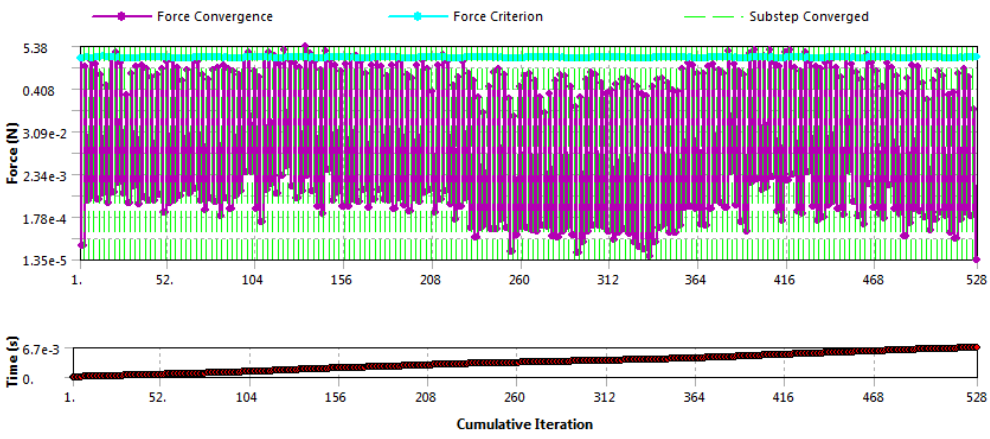

Figure B.5: System Convergence Modal Dynamic Analysis Mechanism 1

B.2 Deformations

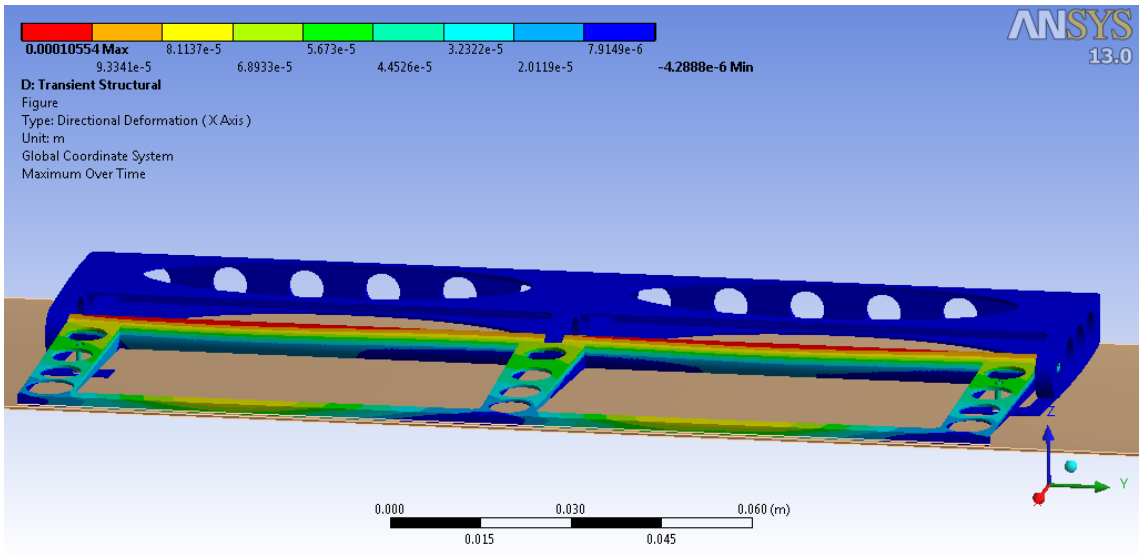

Figure B.6: Deformation X Axis Mechanism 1

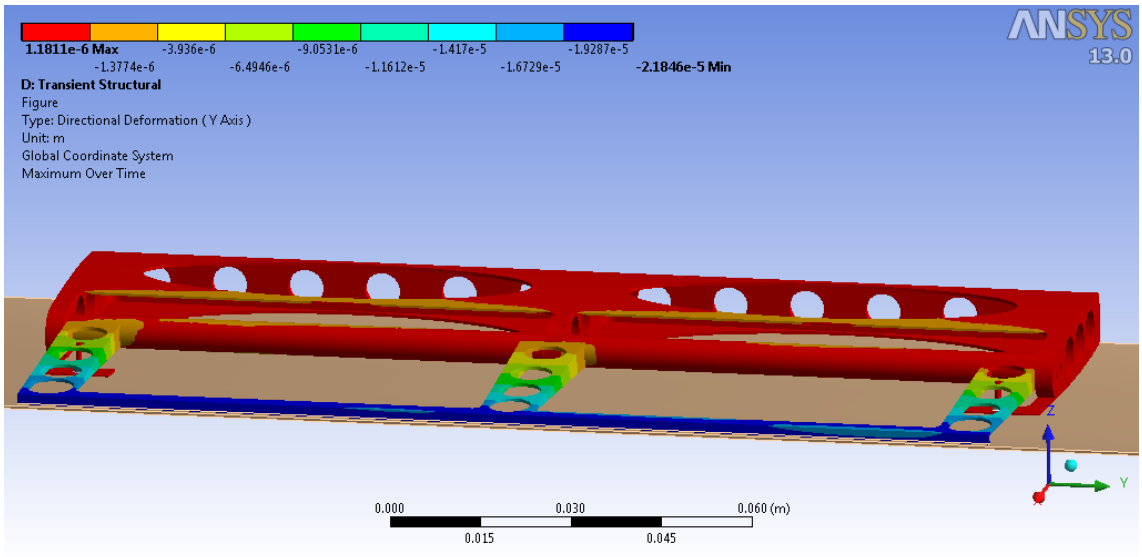

Figure B.7: Deformation Y Axis Mechanism 1

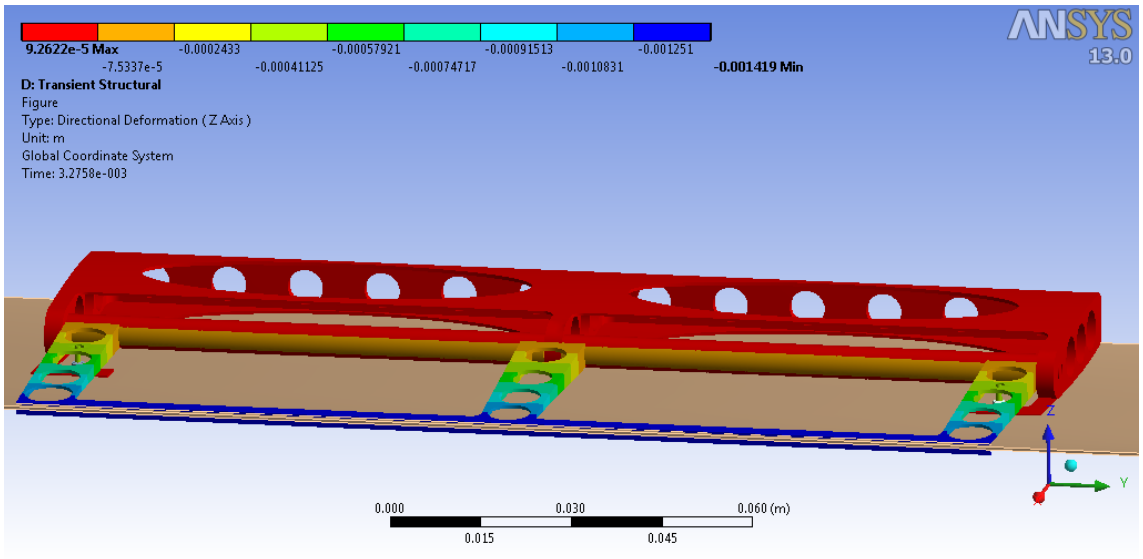

Figure B.8: Deformation Z Axis Mechanism 1

B.3 Stress and Safety Facttor

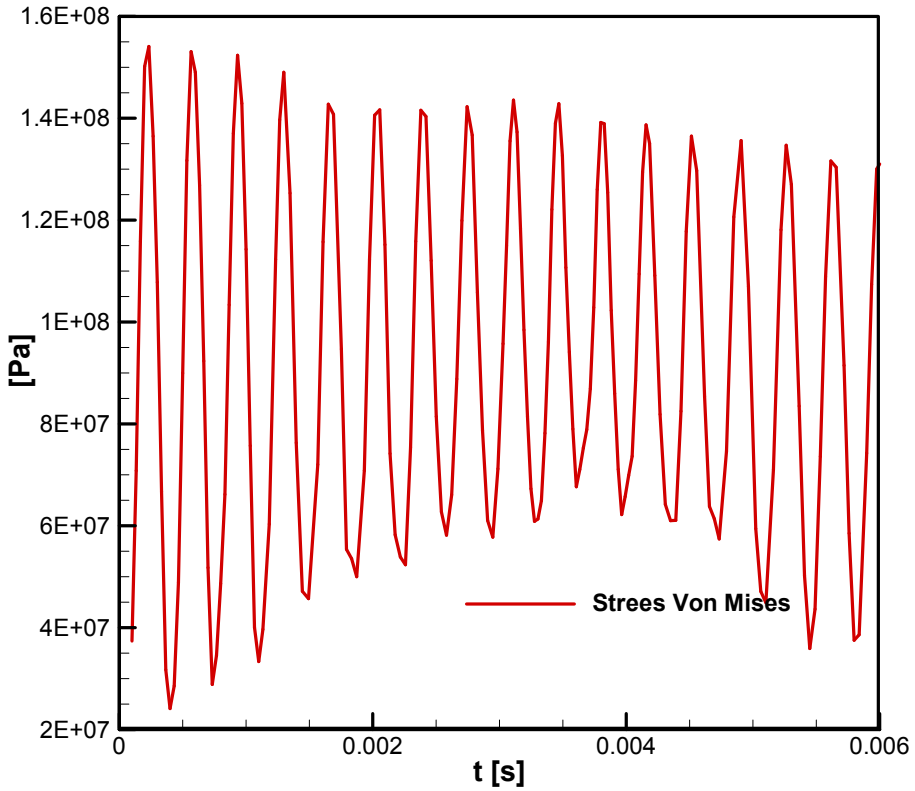

Figure B.9: Stress Von Mises vs time Mechanism 1

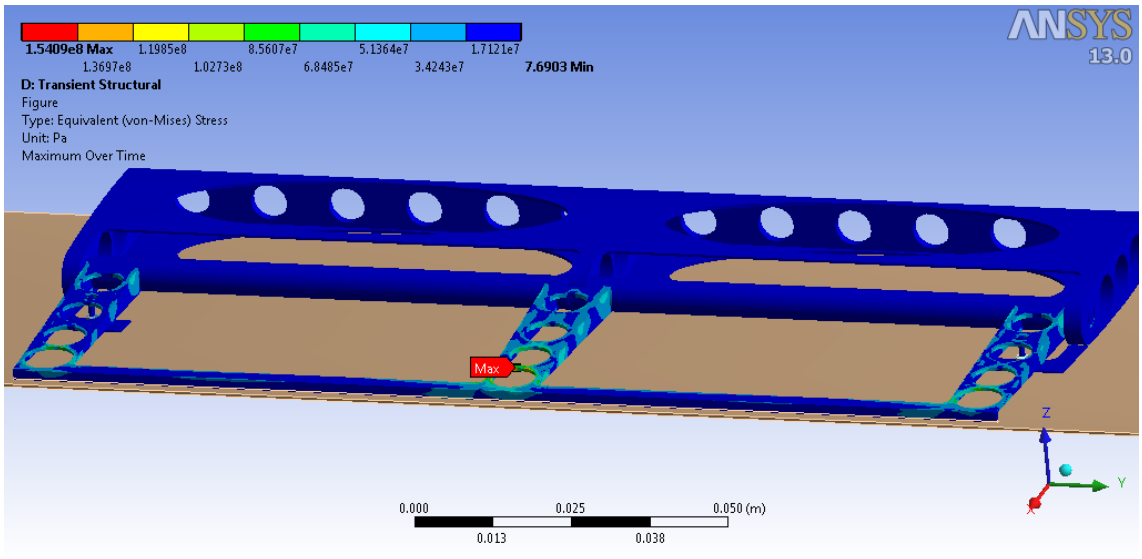

Figure B.10: Stress Von Mises Mechanism 1

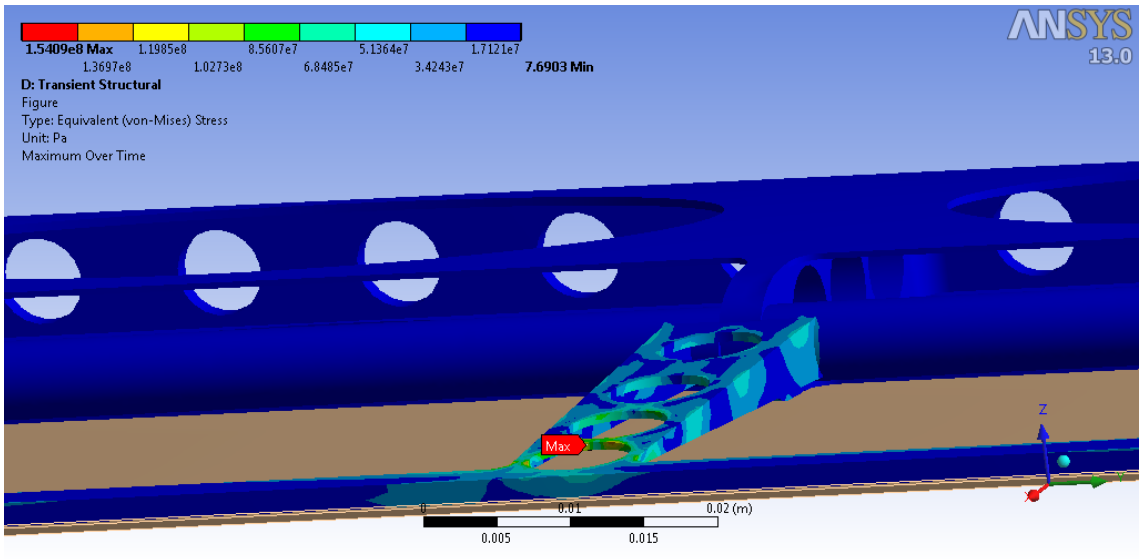

Figure B.11: Stress Von Mises Zoom Mechanism 1

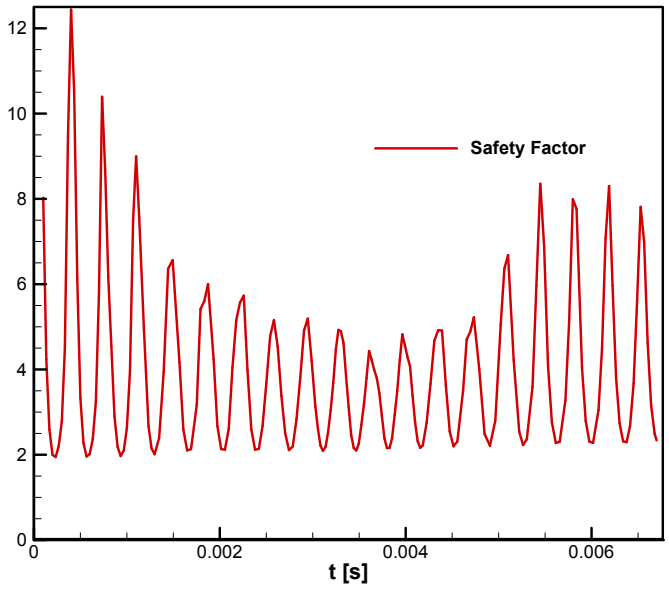

Figure B.12: Safety Factor vs time Mechanism 1

B.4 Dynamics of the Actuator

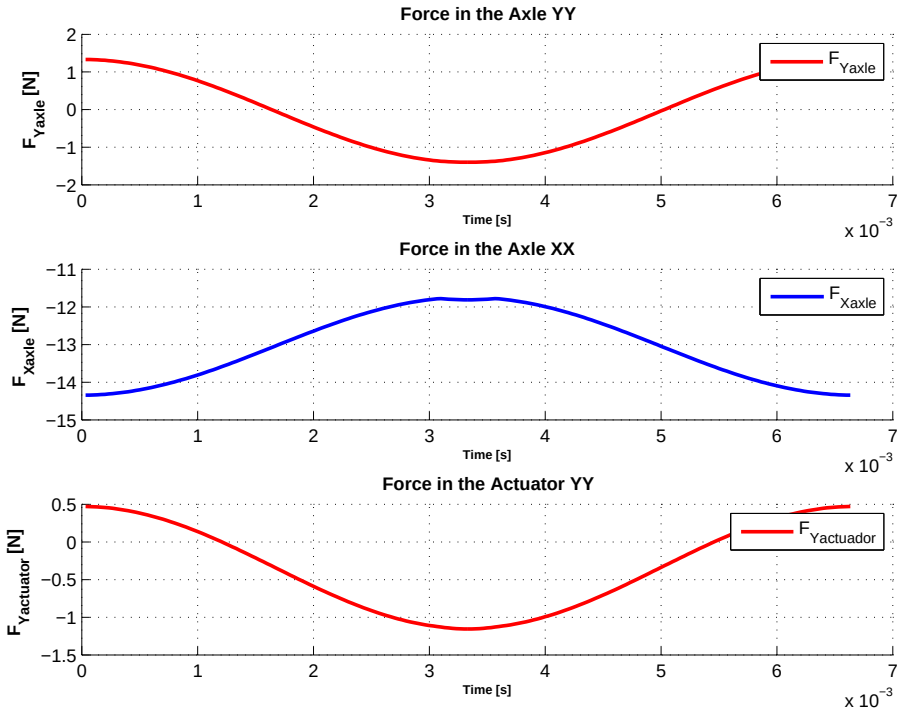

Figure B.13: Necessary Force of the Actuator Mechanism 1

Appendix C

Aluminum Alloy Aluminum 6061-T6 80 HF

Table C.1: Physical Properties

Density	2.7g/cc

Table C.2: Mechanical Properties

Hardness, Brinell	95
Hardness, Knoop	120
Hardness, Rockwell A	40
Hardness, Rockwell B	60
Hardness, Vickers	107
Ultimate Tensile Strength	310 MPa
Tensile Yield Strength	276 MPa
Elongation at Break	12 %
Elongation at Break	17 %
Modulus of Elasticity	68.9 GPa
Notched Tensile Strength	324 MPa
Ultimate Bearing Strength	607 MPa
Bearing Yield Strength	386 MPa
Poisson's Ratio	0.33
Fatigue Strength	96.5 MPa
Fracture Toughness	29 MPa-$m^{1/2}$
Machinability	50 %
Shear Modulus	26 GPa
Shear Strength	207 MPa

Table C.3: Thermal Properties

CTE, linear 68°F	23.6 μ $m-$°C
CTE, linear 250°C	25.2 μ $m/m-$°C
Specific Heat Capacity	0.896 $J/g-$°C
Thermal Conductivity	167 W/m-K
Melting Point	582 - 652°C
Solidus	582°C
Liquidus	652°C

Appendix D

Characteristics of the Piezo Actuatores

Table D.1: Piezoelectric actuators

Reference	**Dimensions [mm]**	**Block Force [N]**	**Stroke [μm]**	**y [mm]**	**L [mm]**	**e [mm]**	**l [mm]**	**Fresult[N]**	**Qty**	**Ftotal [N]**
FPA-0080E-S-0509	10x19x8	56	80	0,133	120	0,08	36,1	33,68	2	67,368
FPA-0085E-S-0518	15x28x10	195	85	0,133	120	0,085	38,3	124,6	2	249,25
APA 35XS	5,5x13,25x9	27	55	0,133	120	0,055	24,8	11,17	2	22,331
APA 50XS	4,7x12,8x9	18	78	0,133	120	0,078	35,2	10,56	2	21,113
APA 60S	15x29,2x9	102	80	0,133	120	0,08	36,1	61,35	2	122,71
APA 120S	13x28,7x9	39	130	0,133	120	0,13	58,6	38,12	2	76,241
APA 150M	22x55,1x9	100	169	0,133	120	0,169	76,2	127,1	2	254,14
APA 100M	25x55,1x9	184	110	0,133	120	0,11	49,6	152,2	2	304,36
APA 200M	17x55x9	73	230	0,133	120	0,23	104	126,2	2	252,48

Appendix E

Gurney Flap Optimization Parameters

Table E.1: Optimization Parameters

Radius 2 [mm]	Radius 1 [mm]	Radius 3 [mm]	Direct. Max. Deformation (m)	Equiv. Max. Stress (Pa)	Geom. Mass (kg)
3.5	3.5	3.5	9.23E-05	88300194.55	0.013509972
3	3.5	3.5	8.69E-05	60003334.03	0.013524732
4	3.5	3.5	0.000102613	152897380.4	0.013493292
3.5	3	3.5	9.23E-05	88434177.63	0.013524747
3.5	4	3.5	9.40E-05	90428996.55	0.013493295
3.5	3.5	3	8.89E-05	88167986.91	0.013524717
3.5	3.5	4	0.000102188	112817697.7	0.013493302
3.093483025	3.093483025	3.093483025	8.46E-05	62364836.08	0.013546314
3.906516975	3.093483025	3.093483025	9.67E-05	130149852.4	0.013520766
3.093483025	3.906516975	3.093483025	8.95E-05	62512952.92	0.013520759
3.906516975	3.906516975	3.093483025	9.94E-05	133716929.6	0.013495165
3.093483025	3.093483025	3.906516975	9.46E-05	94339400.2	0.013520786
3.906516975	3.093483025	3.906516975	0.000108059	136310074.4	0.013495192
3.093483025	3.906516975	3.906516975	9.48E-05	95013942.97	0.013495185
3.906516975	3.906516975	3.906516975	0.000108532	138313682.3	0.013469591

Appendix F

Gurney Flap Draft

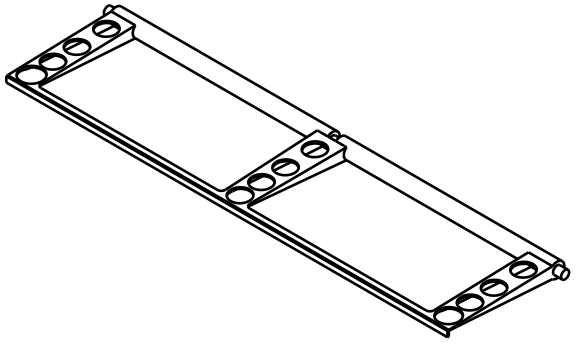

Isometric view
Scale: 1:2

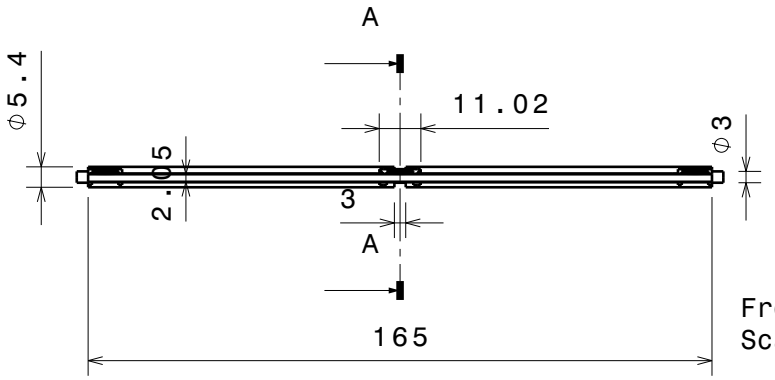

Front view
Scale: 1:2

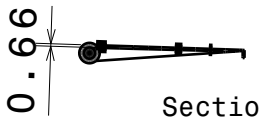

Section view A-A
Scale: 1:2

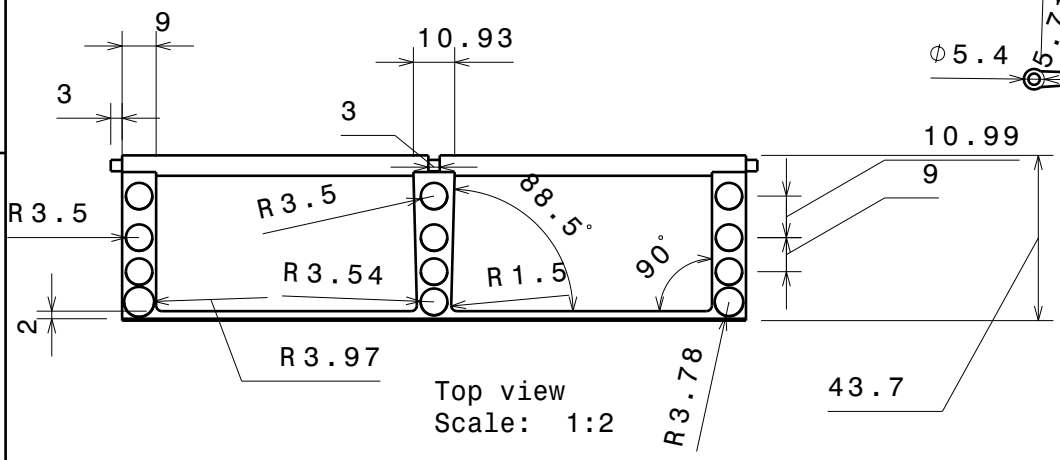

Top view
Scale: 1:2

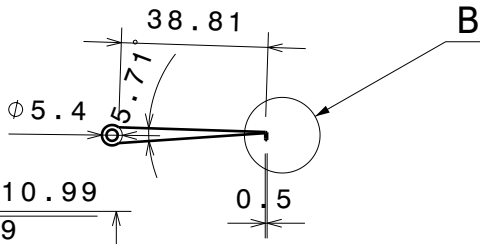

Left view
Scale: 1:2

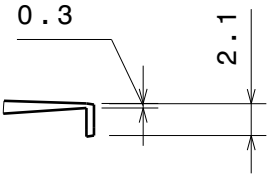

Detail B
Scale: 2:1

UBI

DRAWING TITLE

DRAWN BY: Bruno Dias	DATE: 23-09-2013			
CHECKED BY: XXX	DATE: XXX	SIZE: A4	DRAWING NUMBER: Gurney1	REV: X
DESIGNED BY: Bruno Dias	DATE: XXX	SCALE: 1:2	WEIGHT(kg): 0.01	SHEET: 1/1

Appendix G

Support Draft

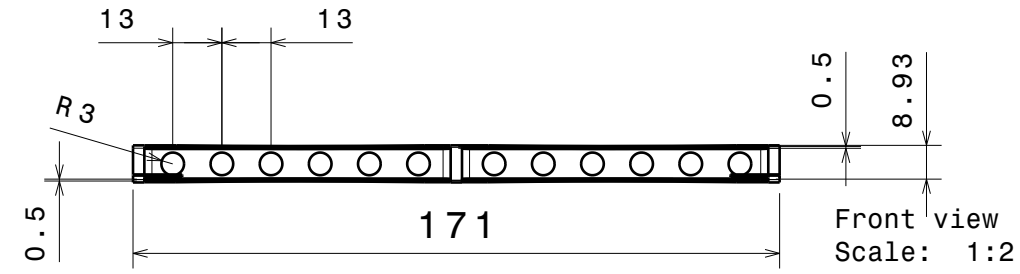

Front view
Scale: 1:2

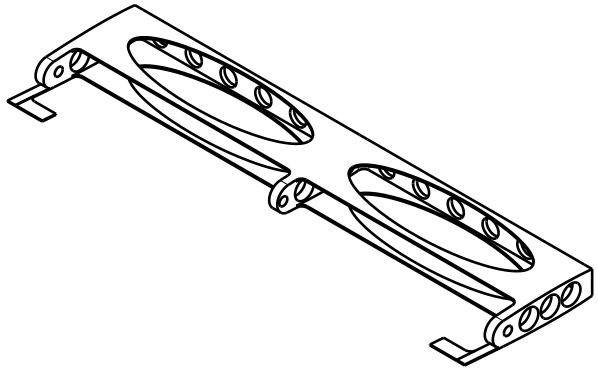

Isometric view
Scale: 1:2

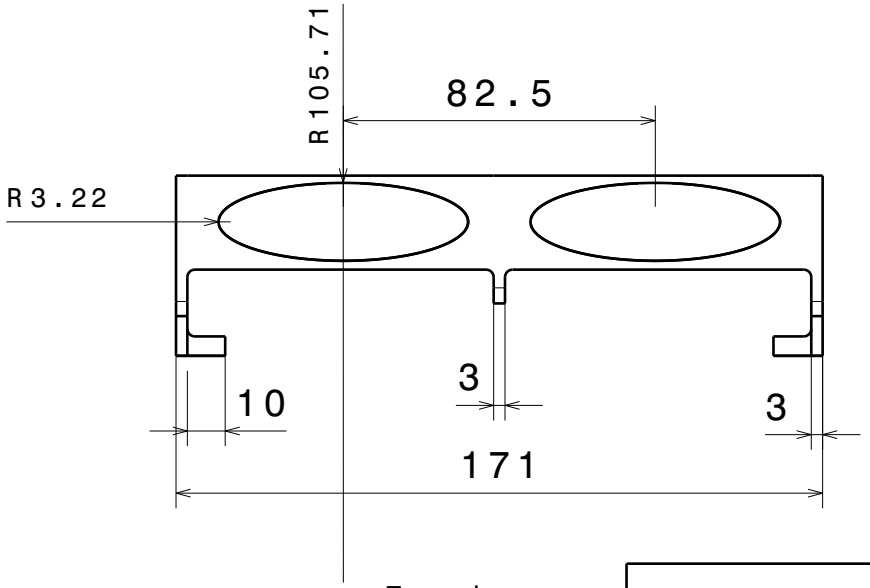

Top view
Scale: 1:2

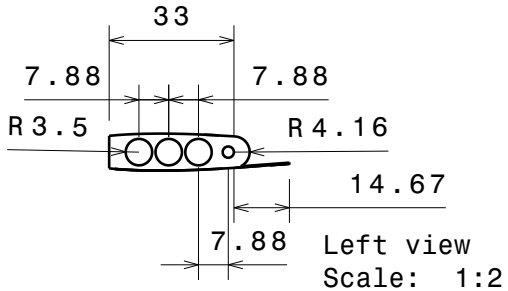

Left view
Scale: 1:2

DRAWN BY: Bruno Dias	DATE: 24-09-2013	UBI			
		DRAWING TITLE: Suport			
CHECKED BY: XXX	DATE: XXX	SIZE: A4	DRAWING NUMBER: Support		REV: X
DESIGNED BY: Bruno Dias	DATE: XXX	SCALE: 1:2	WEIGHT(kg): 0.01		SHEET: 1/1

Appendix H

Matlab code for Mechanim 1

```
clc
clear all
close all
format short
tic
%% Variaveis
 syms theta real  freq x Fy_apoio Fx_apoio Fy_actua y
corda=0.09;              % Corda do perfil
percentagem=0.016;       % Percentagem do Flap
Flap=corda*percentagem; % Tamanho do Flap
espesflap=0.000506;      % Espessura do Flap

b1=4.2958e-002;

 a=0.013551;
g=-9.81;                 % AceleraÃ§Ã£o gravitica
H_max=0.0017;
displacement_act=2.3e-4;    % Displacement do actuador APA200M
tempo_actua=5.61e-4;        % Tempo de actuaÃ§Ã£o APA200M
V_actu=displacement_act/tempo_actua;  % Velocidade do actuador APA200M
Cumprimentoflap=0.165;      %Cumprimento Fla segundo ZZ
Dy_m=-4.03/3;                 % ForÃ§a Aerodinamica segundo YY N/m
Dx_m=31.1/3;                 % ForÃ§a Aerodinamica segundo XX N/m
Dy=Dy_m*Cumprimentoflap;    % ForÃ§a Aerodinamica segundo YY N
Dx=Dx_m*Cumprimentoflap;    % ForÃ§a Aerodinamica segundo XX N
rho=2697;                   % Densidade do Aluminio kg/m3
basemaior=0.004636;         % Base maior do trapezio do braÃ§o de rotaÃ§Ã£o
basemenor=0.0003;          % Base menor trapezio do braÃ§o de rotaÃ§Ã£o
 cumpTrap=0.043025;
Largura=0.009;
A_trap=((basemaior-((basemaior-basemenor)/cumpTrap)*x)*Largura); % Area ...
    do trapezio em funÃ§Ã£o de x
A_flap=(Largura*Flap)*x;              % Area do flap em funÃ§Ã£o de x
R_cili=0.0027;
A_Cili=pi*(R_cili^2);
mass_trap=(A_Cili+A_trap)*rho;       % Massa do trapezio em funÃ§Ã£o de x
mass_Flap=A_flap*rho;       % Massa do Flap em funÃ§Ã£o de x
Momento de Inercia do braÃ§o de rotaÃ§Ã£o(Trapezio)
a_inerc_y=100;
```

```
39 a_inerc_x=-1500;
40 I_trap_flap=1.704e-006/3;  %Momento Inercia segundo o eixo de rotaÃ§Ã£o
41 cg=0.004923;               %centro de gravidade
42 theta_max=atan(Flap/b1);    %Angulo Maximo de ActuaÃ§Ã£o
43 Frequencia=150;          %FrequÃªncia Maxima de actuaÃ§Ã£o;
44 t_max=1/Frequencia;      %PerÃdo Maxima de actuaÃ§Ã£o;
45 subtrac=-0.1;            %Valor inical (importante para Loop de ...
       posiÃ§Ã£o ideal do actuador)
46 %% Loop Cinematica
47 V_actu=0.216816;
48 % Ponto 1( ponto de conecÃ§Ã£o entre actuador e braÃ§o de rotaÃ§Ã£o)
49 y1=a*sin(theta);        %PosiÃ§Ã£o segundo YY
50 x1=0;                   %PosiÃ§Ã£o segundo XX
51 vy_1=V_actu*sin(2*pi*(freq/t_max)); %Velocidade segundo YY
52 vx_1=0;                 %Velocidade segundo XX
53 ay_1=diff(vy_1);        %AceleraÃ§Ã£o segundo YY
54 ax_1=0;                 %AceleraÃ§Ã£o segundo XX
55
56 % Velocidade e aceleraÃ§Ã£o Angular
57
58 vy_1_n=vy_1*cos(theta);
59 omega=vy_1/a;
60 alpha=diff(omega);
61
62 % Ponto 2 (Ponto no Topo do Flap)
63 y2=cos((pi/2)-theta)*b1;     %PosiÃ§Ã£o segundo YY
64 x2=cos(theta)*b1;            %PosiÃ§Ã£o segundo XX
65 vy_2_n=b1*omega;             %Velocidade Normal
66 vy_2=vy_2_n*cos(theta);      %Velocidade segundo YY
67 vx_2=vy_2_n*sin(theta);      %Velocidade segundo XX
68
69 %Ponto 3 (Ponto na Base do Flap)
70 y3=-cos(theta)*Flap+cos((pi/2)-theta)*b1;    %PosiÃ§Ã£o segundo YY
71 x3=sin(theta)*Flap+cos(theta)*b1;            %PosiÃ§Ã£o segundo XX
72 vy_3=vy_2+Flap*omega;                       %Velocidade segundo YY
73 vx_3=vx_2+Flap*omega;                      %Velocidade segundo XX
74
75
76 theta_int=int(omega);
77
78 %%
79
80 t=0;
81 t_step=t_max/200;            %Incremento de tempo
82 i=1;
83  P=t_max;
84  tau=t/P;
```

```
85
86      while t≤t_max
87  %
88  %
89  %    if (0≤tau)&(tau<0.5)
90  %        theta_1=2*sin(theta_max*tau);
91  %
92  %    end
93  %
94  %    if (0.5≤tau)&(tau<1)
95  %        theta_1=theta_max-2*theta_max*(tau-0.5);
96  %
97  %    end
98    T_t(i)=t;
99
100     theta_1=subs(theta_int,{freq},{t})-subs(theta_int,{freq},{T_t(1)});
101    theta_2(i)=theta_1;
102   % Ponto 1
103 y1_n(i)=subs(y1,{theta},{theta_1});
104 x1_n(i)=0;
105 vy_n1(i)=subs(vy_1,{freq},{t});
106 vx_n1(i)=0;
107 vt_n1(i)=sqrt(vy_n1(i)^2+vx_n1(i)^2);
108 ay_n1(i)=subs(ay_1,{freq},{t});
109 ax_n1(i)=0;
110 at_n1(i)=sqrt(ay_n1(i)^2+ax_n1(i)^2);
111
112 % Ponto 2
113 y2_n(i)=subs(y2,{theta},{theta_1});
114 x2_n(i)=subs(x2,{theta},{theta_1});
115 vy_n2(i)=subs(vy_2,{freq,theta},{t,theta_1});
116 vx_n2(i)=subs(vx_2,{freq,theta},{t,theta_1});
117
118
119 % Ponto 3
120
121 y3_n(i)=subs(y3,{theta},{theta_1});
122 x3_n(i)=subs(x3,{theta},{theta_1});
123 vy_n3(i)=subs(vy_3,{freq,theta},{t,theta_1});
124 vx_n3(i)=subs(vx_3,{freq,theta},{t,theta_1});
125
126
127 % Velocidade e aceleraÃ§Ã£o Angular
128 omega_n(i)=subs(omega,{freq},{t});
129 alpha_n(i)=subs(alpha,{freq},{t});
130
131  tau=tau+t_step/P;
```

```
132 if tau>1
133    tau=0;
134 %   P=P+t_max;
135 end
136
137
138 t=t+t_step;
139 i=i+1;
140
141    end
142
143
144  tamanho=numel(vy_n2);
145  for i=1:tamanho-1
146
147 i=i+1;
148 T_tA(i-1)=T_t(i-1);
149 ay_n2(i-1)=(vy_n2(i)-vy_n2(i-1))/t_step;
150 ax_n2(i-1)=(vx_n2(i)-vx_n2(i-1))/t_step;
151 ay_n3(i-1)=(vy_n3(i)-vy_n3(i-1))/t_step;
152 ax_n3(i-1)=(vx_n3(i)-vx_n3(i-1))/t_step;
153  end
154 %% Dinamica
155 yposicao(1)=y3_n(1);
156 alpha_n1(1)=alpha_n(1);
157 for t=2:i-1
158
159 T_tD(t-1)=T_t(t);
160 yposicao(t)=y3_n(t);
161 alpha_n1=alpha_n(t);
162 omega_n1=omega_n(t);
163       Dyy=Dy;
164       Dxx=(Dx*abs(yposicao(t)))/Flap;
165       Dxxx(t-1)=Dxx;
166
167 Forca_Iy=(alpha_n1*(int(mass_trap*x,0,cumpTrap)+...
168 int(mass_Flap*x,0,espesflap)))-(a_inerc_y*(int(mass_trap,0,cumpTrap)...
169 +int(mass_Flap,0,espesflap)));
170 MassCarre=(g*(int(mass_trap,0,cumpTrap)+int(mass_Flap,0,espesflap)));
171
172 MomentoMassa=(g*(int(mass_trap*x,0,cumpTrap)+int(mass_Flap*x,0,espesflap)));
173 MomentoIner=(alpha_n1*(I_trap_flap));
174
175 Forca_Ix=(a_inerc_x*(int(mass_trap,0,cumpTrap)+int(mass_Flap,0,espesflap)));
176 Forcas_Y=Fy_apoio+Fy_actua+Dyy+MassCarre-Forca_Iy;
177 Forcas_X=Fx_apoio+Dxx-Forca_Ix;
178
```

```
179 Momento_ace_I_y=a_inerc_y*(int(mass_trap*x,0,cumpTrap)...
180 +int(mass_Flap*x,0,espesflap));
181 Momento_ace_I_x=a_inerc_x*(int(mass_trap*x,0,basemaior)...
182 +int(mass_Flap*x,0,espesflap));
183
184
185
186 Momentos=Dyy*cumpTrap+Dxx*Flap+(Fy_actua*(a))+MomentoMassa-MomentoIner+...
187         Momento_ace_I_y-Momento_ace_I_x;
188 [Fx_apoio Fy_actua Fy_apoio]=solve(Forcas_Y,Forcas_X,Momentos);
189 Fx_apoio1(t-1)=Fx_apoio;
190 Fy_apoio1(t-1)=Fy_apoio;
191 Fy_actua1(t-1)=Fy_actua;
192 syms Fy_apoio Fx_apoio Fy_actua
193
194 end
195
196
197
198 toc
```

Appendix I

Matlab code for Mechanim 2

```
clc
clear all
close all
format long
tic
%% Variaveis
 syms theta real  freq x y Fy_apoio Fx_apoio Fx_actua
corda=0.09;             % Corda do perfil
percentagem=0.016;      % Percentagem do Flap
Flap=corda*percentagem; % Tamanho do Flap
espesflap=0.000506;     % Espessura do Flap
b1=4.2958e-002;
 a=1.757248E-3;             % PosiÃ§Ã£o orginal do Actuador

g=-9.81;                 % AceleraÃ§Ã£o gravitica
H_max=0.0017;
displacement_act=2.3e-4;    % Displacement do actuador APA200M
tempo_actua=5.61e-4;        % Tempo de actuaÃ§Ã£o APA200M
V_actu=displacement_act/tempo_actua;  % Velocidade do actuador APA200M
Cumprimentoflap=0.165;      %Cumprimento Fla segundo ZZ
Dy_m=-4.03/3;                 % ForÃ§a Aerodinamica segundo YY N/m
Dx_m=31.1/3;                % ForÃ§a Aerodinamica segundo XX N/m
Dy=Dy_m*Cumprimentoflap;    % ForÃ§a Aerodinamica segundo YY N
Dx=Dx_m*Cumprimentoflap;    % ForÃ§a Aerodinamica segundo XX N
rho=2697;                   % Densidade do Aluminio kg/m3
basemaior=0.004636;         % Base maior do trapezio do braÃ§o de rotaÃ§Ã£o
basemenor=0.0003;         % Base menor trapezio do braÃ§o de rotaÃ§Ã£o
 cumpTrap=0.043025;            %Cumprimento do Trapezio
Largura=0.009;
A_trap=((basemaior-((basemaior-basemenor)/cumpTrap)*x)*Largura); % Area ...
    do trapezio em funÃ§Ã£o de x
A_flap=(Largura*Flap)*x;              % Area do flap em funÃ§Ã£o de x
R_cili=0.0027;
A_Cili=pi*(R_cili^2);
mass_trap=(A_Cili+A_trap)*rho;       % Massa do trapezio em funÃ§Ã£o de x
mass_Flap=A_flap*rho;       % Massa do Flap em funÃ§Ã£o de x
a_inerc_y=100;
a_inerc_x=-1500;
I_trap_flap=I_flap+I_trap;
```

```
39 I_trap_flap=1.704e-006/3;  %Momento Inercia segundo o eixo de rotaÃ§Ã£o
40 cg=0.004923;               %centro de gravidade
41 theta_max=atan(Flap/b1);    %Angulo Maximo de ActuaÃ§Ã£o
42 Frequencia=150;          %FrequÃªncia Maxima de actuaÃ§Ã£o;
43 t_max=1/Frequencia;      %PerÃdo Maxima de actuaÃ§Ã£o;
44 subtrac=-0.1;            %Valor inical (importante para Loop de ...
       posiÃ§Ã£o ideal do actuador)
45 %% Loop Cinematica
46
47 V_actu=2.85e-002;
48
49 % Ponto 1( ponto de conecÃ§Ã£o entre actuador e braÃ§o de rotaÃ§Ã£o)
50 y1=cos(theta)*a;
51 x1=sin(-theta)*a;
52 vx_1=V_actu*sin(2*pi*(freq/t_max)); %Velocidade segundo YY
53
54
55
56 % Velocidade e aceleraÃ§Ã£o Angular
57
58 vy_1_n=vx_1*cos(theta);
59 vy_1=vy_1_n*sin(theta);
60 ay_1=diff(vy_1);       %AceleraÃ§Ã£o segundo YY
61 ax_1=diff(vx_1);                %AceleraÃ§Ã£o segundo XX
62 omega=vx_1/a;
63 alpha=diff(omega);
64
65 % Ponto 2 (Ponto no Topo do Flap)
66 y2=cos((pi/2)-theta)*b1;    %PosiÃ§Ã£o segundo YY
67 x2=cos(theta)*b1;           %PosiÃ§Ã£o segundo XX
68 vy_2_n=b1*omega;            %Velocidade Normal
69 vy_2=vy_2_n*cos(theta);     %Velocidade segundo YY
70 vx_2=vy_2_n*sin(theta);     %Velocidade segundo XX
71
72 %Ponto 3 (Ponto na Base do Flap)
73 y3=-cos(theta)*Flap+cos((pi/2)-theta)*b1;   %PosiÃ§Ã£o segundo YY
74 x3=sin(theta)*Flap+cos(theta)*b1;           %PosiÃ§Ã£o segundo XX
75 % vy_3_n=vy_2_n+Flap*omega;                   %Velocidade Normal
76 vy_3=vy_2+Flap*omega;                      %Velocidade segundo YY
77 vx_3=vx_2+Flap*omega;                     %Velocidade segundo XX
78
79
80 theta_int=int(omega);
81
82 %%
83
84 t=0;
```

```
85
86  t_step=t_max/200;           %Incremento de tempo
87  i=1;
88   P=t_max;
89   tau=t/P;
90
91     while t≤t_max
92  %
93  %
94  %    if (0≤tau)&(tau<0.5)
95  %        theta_1=2*sin(theta_max*tau);
96  %
97  %    end
98  %
99  %    if (0.5≤tau)&(tau<1)
100 %        theta_1=theta_max-2*theta_max*(tau-0.5);
101 %
102 %    end
103   T_t(i)=t;
104
105     theta_1=subs(theta_int,{freq},{t})-subs(theta_int,{freq},{T_t(1)});
106    theta_2(i)=theta_1;
107  % Ponto 1
108 y1_n(i)=subs(y1,{theta},{theta_1});
109 x1_n(i)=subs(x1,{theta},{theta_1});
110 vx_n1(i)=subs(vx_1,{freq},{t});
111 vy_n1(i)=subs(vy_1,{freq,theta},{t,theta_1});
112 vt_n1(i)=sqrt(vy_n1(i)^2+vx_n1(i)^2);
113
114
115 % Ponto 2
116 y2_n(i)=subs(y2,{theta},{theta_1});
117 x2_n(i)=subs(x2,{theta},{theta_1});
118 vy_n2(i)=subs(vy_2,{freq,theta},{t,theta_1});
119 vx_n2(i)=subs(vx_2,{freq,theta},{t,theta_1});
120
121
122 % Ponto 3
123
124 y3_n(i)=subs(y3,{theta},{theta_1});
125 x3_n(i)=subs(x3,{theta},{theta_1});
126 vy_n3(i)=subs(vy_3,{freq,theta},{t,theta_1});
127 vx_n3(i)=subs(vx_3,{freq,theta},{t,theta_1});
128
129
130 % Velocidade e aceleraÃ§Ã£o Angular
131 omega_n(i)=subs(omega,{freq},{t});
```

```
alpha_n(i)=subs(alpha,{freq},{t});

 tau=tau+t_step/P;
if tau>1
   tau=0;
%   P=P+t_max;
end


t=t+t_step;
i=i+1;

   end


 tamanho=numel(vy_n2);
 for i=1:tamanho-1

i=i+1;
T_tA(i-1)=T_t(i-1);
ay_n1(i-1)=(vy_n1(i)-vy_n1(i-1))/t_step;
ax_n1(i-1)=(vx_n1(i)-vx_n1(i-1))/t_step;
ay_n2(i-1)=(vy_n2(i)-vy_n2(i-1))/t_step;
ax_n2(i-1)=(vx_n2(i)-vx_n2(i-1))/t_step;
ay_n3(i-1)=(vy_n3(i)-vy_n3(i-1))/t_step;
ax_n3(i-1)=(vx_n3(i)-vx_n3(i-1))/t_step;
 end


%% Dinamica
yposicao(1)=y3_n(1);
alpha_n1(1)=alpha_n(1);
for t=2:i-1

T_tD(t-1)=T_t(t);
yposicao(t)=y3_n(t);
alpha_n1=alpha_n(t);
omega_n1=omega_n(t);
      Dyy=Dy;
      Dxx=(Dx*abs(yposicao(t)))/Flap;
% Dyy=Dy;
% Dxx=Dx;

Forca_Iy=(alpha_n1*(int(mass_trap*x,0,cumpTrap)+int(mass_Flap*x,0,espesflap)));
Forca_YY=(a_inerc_y*(int(mass_trap,0,cumpTrap)+int(mass_Flap,0,espesflap)));
MassCarre=(g*(int(mass_trap,0,cumpTrap)+int(mass_Flap,0,espesflap)));
```

```
179
180 MomentoMassa=(g*(int(mass_trap*x,0,cumpTrap)+int(mass_Flap*x,0,espesflap)));
181 MomentoIner=(alpha_n1*(I_trap_flap));
182
183 Forca_Ix=((int(mass_trap*(int(alpha_n1*x,0,basemaior)+...
184     a_inerc_x),0,cumpTrap)+int(mass_Flap*...
185     (alpha_n1*x+a_inerc_x),0,espesflap)));
186
187
188 Forcas_Y=Fy_apoio+Dyy+MassCarre-Forca_YY-Forca_Iy;
189 Forcas_X=Fx_apoio+Dxx+Fx_actua-Forca_Ix;
190
191
192 Momento_ace_I_y=a_inerc_y*(int(mass_trap*x,0,cumpTrap)+...
193     int(mass_Flap*x,0,espesflap));
194 Momento_ace_I_x=a_inerc_x*(int(int(mass_trap,0,cumpTrap)*y,0,basemaior)...
195     +int(int(mass_Flap*x,0,espesflap)*y,0,basemaior));
196
197 Momentos=Dyy*cumpTrap+Dxx*Flap+(Fx_actua*(a))+MomentoMassa-MomentoIner-...
198         Momento_ace_I_y-Momento_ace_I_x;
199 [Fx_apoio Fx_actua Fy_apoio]=solve(Forcas_Y,Forcas_X,Momentos);
200 Fx_apoio1(t-1)=Fx_apoio;
201 Fy_apoio1(t-1)=Fy_apoio;
202 Fx_actua1(t-1)=Fx_actua;
203 syms Fy_apoio Fx_apoio Fx_actua
204
205 end
206 toc
```